

Editor-in-Chief B.E.Paton

Editorial board:

- Yu.S.Borisov V.F.Grabin
Yu.Ya.Gretskii A.Ya.Ishchenko
B.V.Khitrovskaya V.F.Khorunov
I.V.Krivtsun
S.I.Kuchuk-Yatsenko
Yu.N.Lankin V.K.Lebedev
V.N.Lipodaev L.M.Lobanov
V.I.Makhnenko A.A.Mazur
V.F.Moshkin O.K.Nazarenko
I.K.Pokhodnya I.A.Ryabtsev
Yu.A.Sterenbogen N.M.Voropai
K.A.Yushchenko V.N.Zamkov
A.T.Zelnichenko

International editorial council:

- N.P.Alyoshin (Russia)
B.Braithwaite (UK)
C.Boucher (France)
Guan Qiao (China)
U.Diltey (Germany)
P.Seyffarth (Germany)
A.S.Zubchenko (Russia)
T.Eagar (USA)
K.Inoue (Japan)
N.I.Nikiforov (Russia)
B.E.Paton (Ukraine)
Ya.Pilarczyk (Poland)
D.von Hofe (Germany)
Zhang Yanmin (China)
V.K.Sheleg (Belarus)

Promotion group:

- V.N.Lipodaev, V.I.Lokteva
A.T.Zelnichenko (exec. director)

Translators:

- A.V.Gorskaya, I.N.Kutianova,
T.K.Vasilenko

Editor:

N.A.Dmitrieva

Electron galley:

- I.S.Batasheva, T.Yu.Snegiryova

Address:

E.O. Paton Electric Welding Institute,
International Association «Welding»,
11, Bozhenko str., 03680, Kyiv, Ukraine
Tel.: (38044) 287 67 57
Fax: (38044) 528 04 86
E-mail: journal@paton.kiev.ua
http://www.nas.gov.ua/pwj

State Registration Certificate
KV 4790 of 09.01.2001

Subscriptions:

12 issues per year;
460\$ — regular, 390\$ — for subscription
agencies, 260\$ — for students;
postage and packaging included.
Back issues available.

All rights reserved.

This publication and each of the articles
contained herein are protected by copyright.
Permission to reproduce material contained in
this journal must be obtained in writing from
the Publisher.
Copies of individual articles may be obtained
from the Publisher.

CONTENTS

SCIENTIFIC AND TECHNICAL

Grigorenko G.M., Golovko V.V., Kostin V.A. and Grabin V.F. Effect of microstructural factors on sensitivity of welds with ultra-low carbon content to brittle fracture ..... 2
Maksimov S.Yu. Evaluation of the influence of wet underwater welding conditions on the probability of pore formation in the weld metal ..... 10
Kuzmenko V.G. and Guzej V.I. Pore formation in weld metal in submerged arc welding with surface saturation of grains with fluorine ..... 14
Shonin V.A., Gushcha O.I., Mashin V.S., Kovalchuk V.S. and Kuzmenko A.Z. Influence of the dimensions of a specimen of aluminium alloy welded joint on the residual stressed state and fatigue resistance ..... 18
Ulshin V.A. and Kharlamov M.Yu. Optimization of parameters of detonation-gas spraying using a genetic algorithm ..... 29

INDUSTRIAL

Blashchuk V.E. and Shelenkov G.M. Fusion welding of titanium and its alloys (Review) ..... 35
Shelyagin V.D., Khaskin V.Yu. and Lukashenko A.G. CO2-laser cutting of disk saw bodies ..... 43
Vornovitsky I.N., Zakharova N.V., Shishkova O.V., Vilisov A.A. and Zinchenko A.V. Technological peculiarities of high-alloy steel welding by electrodes with rutile coating ..... 46
Illarionov S.Yu., Dobrushin L.D., Polyakov S.G. and Boeva G.E. Increase of corrosion resistance of welded joints of high-strength aluminium alloys by explosion cladding ..... 48
Zhadkevich A.M. Sources of beam heating for brazing (Review) ..... 51

BRIEF INFORMATION

Kiselevsky F.N., Dolinenko V.V. and Topchev D.D. Method of software development using control graphs and languages means ISaGRAF for intelligent welding controllers ..... 58
Theses for scientific degrees ..... 60



# EFFECT OF MICROSTRUCTURAL FACTORS ON SENSITIVITY OF WELDS WITH ULTRA-LOW CARBON CONTENT TO BRITTLE FRACTURE

G.M. GRIGORENKO, V.V. GOLOVKO, V.A. KOSTIN and V.F. GRABIN  
E.O. Paton Electric Welding Institute, NASU, Kiev, Ukraine

Morphological features of microstructure of weld metal with ultra-low carbon content have been studied. It is shown that in such welds both MAC-phase and lamellar forms of ferrite are the structural factors that cause instability of properties. It has been found that the content of the MAC-phase should not exceed 5–6 vol.% at a low content of ferrite with an ordered secondary phase to provide consistently high properties at low temperatures. It is shown that impact toughness of the welds studied rises with increase in the content of the ductile component in fracture.

**Keywords:** arc welding, low-alloy steels, weld metal, ultra-low content of carbon, structure, acicular ferrite, MAC-phase, ferrite with ordered and disordered secondary phase, structural components, quasi-cleavage, impact toughness

Optimal strength and ductile properties of metal of the welds in low-alloy steels are achieved primarily owing to a favourable combination of a set of ferrite-cementite structures. The following structural components are formed in such a weld metal: acicular ferrite (AF), polygonal (allotriomorphic) ferrite (PF), Widmanstätten ferrite (WF), ferrite with ordered (OSP) and disordered secondary phase (DSP), as well as martensite-austenite-carbide phase (MAC-phase) formed during the austenite dissociation process.

It is reported [1, 2] that, among all the above structural components, AF has the best properties in terms of resistance to brittle fracture, which is caused by its morphological peculiarities: AF is formed mainly inside primary crystalline grains, its needles are 2–8  $\mu\text{m}$  long and 1–2  $\mu\text{m}$  thick, and the ratio of their sides is 1:3 to 1:10, high-angle boundaries with a disorientation angle of more than  $20^\circ$  are formed between the needles, micro-phases, i.e. carbides or MAC-phase, are formed at the interface between the ferrite grains, and dislocations inside the AF grains have high density ( $\rho = 1 \cdot 10^{12} \text{ cm}^{-2}$ ).

At the same time, analysis of literature data shows that there are cases where it is impossible to achieve high cold resistance of the weld metal, despite the presence of AF in it [3, 4]. It can be seen from the data shown in Figure 1 that impact toughness somewhat decreases at a content of AF in the weld metal equal to more than 70 vol.%. Given that these results were obtained for welds with a carbon content of 0.12–0.15 wt.%, it can be suggested that this effect is caused by contribution of an unaccounted structural factor, e.g. MAC-phase.

Study [4] explains decrease in impact toughness of the weld metal with a high content of alloying elements by growth of its tensile strength without a corresponding decrease in grain size. However, there is a different opinion, according to which decrease in impact toughness is related to the fact that the weld metal contains micro-phases that act, similar to oxide inclusions, as brittle crack initiation centres [5, 6].

The purpose of this study was to investigate the effect of structural components of the weld metal on its sensitivity to brittle fracture at low temperatures, and to reveal factors that lead to decrease in properties of the weld metal containing AF.

**Experimental procedure.** The studies were conducted on specimens of metal of the welds with an experimentally found decrease in impact toughness at negative temperatures at a content of AF in their structure equal to more than 70 vol.%. These welds were made by butt welding with V-groove preparation (included angle  $60^\circ$ ) on 32 mm thick steel 10KhSND

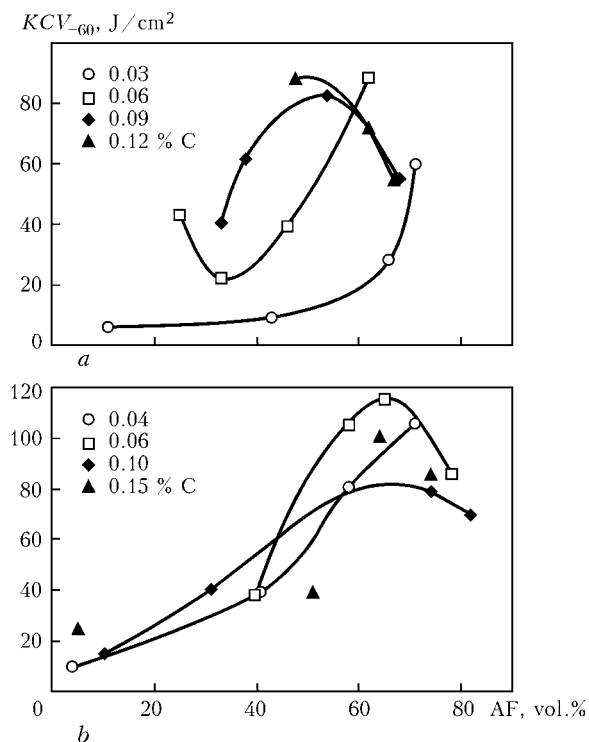


Figure 1. Effect of volume content of AF on impact toughness KCV according to experimental data given in [3] (a) and [4] (b)



**Table 1.** Chemical composition (wt.%) of weld metal and welding wire for the specimens studied

Wire grade, weld No.	N	Al	Si	Ti	Ni	Mn	Mo	Cr	Cu	S	P
Sv-03G2N2MTA, 1	0.030	0.003	0.140	0.004	2.63	1.16	0.60	0.27	0.15	0.011	0.011
Sv-03G2N2TA, 2	0.030	0.002	0.160	0.004	2.58	1.65	0.17	0.28	0.15	0.011	0.010
Sv-04N3GMTA, 3	0.036	0.002	0.235	0.018	2.53	1.01	0.26	0.10	0.16	0.014	0.007
Sv-06G2NMTA, 4	0.060	0.002	0.200	0.008	1.20	1.40	0.52	0.26	0.16	0.011	0.016
	0.073	0.013	0.420	0.013	1.27	1.28	0.27	0.28	0.40	0.010	0.016

(wt. %: 0.12C, 0.5–0.8Mn, 0.8–1.1Si, 0.6–0.9Cr, 0.5–0.8Ni, 0.4–0.65Cu) using neutral flux ANK-57 (DIN 32 522, BFB 155, DC 8, KMHP 5) and four welding wires Sv-03G2N2MTA, Sv-03G2N2TA, Sv-04N3GMTA and Sv-06G2NMTA (TU 14-143-508-99). The choice of the types of welding wire was based on the task to provide welds with a different content of carbon, nickel and molybdenum. Welding was performed at a direct current of reversed polarity under the following conditions:  $I_w = (620 \pm 5) \text{ A}$ ,  $U_a = (30 \pm 1) \text{ V}$ ,  $v_w = (20 \pm 5) \text{ m/h}$ , and  $q_w \cong 48 \text{ kJ/cm}$ . The rate of cooling of a weld was 4–7 °C/s in a temperature range of 800–500 °C.

Chemical composition of metal of the last pass of the weld was determined by spectral analysis using the Baird unit equipped with IBM PC. From three to five measurements were made for each specimen, and the results thus obtained were averaged. The results of analysis of chemical composition of the weld metals and welding wires are given in Table 1.

Specimens for evaluation of mechanical properties of the deposited metal were made from metal of the welds studied (Figure 2).

Quantitative determination of microstructural components was done in accordance with the IIW procedure [7]. The content of alloying elements in solid solution and composition of non-metallic inclusions were determined by the method of X-ray spectral microanalysis using the Link System energy-dispersive spectrometer Link 860/500 and wave-dispersive spectrometer Ortec. Microstructure of metal of the welds studied is shown in Figure 3.

**Investigation results.** As found as a result of metallographic examinations, all specimens of the deposited metal were characterised by the presence of such

components as AF, PF and MAC-phase. In addition, a small amount of lamellar forms of ferrite was revealed. According to the IIW classifications, these forms are OSP and DSP. They have to be taken into account, as this type of structure may have a marked effect on sensitivity of the weld metal to brittle fracture. Data on the content of structural components in the specimens studied are given in Table 2.

The weight content of elements in AF and PF was determined by the method of quantitative microanalysis using scanning electron microscope JSM-840 and software ZAF4/FLS for analysis of flat surfaces on etched specimens. The content of alloying elements in the MAC-phase and on the fracture surface was determined using software ZAF/PB intended for analysis of particles and rough surfaces (fractures). The results obtained are given in Table 3. As shown by the studies, compared with PF, AF is richer in

**Table 2.** Content (vol.%) of main structural components in weld metal

Weld No.	PF	AF	OSPF	DSPF	MAC-phase
1	13.7	61.1	1.5	18.5	5.15
2	29.4	51.0	2.5	11.5	5.00
3	19.4	70.5	2.6	2.5	6.97
4	15.8	73.4	4.5	3.5	6.42

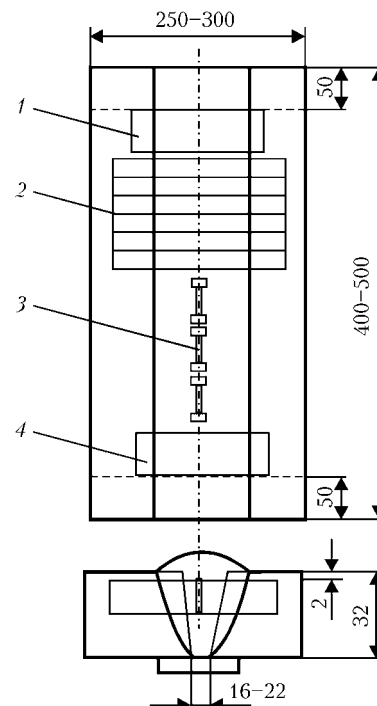


**Figure 2.** Schematic diagram of sampling for metallographic examination and evaluation of mechanical properties of deposited metal of the welds: 1, 4 — sections for metallographic examinations; 2, 3 — specimens for evaluation of impact toughness and strength, respectively

**Table 3.** Content of alloying elements (wt.%) in structural components of weld metal

Weld No.	Structural components	Al	Si	Ti	Ni	Mn	Mo	Cr	Cu	S	P
1	AF	0.007	0.326	0.024	2.120	0.795	1.574	0.269	0.438	0.005	0.009
	PF	0.104	0.357	0.004	1.824	0.911	0.085	0.333	0.257	0.008	0.004
	MAC-phase	0.002	0.392	0.037	2.184	0.680	1.944	0.180	0.259	0	0.025
2	AF	0.007	0.263	0.048	1.890	0.686	0.548	0.276	0.350	0.006	0.005
	PF	0.155	0.352	0.004	1.712	0.378	0.109	0.229	0.372	0.005	0.007
	MAC-phase	0	0.321	0	2.302	0.598	1.208	0.069	0.202	0	0.007
3	AF	0.055	0.438	0.045	1.924	0.848	0.833	0.242	0.283	0.009	0.003
	PF	0.097	0.504	0.007	1.689	0.769	0.045	0.189	0.200	0.004	0.009
	MAC-phase	0.002	0.405	0.001	2.381	0.611	2.508	0.143	0.326	0	0.007
4	AF	0.009	0.367	0.052	1.831	1.123	0.741	0.257	0.397	0.006	0.006
	PF	0.079	0.375	0.007	1.558	0.665	0.157	0.251	0.440	0.005	0.011
	MAC-phase	0.005	0.365	0.013	2.228	0.727	1.590	0.214	0.109	0	0.009

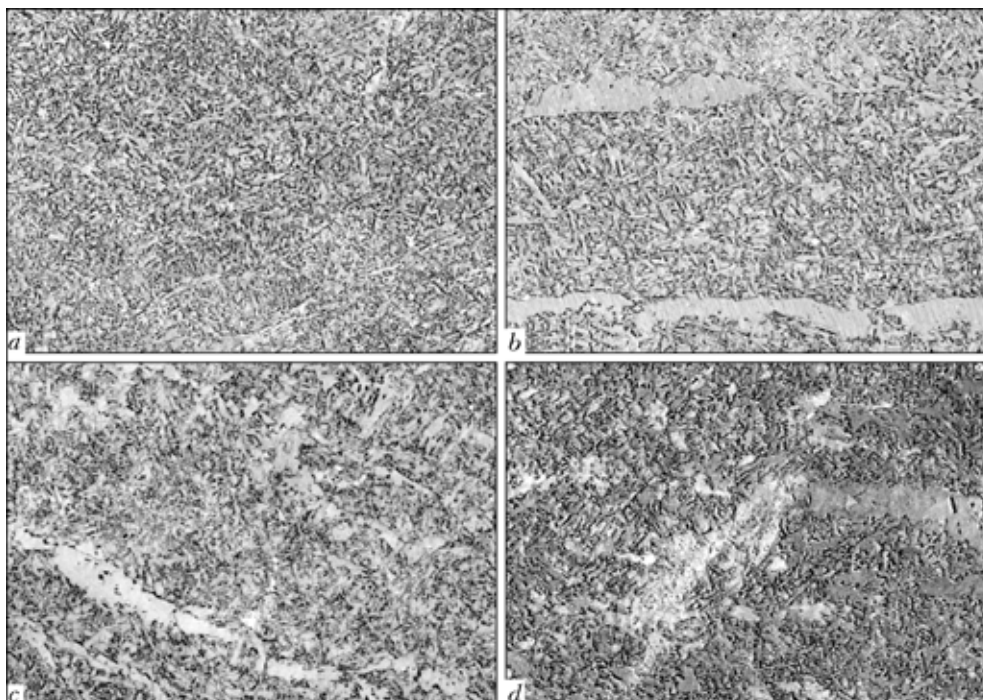
nickel and molybdenum, while the MAC-phase has the highest content of these elements.

Fractography of the fracture surface (Figure 4) shows that fracture occurs by the same mechanism in all the specimens. Regions of quasi-cleavage (tough cleavage), which are small brittle fracture facets 2–5  $\mu\text{m}$  in size separated by high-angle boundaries, as well as regions of tough pitting fracture can be seen on the fracture surfaces. Extended branching lines called combs are a characteristic element of the fracture surfaces of the welds studied. The metal of weld 1 is characterised by a uniform distribution of the quasi-cleavage facets, the size of which is comparable with size of the ferrite needles (1–6  $\mu\text{m}$ ). The studies show that welds 2–4 have extended cleavage regions 10–20  $\mu\text{m}$  wide and 50–100  $\mu\text{m}$  long, elongated in the same direction.

To determine structural components in which the fracture occurs, it is necessary to investigate composition of metal of the characteristic fracture regions of the welds and compare them with that of the structural components given in Table 3. The regions of quasi-cleavage, tough pitting fracture and fracture surface of the type of the combs, i.e. the region of plastic deformation, were selected for analysis.

The results of microanalysis of the characteristic regions of fracture of the weld metal are given in Table 4.

Fracture was found to occur in certain structural components. Comparison of the results of analysis of chemical composition of metal of the fracture surfaces given in Tables 3 and 4, as well as characteristic sizes and morphology of fracture (quasi-cleavage, pitting, combs) and structure elements (AF, PF, MAC-phase),

**Figure 3.** Microstructure of metal of the welds (a–d correspond to welds Nos. 1–4 in Table 2) ( $\times 500$ )

**Table 4.** Content of alloying elements (wt.%) in metal of characteristic regions of fracture of the welds

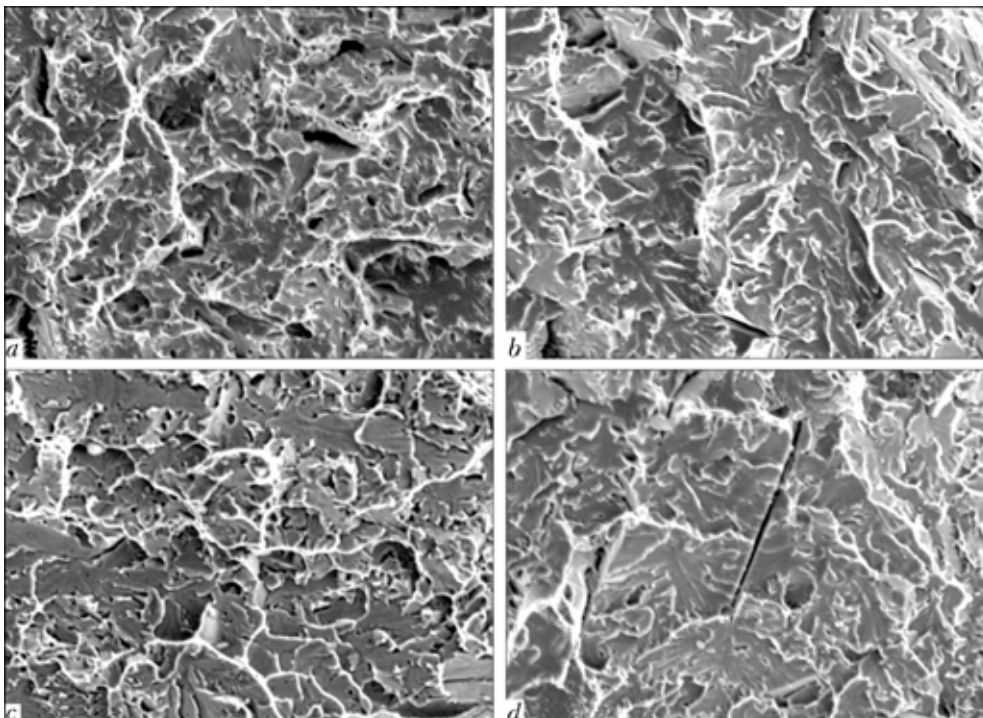
Weld No.	Type of fracture	Al	Si	Ti	Ni	Mn	Mo	Cr	Cu	S	P
1	Quasi-cleavage	0.032	0.408	0.139	2.145	0.878	1.656	0.497	0.253	0	0.008
	Pitting	0	0.392	0.089	1.821	1.056	0.040	0.477	0.431	0	0
	Combs	0.266	0.569	0.017	2.028	0.810	1.540	0.312	0.405	0.181	0
2	Quasi-cleavage	0	0.360	0	1.834	0.782	0.430	0.466	0.276	0	0
	Pitting	0.056	0.293	0	1.617	0.526	0.135	0.444	0.123	0	0
	Combs	0	0.562	0.086	2.426	0.871	1.120	0.205	0.540	0	0
3	Quasi-cleavage	0.193	0.454	0.276	1.902	0.878	0.865	0.504	0.765	0	0
	Pitting	0	0.525	0.057	1.613	0.746	0.120	0.450	0.109	0	0
	Combs	0	0.528	0.020	2.596	0.872	2.108	0	0.108	0	0
4	Quasi-cleavage	0.203	0.272	0.013	1.896	0.995	0.782	0.122	0.578	0.046	0
	Pitting	0.077	0.224	0.057	1.573	0.753	0.090	0.298	0.489	0	0.002
	Combs	0.158	0.647	0.047	2.167	0.882	0.816	0.319	0.495	0.050	0.085

allowed a conclusion that the quasi-cleavage regions are related primarily to AF, and the tough regions are related mainly to PF. Analysis of fractures showed that fracture of metal of the welds studied occurred mostly in grains of AF and ferrite with OSP. The only difference was the quantitative proportion of fracture surfaces occupied by AF and ferrite with OSP.

The use of the traditional procedure for analysis of fractures from macro images of the welds, where fracture occurred by quasi-cleavage, turned out to be of a low efficiency. This is associated with the fact that with the standard classification the regions of quasi-cleavage are entirely classed as a brittle fracture component. In fact, the content of the brittle component (dark regions in Figure 5, *a, c, e, g*) in the quasi-cleavage regions constitutes only part of frac-

ture. This type of fracture is characterised by the presence of a substantial content of a ductile component (white regions in Figure 5, *a, c, e, g*), which is directly related to the process of crack propagation. In this connection, it is of interest to analyse relationship between the content of the ductile component in quasi-cleavage and impact toughness. We marked out the ductile component (white regions in Figure 5, *b, d, f, h*) in the quasi-cleavage regions using the image analysis software Image-Pro-Plus, version 3.0, and considered relationship between the content of the ductile component and impact toughness of the weld metal (Figure 6).

Mechanical properties of the welds were evaluated on specimens made from their metal. The results are given in Table 5.

**Figure 4.** Fractography of fracture surfaces of metal of the welds (*a-d* correspond to welds Nos. 1-4 in Table 2) ( $\times 1000$ )

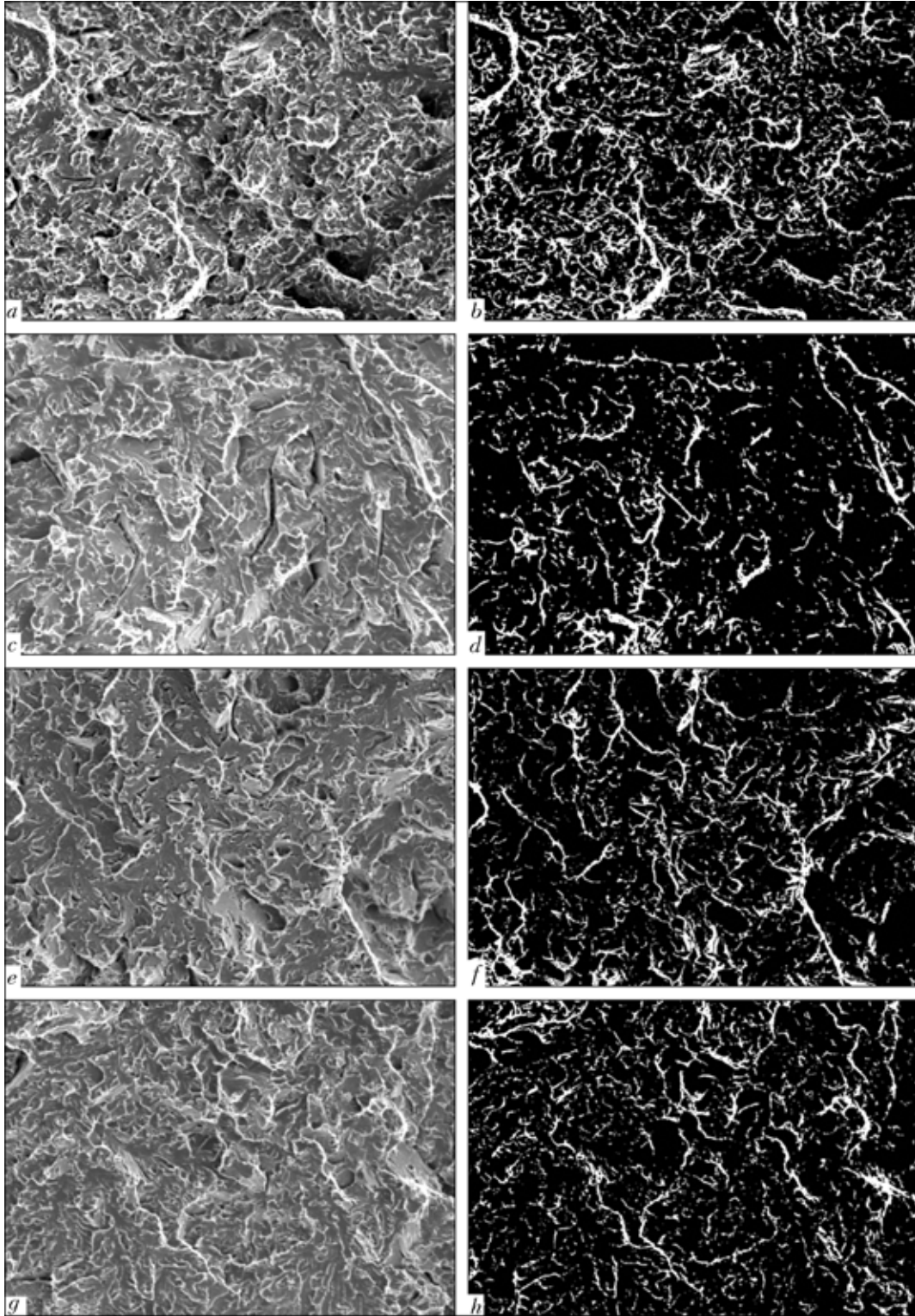


**Figure 5.** Fractography of fracture of weld metals and ductile zones marked in them (*b, d, f, h*), constituting 15.7 (*b*), 8.5 (*d*), 9.7 (*f*) and 8.7 (*h*) vol.% (*a* and *b*, *c* and *d*, *e* and *f* and *g*, *h* correspond to welds Nos. 1–4 in Table 2) ( $\times 500$ )

The studies show that increase in the content of the ductile component in the quasi-cleavage region leads to increase in low-temperature impact toughness (see Figure 6).

To determine the role of this or that structural component in the brittle fracture process, it is necessary to detect them on the fracture surfaces. This was done by the special procedure developed for etching the fracture surfaces. The problem in this case is that

air bubbles hindering the etching process are present on a developed rough surface. The ultrasonic disperser generating the standing waves in a solution was used to remove the air bubbles, thus providing a continuous washing of the fracture surface with an etchant. Alkali solution of picric acid (picrate) and 4 % solution of nitric acid in alcohol (nital) were used as an etchant. Microstructure of the weld metal on the fracture surface is shown in Figure 7.

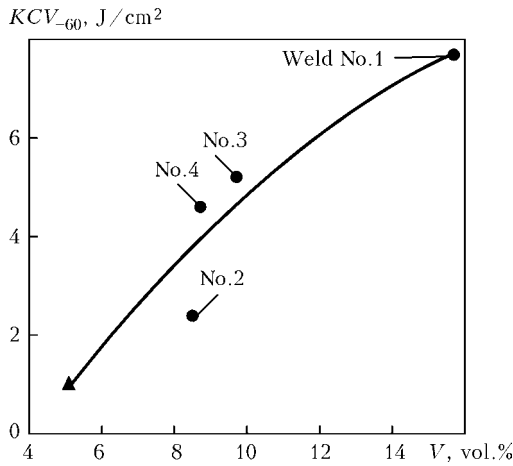


**Figure 6.** Effect of volume content  $V$  of ductile component in quasi-cleavage regions on impact toughness  $KCV_{-60}$  of welds in low-alloy steels:  $\blacktriangle$  — results obtained at a temperature of  $-196\text{ }^{\circ}\text{C}$

The studies revealed that cracks in metal of weld 1 propagated mainly in AF, a substantial content of the MAC-phase being detected on the fracture surface (Figure 8, a) ( $V_{MAC} = 3.56\%$ ), which, as noted above, was precipitated along the boundaries of ferrite lamellae. The MAC-phase was revealed and its volume content on the surface of fractured specimens was determined by the method of analysis of images of the weld fracture surfaces (Figure 9, b).

Examination of fractographs of fractures of welds 2–4 showed that fracture planes propagated both in grains with the AF structure and in grains where ferrite with OSP was formed. It can be assumed that here we have two probable mechanisms of crack propagation. In the first case the crack propagates across the grains of ferrite with OSP (Figure 10, a), the carbide phases (MAC-phase in particular) serving as efficient barriers in a way of its propagation. In the second case the crack is initiated at the carbide–ferrite interface and propagates along the boundaries of grains of ferrite with OSP (Figure 10, b). As a result, the longitudinal type of carbide particles is fixed on the fracture surface. No differences in composition of the carbide phases with longitudinal and transverse propagation of the crack in grains of ferrite with OSP were revealed.

**Results and discussion.** The results obtained allow an assumption of a probable character of the

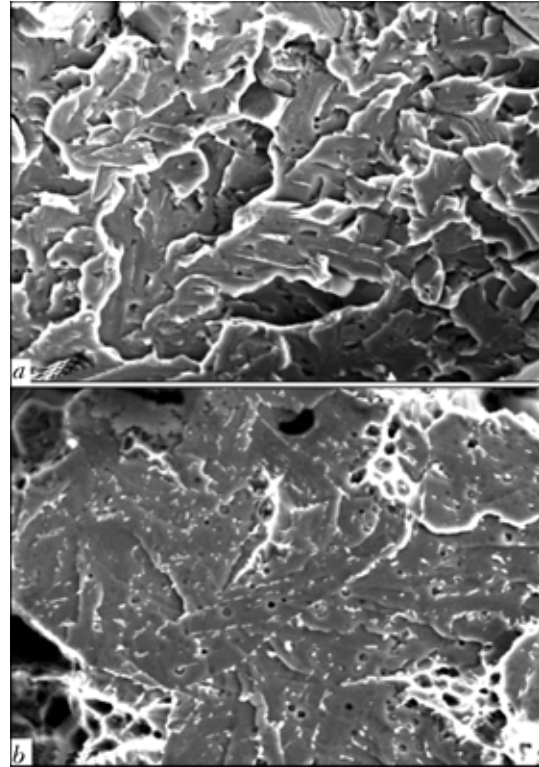


**Figure 7.** Microstructure of metal of weld No. 1 on fracture surfaces in etching in picrate (a) and nital (b) ( $\times 2000$ )

mechanism of fracture of the weld specimens. Fracture occurred by cleavage in a body of the ferrite needles in the AF grains. As there are high-angle boundaries between the needles, the cracks change their propagation directions, which leads to formation of a new fracture facet. A change in the crack propagation directions requires an additional energy to occur. Therefore, the smaller the size of the needles and the higher the space disorientation of two neighbouring needles in the AF grains, the higher the energy required for a crack to propagate and the higher the values of impact toughness [8]. A change in the crack propagation directions occurs along the boundaries of the ferrite needles to form fracture of the comb type on the surface. As shown by the studies (see Figure 3), the MAC-phase is formed mainly along the boundaries of the ferrite needles. Therefore, we may expect coincidence of the results of microanalysis of chemical composition of the MAC-phase and combs on the frac-

**Table 5.** Mechanical properties of the welds studied

Weld No.	Yield stress, MPa	Tensile strength, MPa	Elongation, %	Reduction in area, %	Impact toughness $KCV_{-60}$ , J/cm <sup>2</sup>	Impact toughness $KCV_{-173}$ , J/cm <sup>2</sup>
1	562.0–572.5	701.7–719.1	23.3–27.0	69.5–73.1	75–120	6.2–9.4
	568.5	709.1	25.0	70.8	100.6	7.7
2	520.1–520.8	637.8–638.8	26.7–27.7	71.4–73.1	39–50	2.0–3.1
	564.9	638.5	27.4	72.0	43.0	2.4
3	562.0–568.9	683.8–693.7	24.0–25.3	65.9–76.8	48–59	4.8–5.6
	564.9	688.2	24.7	66.6	52.7	5.2
4	572.4–598.5	720.3–727.3	25.7–26.7	67.8–69.7	36–46	4.3–5.0
	585.2	722.6	26.2	69.1	42.7	4.6

Note. Minimal and maximal values are given in numerator, and average values are given in denominator.

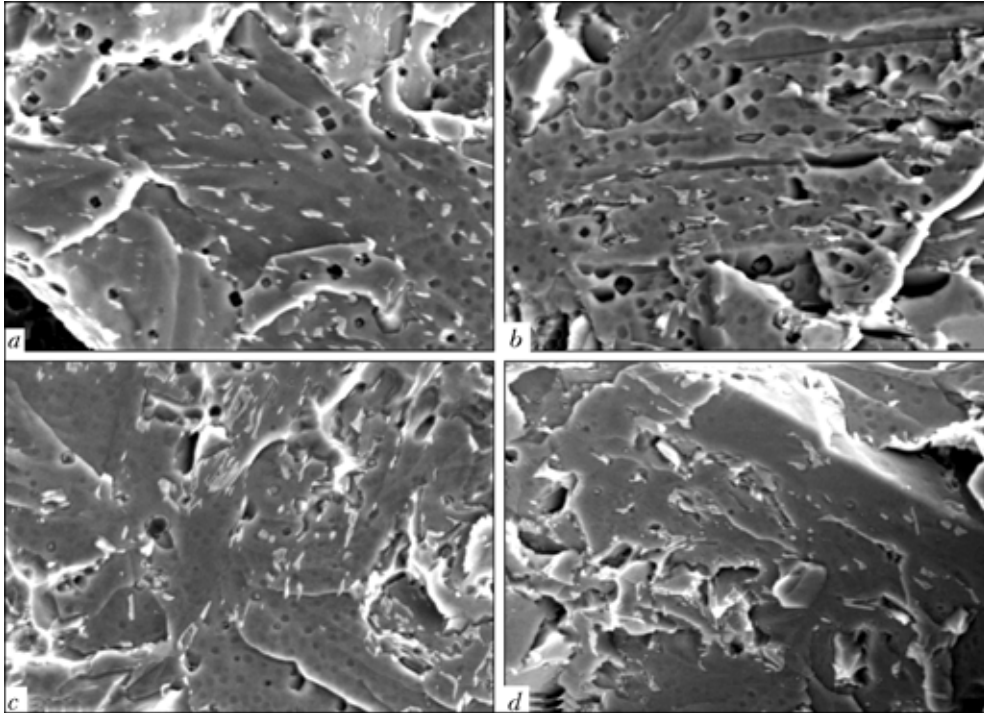


**Figure 8.** Microstructure with the MAC-phase marked out on the fracture surface of metal of the welds in low-alloy high-strength steels (a–d correspond to welds Nos. 1–4 in Table 2) ( $\times 3000$ )

ture surface. This assumption was experimentally proved (see Tables 3 and 4).

The presence of the MAC-phase at the ferrite needle boundaries and angle of disorientation of the neighbouring AF needles inhibit the quasi-cleavage fracture process [9]. Analysis of the results shows that an insignificant increase in the volume content of the MAC-phase (from 0 to 5–6 %) leads to increase in

impact toughness (Figure 11), while at a MAC-phase content of more than 6 vol.% the value of impact toughness decreases. To have a more detailed picture of the effect of the MAC-phase on impact toughness, it is necessary to study the welds with a higher volume content of the MAC-phase. To plot curves for a range of high values of the MAC-phase, we used the data given in [10] and data obtained experimentally on specimens in which the volume content of the MAC-phase was approximately 19 %.

The character of relationship between the MAC-phase and impact toughness shown in Figure 11 seems to be related to a change in the mechanism of its effect

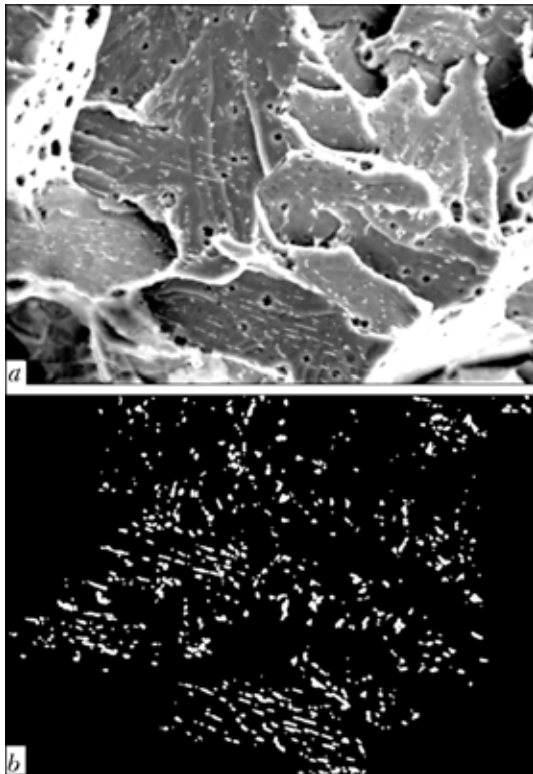


**Figure 9.** Microstructure of fracture surface of metal of weld No. 1 (a) (Table 2) and MAC-phase marked out on it (b) ( $\times 2000$ )

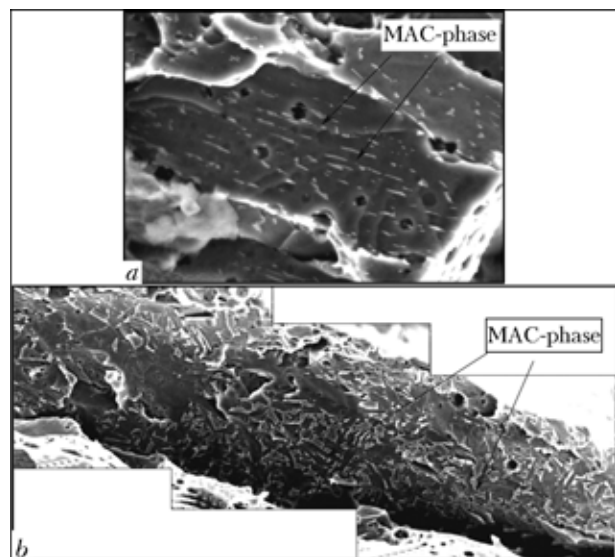


**Figure 10.** Fracture in ferrite with the ordered secondary phase: a — propagation of crack across grains of ferrite with OSP (weld No. 1 in Table 2); b — propagation of crack along grains of ferrite with OSP (weld No. 3 in Table 2) ( $\times 2300$ )

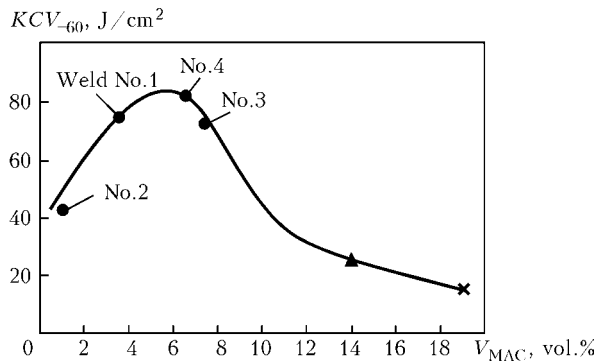


**Figure 11.** Effect of volume content of the MAC-phase in fracture on impact toughness of weld metal:  $\blacktriangle$  — according to data of [1];  $\times$  — results obtained after heat treatment of weld No.1 (heating to 730 °C and rapid water cooling)

on initiation and propagation of cracks. If the volume content of the MAC-phase is insignificant (up to 5–6 %), it plays the role of a hardening secondary phase and hampers crack propagation. At  $V_{MAC} > 5-6$  %, the MAC-phase becomes a source of crack initiation, as it contains a brittle component, i.e. martensite (and, probably, retained austenite). Therefore, increase in the volume content of the MAC-phase in metal of the studied welds to more than 5–6 % leads to decrease in impact toughness.

The change in the mechanism of the effect exerted by the MAC-phase on the fracture process depends upon its composition. Stresses at the interface between the MAC-phase and ferritic matrix are related to their composition, which is caused by their different linear thermal expansion coefficients. Composition of the MAC-phase may affect the stressed state at the interface between the phases. As a result, the process of crack formation may be either hampered or, on the contrary, further developed. Unfortunately, our studies did not prove this fact (see Tables 3 and 4), which seems to be associated with peculiarities of determination of compositions of small particles (less than 1  $\mu m$ ). This issue needs to be further investigated.

The fact of decrease in impact toughness of the weld metal with a high (more than 70 vol.%) content of AF can be explained in terms of the above results. As found in study [11], the amount of the MAC-phase grows with growth of the volume content of AF in the weld metal. Our results showed that if the volume content of the MAC-phase is in excess of a certain value (about 6 % for the welds studied), impact toughness of the weld metal decreases. Therefore, the positive effect of AF is levelled out by the negative effect of the MAC-phase. As a result, impact toughness does not only increase or remain at the same level, but also may markedly decrease (see Figure 1). It is clear that the higher the content of carbon or carbide-forming elements, the stronger this effect.

In addition to the content of the MAC-phase, the character of fracture is also affected by the topography of its distribution. According to the IIW classification [7], in a case where particles of the MAC-phase are parallel to each other and oriented along the ferrite boundaries, this structural component is classed as

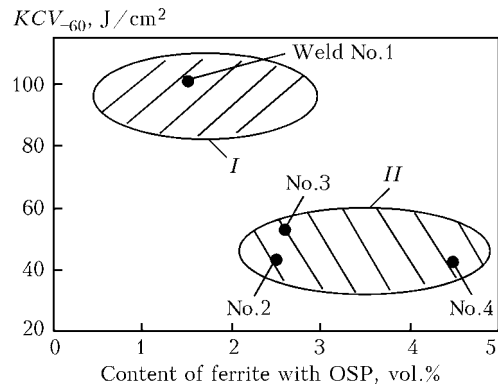


**Figure 12.** Effect of content of ferrite with OSP on impact toughness of welds: I, II — regions in which fracture occurs across grains of ferrite with OSP and in a mixed way, respectively

ferrite with OSP. It can affect impact toughness of metal of the welds in low-alloy steels [12], although authors of this study call it a bainite pack.

The presence of ferrite with OSP on the fracture surface (see Figure 10, a) allows a conclusion that this may also be a factor causing instability of low-temperature impact toughness of metal of the welds in low-alloy steels. Analysis of fractures of the welds studied suggests that in the case of high values of impact toughness the crack propagates across the grains of ferrite with OSP (Figure 12), which is characteristic of metal of weld 1. In metal of the welds with low values of impact toughness (2–4) the avalanche crack propagation is of a mixed character and occurs both across and along the boundaries of ferrite lamellae (see Figure 10, b). A different level of impact toughness in metal of welds 1 and 3 (Table 5) is attributable to a different character of crack propagation.

Upon establishing that the MAC-phase and ferrite with OSP are responsible for decrease in low-temperature brittleness of the welds in low-alloy high-strength steels, it was necessary to perform quantitative evaluation of the ability of structure of the weld metal to resist fracture at low temperature. The content of a lamellar component in fracture of the specimens determined in impact toughness tests at a temperature of occurrence of purely brittle fracture, i.e.  $-173$  °C (Table 5), was selected as such a parameter. To consider this issue, we used a microscopic approach to description of fracture, instead of the traditional macroscopic approach. The content of the ductile component was determined from fractographs of fractures. In addition to the traditional «tough» pitting fracture, it allowed also for the ductile component formed in propagation of a crack from one brittle fracture facet to the other (see Figure 5). A good correlation was found between the content of the ductile component in fracture and impact toughness of the weld metal (see Figure 6).

## CONCLUSIONS

1. The MAC-phase on the fracture surface was determined and decrease in impact toughness at low temperature was detected using the suggested procedure.



2. The procedure for marking out of the ductile component in regions of quasi-cleavage was used to establish relationship between its content and impact toughness of metal of the welds in low-alloy steels. It was found that impact toughness increased with increase in the content of the ductile component in quasi-cleavage fracture.

3. Both MAC-phase and ductile forms of ferrite, in particular ferrite with OSP, may act as a structural factor causing instability of properties (such as low-temperature impact toughness) of metal of the welds in low-alloy steels.

4. To provide a consistently high low-temperature impact toughness of the weld metal, it is required that the volume content of the MAC-phase be not in excess of 5–6 %, and that the content of ferrite with OSP be low.

1. Pokhodnya, I.K., Golovko, V.V., Denisenko, A.V. et al. (1999) Effect of oxygen on formation of acicular ferrite structure in low-alloy weld metal. *Avtomatich. Svarka*, **2**, 3–10.
2. Ito, G., Nakanishi, M. (1975) Study on Charpy impact properties of weld metals with submerged arc welding. *IIW Doc. XI-A-113–75*.

3. Svensson, L.-E., Grefott, B. (1990) Microstructure and impact toughness of C-Mn weld metals. *Welding Res. Supplement*, Dec., 454–461.
4. Evans, G.M. (1981) The effect of carbon on the microstructure and properties of C-Mn all-weld-metal deposits. *IIW Doc. II-A-546–81*.
5. Curry, D.C., Knott, J.F. (1978) Effects of microstructure on cleavage fracture stress in steel. *Metal Sci.*, **12**, 511.
6. Garland, J.G., Kirkwood, P.R. (1975) Towards improved submerged arc weld metal. *Metal Construction*, **7**, 275–283.
7. (1986) Guidelines for the classification of ferritic steel weld metal microstructural constituents using the light microscope. *Welding in the World*, **24(7/8)**, 144–148.
8. Romaniv, O.N. (1979) *Fracture toughness of structural steels*. Moscow: Metallurgiya.
9. Ohkita, S., Horii, Y. (1995) Recent development in controlling the microstructure and properties of low alloy steel weld metals. *ISIJ Int.*, **35(10)**, 1170–1182.
10. Evans, G.M. (1984) The effect of heat-treatment on the microstructure and properties of C-Mn all-weld-metal deposits. *IIW Doc. A-605–84*.
11. Grabin, V.F., Golovko, V.V., Solomijchuk, T.G. et al. (2003) Analysis of structural state of weld metal produced by using welding wires of the ferritic-pearlitic grade. *The Paton Welding J.*, **8**, 17–22.
12. Pokhodnya, I.K., Makarenko, V.D., Korsun, A.O. et al. (1986) Effect of nickel on structure and mechanical properties of weld produced by using basic electrodes. *Avtomatich. Svarka*, **2**, 1–5.

## EVALUATION OF THE INFLUENCE OF WET UNDERWATER WELDING CONDITIONS ON THE PROBABILITY OF PORE FORMATION IN THE WELD METAL

S.Yu. MAKSIMOV

E.O. Paton Electric Welding Institute, NASU, Kiev, Ukraine

A numerical method was used for evaluation of the influence of hydrostatic pressure, velocity of motion of weld pool solidification front and hydrogen concentration in the molten metal in wet underwater welding on the value of critical radius of gas nuclei. Obtained results enable establishing the regularities of the influence of underwater welding conditions on the susceptibility to pore formation.

**Keywords:** underwater welding, pores, solidification rate, hydrogen, pressure, gas nuclei

Porosity is one of the most often found defects in welds made under the water. In a number of cases, this restrains the underwater welding application. Despite the importance of the above problem, the issues of pore formation and influence of the factors, inherent in welding directly in the water, have been insufficiently studied and remain to be urgent. One of the steps in this direction is a mathematical model [1] that allows describing the physical processes, which proceed in the subsurface layer ahead of the solidification front (zone adjacent to the interphase) under the conditions of underwater welding, and enables studying the regularities of evolution of the gas bubbles formed here, and establishing the main param-

eters of the physical processes that determine further growth or collapse of the nuclei in the weld pool. The model was developed with the following assumptions:

- solidification front is a flat surface with a constant propagation rate;
- hydrogen transfer is performed only through diffusion;
- the liquid is ideal, uncompressed and quiescent over infinity in the absence of thermal convection;
- impurities dissolved in the liquid do not influence the physical parameters of the liquid medium;
- gas bubble is homogeneous, spherical.

Numerical studies conducted with these assumptions, led to the following conclusions:

- critical parameters of the gas bubble, at which the bubble growth rate is zero, are chiefly determined by the external hydrostatic pressure  $P_a$ , solidification front velocity  $v_s$ , and cavity formation time  $t_0$ . Critical

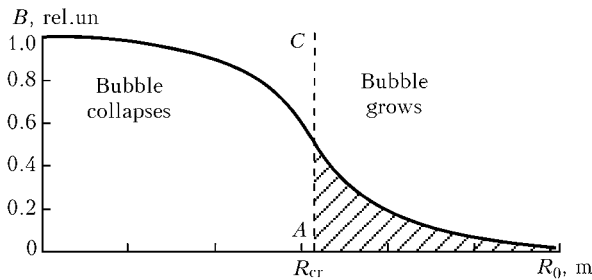


**Figure 1.** Probability *B* of gas cavity formation ahead of the liquid metal solidification front

condition is unstable: a slight disturbance of the bubble parameters leads to an inevitable growth or collapse of the cavity;

- bubble growth dynamics is determined by the moment of its initiation. The later the bubble forms, the earlier the concentration field in the subsurface layer reaches large dimensions, this eventually increasing the amount of hydrogen, diffusing into the bubble cavity, and promoting growth of the latter;

- dynamic characteristics of the gas bubble ahead of the solidification front are largely dependent on the velocity of the flat front propagation in the entire range of the possible initial radii of the gas bubble. At increase of the solidification rate, diffusion processes run faster, and critical parameters of gas bubbles shift towards the smaller dimension region.

Investigations showed that in the parameter range characterizing the underwater welding process (depth, solidification rate, hydrogen concentration) there exist certain values of gas bubble radii, at which their growth rate is zero. In the case of a slight increase of the radius (at other parameters unchanged), the diffusion balance is disturbed, and the gas bubble starts growing. On the other hand, a slight reduction of the radius leads to compression of the cavity and its subsequent disappearance. Critical radius corresponds to an unstable condition of the gas bubble.

The obtained results allows evaluation of the probability of formation of gas bubbles (cavities) in the subsurface layer (Figure 1). The schematic is a qualitative representation of an obvious regularity of the most probable formation of small-sized nuclei. However, fine cavities collapse, and larger ones, contrarily, grow. Existence of a critical radius (*AC* line) determines a region (not hatched in the Figure), the area of which is proportional to the probability of cavities developing during welding. Numerical studies enable evaluation of the nature of the influence of hydrostatic pressure, rate of propagation of the weld pool solidification front and hydrogen concentration in the liquid metal on the critical radius of gas bubble. This enables outlining the basic approaches to development of a welding technology with which the critical radius position would shift much farther to the right.

The developed model [1] was used to study the influence of the main factors, characterizing the specific features of wet underwater welding, on the critical radius of the bubble. The values of the above

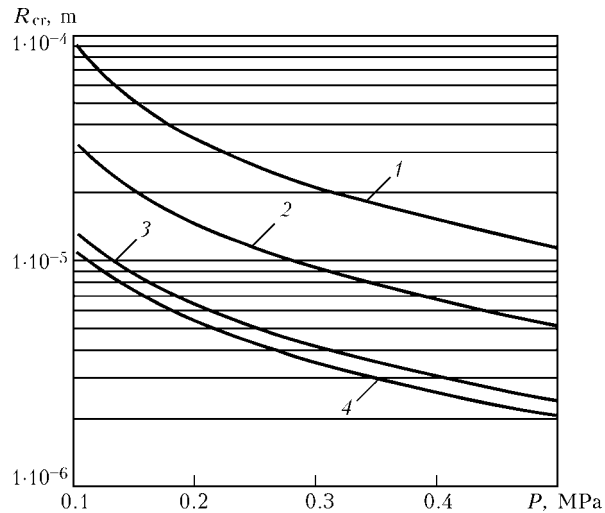
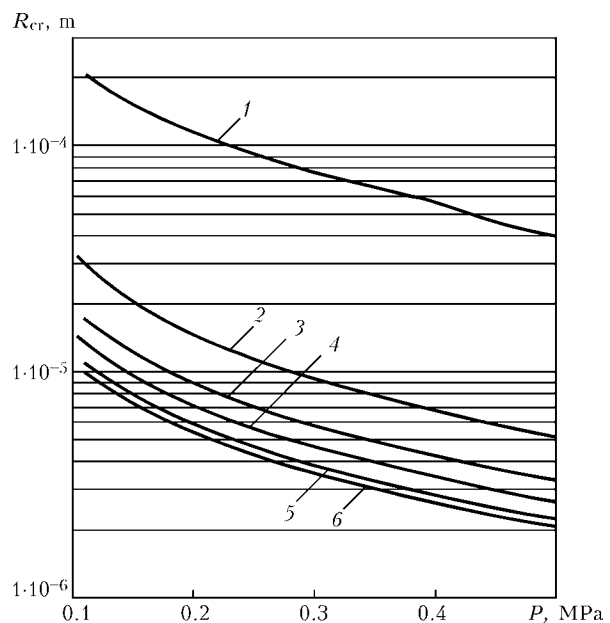


**Figure 2.** Dependence of the critical radius of gas bubble on external pressure at different rates of the solidification front: 1 —  $v_s = 0.0005$ ; 2 — 0.001; 3 — 0.002; 4 — 0.005 m/s

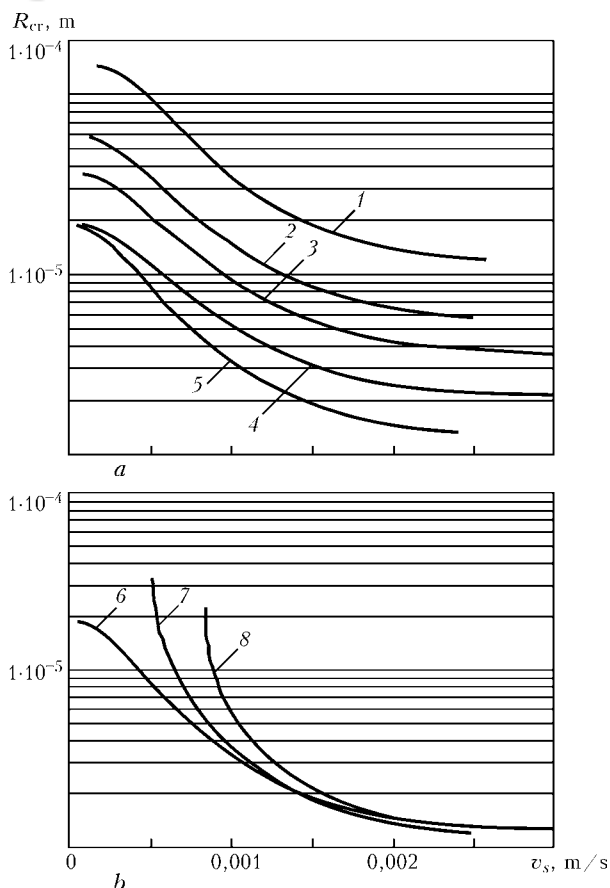
factors varied in the range characteristic for the underwater welding conditions.

Figure 2 gives a dependence of the critical radius of the bubble on the external pressure at different rates of solidification front propagation. With pressure rise, the critical parameter region shifts towards lower values, i.e. the susceptibility to pore formation increases. It should be noted that increase of the solidification rate yields a similar result.

The welding process runs for a certain time during which the subsurface layer is enriched in hydrogen up to its maximum saturation with gas, thus promoting the shifting of the critical radii to lower values (Figure 3). The following tendency should be also noted: with time each curve of critical parameters asymptotically approaches a certain position, corresponding to the moment of time, at which the saturation of the subsurface layer is already over. In keep-



**Figure 3.** Dependence of the critical radius of gas bubble on external pressure at  $v_s = 0.001$  m/s for different moments of nuclei formation: 1 —  $t_0 = 0$ ; 2 — 0.1; 3 — 0.2; 4 — 0.3; 5 — 0.5; 6 — 1.0 s



**Figure 4.** Dependence of the critical radius of gas bubble on the solidification front rate at low (a) and high (b) values of hydrostatic pressure: 1 —  $P_a = 0.1$ ; 2 — 0.2; 3 — 0.3; 4 — 0.5; 5, 6 — 1.0; 7 — 1.5; 8 — 2.0 MPa

ing with our calculations, maximum hydrogen concentration in the liquid metal ahead of the moving solidification front is reached within approximately 1 s after the start of its propagation.

Obtained dependencies of critical dimensions of the gas bubbles on the propagation rate of the solidification front (Figure 4) enable evaluation of the critical radius at variation of the external static pressure. With its increase in the region of values, where the Siverts law for gas solubility in metal is still valid, the curves of critical radii shift to the lower value

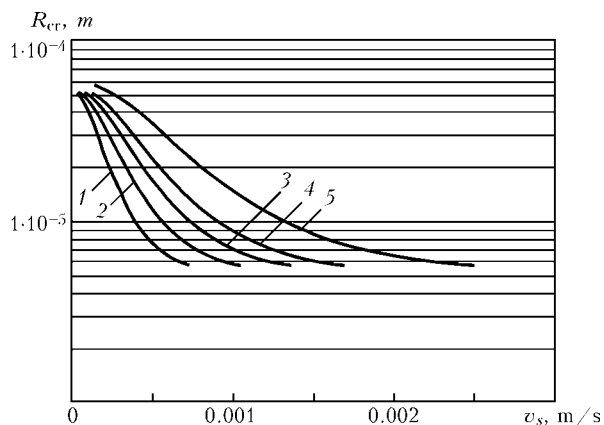


**Figure 5.** Dependence of critical radius of the gas bubble on the solidification front rate for different moments of the time of nuclei formation at  $P_a = 0.2$  MPa: 1 —  $t_0 = 1.0$ ; 2 — 0.5; 3 — 0.3; 4 — 0.2; 5 — 0.1 s

region (Figure 4, a). A certain value of the critical radius corresponds to each solidification rate. The pattern is disturbed at high values of pressure (above 1 MPa), when hydrogen solubility in the liquid phase becomes stabilized. With lowering of the solidification rate, the slope of the equilibrium curves tends to zero (Figure 4, b), and at certain values of the rate the critical points are absent at all.

Dependence of the critical radius of the cavity on the rate of the solidification front for different moments in time, but at unchanged external pressure, is shown in Figure 5. Note that at low rates the value of the critical radius is practically independent on the moment of nuclei formation. This leads to the conclusion that the low rates of solidification are less favourable for a broad range of nuclei dimensions, and, therefore, also the number of pores in the weld metal should decrease.

For any set of initial parameters there exists a quite certain critical value of the dimensions of gas bubbles, formed ahead of the solidification front. With time  $R_{cr}$  is stabilized and remains unchanged for these welding conditions ( $P_a, v_s$ ).

Figure 6 shows the obtained investigation results in the form of dependencies of the critical gas bubble radius on the solidification rate, hydrostatic pressure and hydrogen concentration in the molten metal in the range of values characteristic for underwater welding.

In the case of  $20 \text{ cm}^2/100 \text{ g}$  hydrogen content in the molten weld pool (Figure 6, a) bubbles of  $10\text{--}15 \text{ }\mu\text{m}$  radius can initiate at solidification rate above  $7 \text{ m/h}$  ( $2 \cdot 10^{-3} \text{ m/s}$ ). At slowing down of the solidification process or pressure increase, the probability of pore formation decreases, as the critical radius is increased. 1.5 times increase of hydrogen concentration (Figure 6, b) leads to approximately 2 times decrease of the critical radii of the bubbles, and the pressure effect is decreased.

Depending on the solidification rate, there exists a certain pressure level, at which the probability of pore formation drops abruptly. A section of the curve where the angle of inclination of the tangent to the abscissa axis is close to  $90^\circ$  corresponds to this condition. The above pressure rises with increase of hydrogen content. The greatest effect of the action of the above factors is found in the range of low solidification rates, and at the rate above  $7 \text{ m/h}$  their influence is practically neutralized.

The above conclusions correlate well with the results of investigation of the nature of porosity in wet welding [2]. Study of the fracture of specimens, welded by the rutile and ilmenite electrodes, showed the presence of micropores of  $10\text{--}50 \text{ }\mu\text{m}$  and absence of macropores. At decrease of hydrogen content a great number of pores of more than  $0.5 \text{ mm}$  diameter were additionally found.

Increase of the rate of propagation of the solidification front leads to shifting of the critical parameters of gas bubbles into the region of smaller dimensions,



i.e. at low welding speeds the range of dimensions of nuclei, which grow with time and lead to porosity at weld solidification, becomes smaller.

However, in all the cases with longer of time before the bubble initiation, the range of the dimensions of cavities, where the evolution ends up by pore formation, becomes wider. Critical radii of the bubbles asymptotically tend to values, corresponding to the moment of time, at which hydrogen concentration in the liquid metal is stabilized in a region close to the solidification front.

Allowing for the experimental dependencies of hydrogen solubility in the liquid metal with increase of the external pressure leads to a complex dependence of the critical radius on the pressure, at which welding proceeds. At shallow depths pressure rise promotes shifting of the critical radius into the region of small dimensions of the gas bubbles. At great depths, which are characterized by increase of gas solubility in the metal, a reverse tendency has been noted: pressure rise results in an increase of the critical radius, the further evolution of which leads to pore formation.

As under the actual conditions, only two parameters can be regulated (solidification rate and hydrogen concentration), porosity can only be reduced by decreasing their values. One of the efficient methods to implement such an approach can be stirring of the weld pool molten metal. The action is produced on both the factors simultaneously. On the one hand, stirring promotes degassing of the weld pool, and on the other — equalizing of the molten metal temperature over the entire volume, thus causing a lowering of the solidification rate. In practice, when underwa-

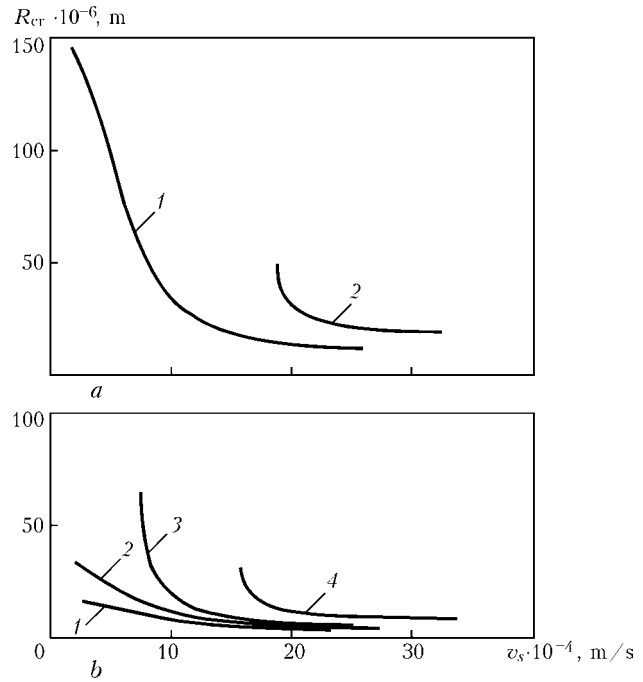


**Figure 6.** Influence of pressure on the critical radius on the gas bubble at hydrogen concentrations of 20 (a) and 30 (b)  $\text{cm}^3/100 \text{ g}$ : 1 —  $P_a = 0.1$ ; 2 — 0.2; 3 — 0.3; 4 — 0.5 MPa

ter welding is performed, this can be achieved using an external electromagnetic action, or applying transverse oscillations of the electrode end or welding head.

1. Maksimov, S.Yu., Gurzhy, A.A. (2004) Modeling the conditions of pore initiation in the weld metal in wet underwater welding. *The Paton Welding J.*, 7, 7-11.
2. Shiming, L., Guorong, W., Yonglun, S. et al. (1987) A study of microporosity in underwater wet welding. *IIW Doc. CREAU 96-87*.



# PORE FORMATION IN WELD METAL IN SUBMERGED ARC WELDING WITH SURFACE SATURATION OF GRAINS WITH FLUORINE

V.G. KUZMENKO<sup>1</sup> and V.I. GUZEJ<sup>2</sup>

<sup>1</sup>E.O. Paton Electric Welding Institute, NASU, Kiev, Ukraine

<sup>2</sup>City State Administration, Kiev, Ukraine

Properties were studied of fused welding fluxes of manganese-silicate type, not containing fluorine and subjected to fluorinating heat treatment together with ammonia salt of hydrofluoric acid ( $\text{NH}_4\text{F}$ ) and magnesium hexafluosilicate ( $\text{MgSiF}_6$ ). It is established that the weld metal resistance to pore formation is achieved, when using 0.5 % each of the above salts for flux treatment. Fluorine content in the flux is equivalent to adding 0.4 %  $\text{CaF}_2$  to it. The effect is achieved due to local arrangement of fluorine on the flux grain surface.

**Keywords:** arc welding, fluxes, gas shielding, porosity, fluorinating heat treatment, nitrogen dissolution

Porosity in the weld metal appears because of excessive solubility of mainly nitrogen and hydrogen from the ambient gas atmosphere in the molten metal and release of these gases during cooling down and solidification of the weld metal [1, 2]. It is possible to prevent porosity in submerged arc welding by regulating a set of physical phenomena including slag and gas shielding of the weld pool.

Slag shielding of the weld pool is based on the commonly accepted idea on existence of the air-tight shell around arc. However, this shield solely is not enough. In [3] it is shown that a continuity of the slag shell is destroyed in the zone of the pre-arc front of the parent metal melting due to a fast shift of the liquid slag under the action of high-velocity gas-plasma flows of the arc towards the rear area of the weld pool. As a result the efficiency of the slag shield-

ing of the molten metal decreases while that of the gas shielding grows.

Introduction of  $\text{CaF}_2$  into the flux composition produces the best results for decrease of a level of gas solubility and restriction of the weld metal porosity under electric arc welding. Hence, addition of 3–5 wt.% of this salt into the manganese-silicate flux decreases nitrogen concentration in the weld metal 2–3 times [4], thus increasing its resistance against pore formation. Initially it was considered that introduction of fluorides into flux increased the efficiency of shielding from the air due to a decrease of the slag viscosity and, thus faster formation of the slag «shelter» on the surface of the weld pool. A specific role of the gaseous silicon tetrafluoride  $\text{SiF}_4$  formed under interaction of  $\text{CaF}_2$  and  $\text{SiO}_2$  contained in fluxes is established in [5]. Peculiarities of this reaction directly between these components as well as in composition of the welding fluxes are considered in [6–8]. Even under normal temperature this gas creates pressure of about 400 kPa (40 atm) [9] rather quickly expelling the air from the arc zone.

Calcium fluoride performs a double function in the welding fluxes. On the one hand, it affects such physical-chemical properties of fluxes as melting temperature, viscosity, solid-liquid interfacial tension, electrical conductivity, activity of the components exerting through them a metallurgical influence on the metal. On the other hand, it provides a gas shielding due to formation of  $\text{SiF}_4$ . It is noteworthy that the necessary physical-chemical properties are provided by a uniform distribution of the components in the volume of the welding fluxes while  $\text{SiF}_4$  is formed on the surface of the flux grains. A surface nature of  $\text{SiF}_4$  isolation is confirmed by the data from [8] where the method of flows was used to study a formation intensity of this gas as a function of temperature. Fluxes were heated from 400 °C up to melting temperature. The quantity of this gas monotonously grew with heating with a considerable increase right before melting and a sharp decrease after flux was melted. A surface nature of  $\text{SiF}_4$  formation is also confirmed by the fact that this gas is released in a greater quantity

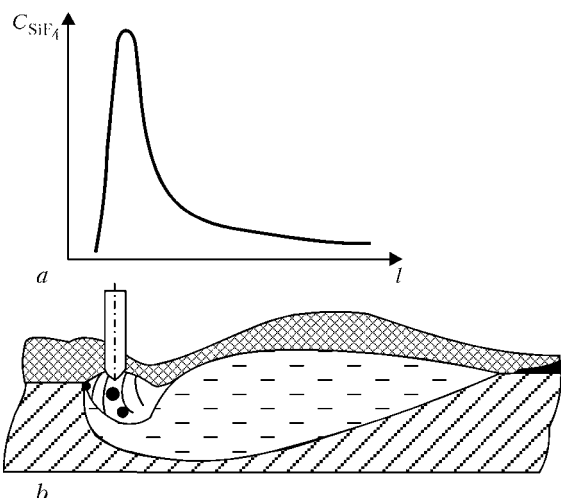


**Figure 1.** Intensity of  $\text{SiF}_4$  release (a) from different parts of the flux charge in the specific zones of the weld pool (b) [6]:  $l$  — length of the weld pool



from pumice-like fluxes than from glass fluxes. The pumice-like fluxes also provide a higher weld metal resistance against pore formation in welding.

Comparison of the SiF<sub>4</sub> release from the parts of flux charge in specific zones of the weld pool (Figure 1) shows that its maximal quantities will form in the pre-arc zone on the upper front of the metal melting, i.e just where there is a break of the slag shell continuity in the weld pool. Considering that penetration of the air into the weld pool is most probable specifically in this zone it seems appropriate to intensify the process of SiF<sub>4</sub> formation on the surface of flux grain. A current technology, which provides a uniform distribution of fluorine in the volume of flux grain, does not allow a local increase of its surface concentration.

Previously we studied the fluorinating treatment of fluxes for its effect on the change in the nature of their hydration [10]. Formation of the fluoride barrier on the flux grain surface essentially decreases the flux tendency to moisture absorption. One can assume that an increased content of fluorides in the surface layer of the flux grain can also influence the pore formation in the weld metal during welding.

A layer enriched with fluorine and depleted with oxygen forms on the surface of the flux grains during heat treatment with gaseous hydrogen fluoride. Evidently, such treatment of fluxes containing silica creates conditions for its more intense interaction with fluorides, so that gaseous silicon tetrafluoride forms more rapidly. We experimentally studied the fluorinating heat treatment of fluxes for its effect on resistance of the weld metal against pore formation resulted from corrosion. For this purpose a fluorine-free flux of the manganese-silicate type approaching in its composition the standard flux of AN-60 grade was fused in the electric flux furnace. This flux was then exposed to fluorinating heat treatment in the closed container together with 1.5, 3.0 and 4.5 wt.% of ammonium fluoride NH<sub>4</sub>F at the temperature 500 °C for 39 min. Chemical composition of fluorine-free flux and the fluxes received after fluorinating heat treatment is shown in Table 1.

Analogous control fluxes with the fluorine content different from that of the fluorinated fluxes and approaching it were produced by the conventional technology introducing CaF<sub>2</sub> into the molten charge. Chemical composition of these fluxes is shown in Table 2.

Fluorinated and control fluxes were used for deposition on the St3 steel plate 16 mm thick with grooves filled with the measured quantity of the air-dry rust [4]. A mass of rust per 100 mm when pores were formed in the deposited metal was assumed as the porosity threshold. Deposition was made with wire Sv-08A 4 mm in diameter under the following condition: welding AC  $I_w = 750\text{--}800$  A; arc voltage  $U_a = 37\text{--}40$  V; welding speed  $v_w = 25$  m/h.

The experimental results are shown in Figure 2. Fluorine was introduced through the gas phase by fluorinating treatment into the fluxes designated with curve 1 and by the conventional technology (by introduction to the charge) into the fluxes designated with curve 2. The quantity of rust when pores ap-

**Table 1.** Chemical composition (wt.%) of fluorine-free flux and the fluxes received after application of the fluorinating heat treatment

Weight fraction of NH <sub>4</sub> F in flux, %	SiO <sub>2</sub>	CaF <sub>2</sub>	CaO	MnO	Al <sub>2</sub> O <sub>3</sub>	Fe <sub>2</sub> O <sub>3</sub>	S	P
0 (AN-60)	46.2	--	9.4	37.2	4.0	0.02	0.03	0.02
1.5	46.1	1.3	7.7	37.3	4.2	0.02	0.03	0.02
3.0	45.4	2.7	6.5	37.4	4.1	0.02	0.03	0.02
4.0	45.8	3.8	6.2	36.8	3.9	0.02	0.03	0.02

**Table 2.** Chemical composition (wt.%) of fluxes of manganese-silicate type with different content of CaF<sub>2</sub>

Weight fraction of CaF <sub>2</sub> in flux, %	SiO <sub>2</sub>	CaF <sub>2</sub>	CaO	MnO	Al <sub>2</sub> O <sub>3</sub>	Fe <sub>2</sub> O <sub>3</sub>	S	P
2.0	46.2	1.4	9.8	38.7	4.3	0.04	0.02	0.03
3.0	45.9	2.3	9.9	38.3	4.3	0.03	0.03	0.02
4.5	45.7	3.9	10.3	38.4	4.2	0.03	0.03	0.02
6.0	45.5	5.0	9.8	38.2	4.3	0.03	0.02	0.04

peared in the weld metal was 3–5 times higher for fluorinated fluxes than for fluxes produced conventionally. Most likely such high indices are specified by a more intensive formation of silicon tetrafluoride because the corresponding reagents are present on the surface of the flux grains. Using the fluorination method we produced a series of manganese-silicate fluxes with a lower fluorine content to obtain the balanced indices for the weld metal resistance against porosity and for the quantity of the formed gaseous fluorides. Chemical composition of fluorine-free and fluorinated fluxes produced with introduction of a smaller NH<sub>4</sub>F quantity is presented in Table 3.

The method of flow with titrimetric ending was used to determine the weight fraction of SiF<sub>4</sub> isolated

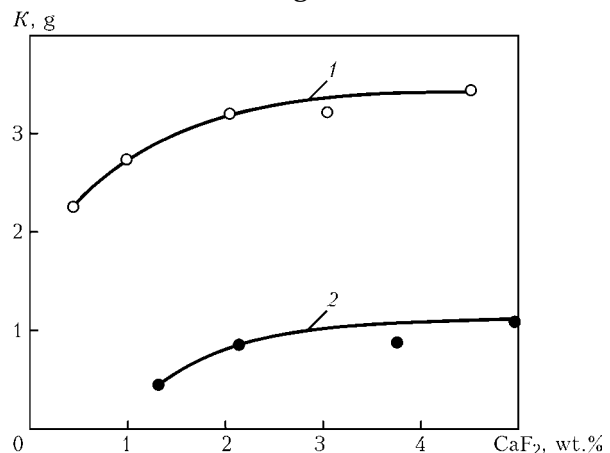


**Figure 2.** Tendency of the weld metal to pore formation during welding using fused flux produced by different technologies depending on the content of CaF<sub>2</sub> in their composition: 1 — surface-fluorinated fluxes (see Table 1); 2 — fluxes produced by fusion of all components in the electric furnace (see Table 2); K — mass of rust per 100 mm of the weld length



**Table 3.** Chemical composition (wt.%) of initial and fluorinated fluxes obtained as a result of heat treatment with a limited weight fraction of  $\text{NH}_4\text{F}$

Weight fraction of $\text{NH}_4\text{F}$ in flux, %	$\text{SiO}_2$	$\text{MnO}$	$\text{CaF}_2$	$\text{CaO}$	$\text{Fe}_2\text{O}_3$
0 (AN-60)	45.3	36.5	--	8.9	0.28
0.4	45.1	36.9	0.22	7.9	0.26
0.6	45.0	36.7	0.48	8.2	0.23
1.0	44.8	37.2	0.84	7.7	0.22
1.5	44.3	36.9	1.28	7.9	0.32

from the fluorinated fluxes (Table 3) and from the standard flux AN-60 under heating within the temperature range 600–900 °C. The results presented in Figure 3 show that more  $\text{SiF}_4$  was released from fluxes after fluorinating treatment (surface-fluorinated (SF) fluxes) with 0.5 %  $\text{NH}_4\text{F}$  than from the standard ones. Hence, it is quite possible to produce fluxes with essentially lower content of fluorine arranged on the flux grain surface providing resistance of weld metal against porosity on par with the standard flux AN-60. To verify this assumption the resistance of weld metal against rust porosity in welding with fluorinated fluxes was studied by the above-described method. These fluxes were produced by heating the pumice-like fluorine-free manganese-silicate flux with 0.1, 0.2, 0.4, 0.6 and 1.0 wt.% of  $\text{NH}_4\text{F}$ . Welding speed was 30, 34.5 and 40 m/h. The standard flux AN-60 was used to conduct control tests. The results of the experiment are shown in Figure 4. With all used variants of changing  $\text{NH}_4\text{F}$  content above 0.48 wt.% in the mixture under fluorinating treatment and with all welding speeds the fluorinated fluxes displayed higher resistance of weld metal against rust porosity than the standard flux AN-60. This index increases with the weight fraction of  $\text{NH}_4\text{F}$  in the mixture.

Gaseous  $\text{SiF}_4$  may also be used as a fluorinating reagent in addition to HF (a product of thermal decomposition of  $\text{NH}_4\text{F}$ ). In this case magnesium hexafluosilicate  $\text{MgSiF}_6$  may be the source of this gas. Fluorine-free flux of AN-60 type (see Table 3) was treated by the previously employed technique in the mixture with  $\text{MgSiF}_6$  at the temperature 500 °C. Weight fraction of salt in the mixture with the flux

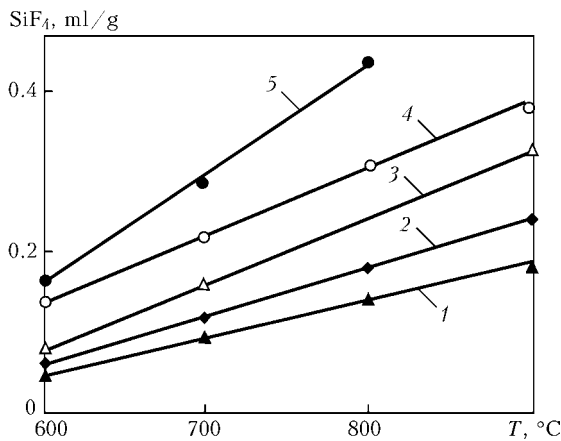


**Figure 3.** Effect of temperature on intensity of the  $\text{SiF}_4$  release from fluxes with different content of  $\text{CaF}_2$ , wt.%. 1 — 0.22 (SF); 2 — 5.70 (AN-60); 3 — 0.84 (SF); 4 — 0.84 (SF); 5 — 1.28 (SF)

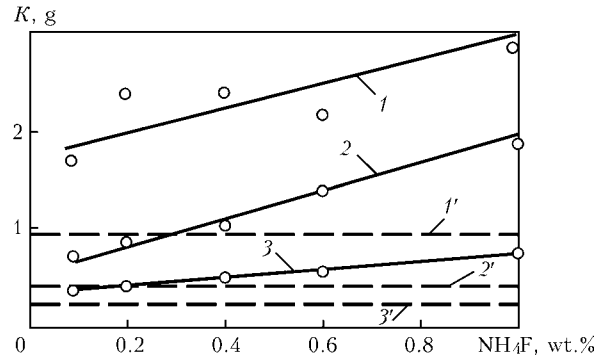


**Figure 4.** Tendency of the weld metal to formation of porosity in welding at different speeds using SF fluxes (see Table 3) depends on the content of  $\text{NH}_4\text{F}$  used for their fluorinating treatment: 1, 1' —  $v_w = 30$ ; 2, 2' — 34.5; 3, 3' — 40 m/h; 1–3 — SF; 1'–3' — AN-60 flux

in terms of  $\text{SiF}_4$  was 0.25, 0.50, 0.75, and 1.00 %. Such fluxes were used to determine the resistance of weld metal against rust porosity by the previously described method. Conditions of the experiment and the used materials were similar to those employed earlier (except  $v_w = 21.5$  m/h). The results of the experiment are shown in Figure 5. Indices of weld metal resistance against rust porosity equal to those for flux AN-60 are obtained by using the test flux treated with 0.4 wt.%  $\text{SiF}_4$ . Further increase of the reagent content under fluorinating treatment did not lead to essential increase of the weld metal resistance against pore formation.

Increase of the  $\text{SiF}_4$  formation intensity under welding heating of fluorinated fluxes should facilitate a more ample use of fluorine in welding. Deposition with test fluxes obtained by treatment with 0.4, 0.5, 1.0 and 1.5 wt.%  $\text{NH}_4\text{F}$  and standard flux AN-60 was performed for estimation of the value of this index. Then the fluorine content was determined in the initial flux and in the slag crust.

These data are presented in Table 4 and in Figure 6. They suggest that the efficiency of using fluorine of SF fluxes essentially exceeds this index in the standard fluxes.

Therefore, fluorinating treatment of fluxes results in a considerable increase of the weld metal resistance against porosity in welding. However, this effect is achieved under fluorine content being 10 times lower than that provided by conventionally produced fluxes.

The use of ammonium salts of hydrofluoric acid as an HF-forming reagent under fluorinating heat treatment of the welding fluxes may lead to an in-

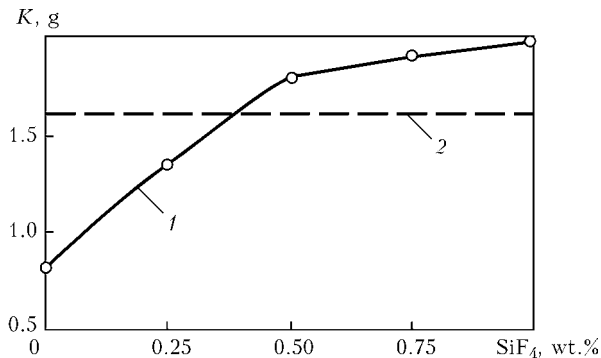


**Figure 5.** Dependence of weld metal resistance against pore formation in welding using SF fluxes on the content of  $\text{SiF}_4$  produced under thermal decomposition of  $\text{MgSiF}_6$  in the mixture with fluorine-free flux: 1 — SF; 2 — AN-60 flux



**Table 4.** Efficiency of using fluorine in the fluxes in welding

Weight fraction of $NH_4F$ in flux, %	Weight fraction of $CaF_2$ , %		$\Delta F^-$ , %	$\Delta F^- / F^-$ , %	Threshold of pore formation
	In flux	In slag crust			
0 (AN-60)	5.70	4.84	0.43	15.1	0.4
0.4	0.22	0.10	0.06	54.4	1.0
0.6	0.48	0.17	0.16	66.6	1.3
1.0	0.84	0.28	0.29	69.0	1.8
1.5	1.28	0.32	0.46	71.8	2.4

Note.  $\Delta F^-$  — weight fraction of released fluorine;  $F^-$  — total weight fraction of fluorine in flux.

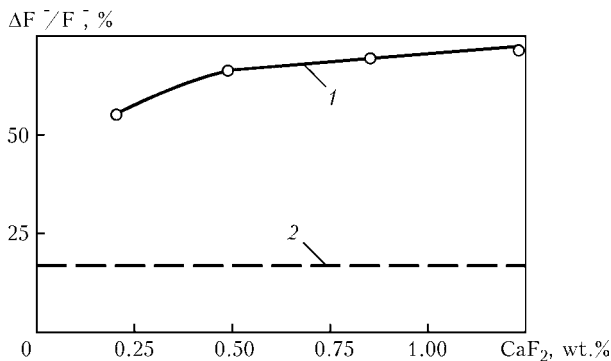


**Figure 6.** Efficiency of the use of fluorine in welding with SF (1) and AN-60 (2) flux

crease of the nitrogen content in their composition due to thermal decomposition of ammonia. This in its turn may foster transition of nitrogen from the flux into weld metal in the course of welding. Figure 7 shows the results of determination of the nitrogen content in the standard flux AN-60 and fluxes of SF types produced by fluorinating technology by introduction of ammonium fluoride into the flux mixture in the range of 0 up to 1.5 % and subsequent heat treatment. As it is seen from the Figure, the content of nitrogen in the flux inconsiderably increases with ammonium fluoride in comparison with the standard flux AN-60 and amounts to 0.011–0.016 wt.%. Nonetheless, we carried out a final verification by control welding and determination of the nitrogen content in the weld metal. The air nitrogen was also studied in these experiments for its effect on metal saturation with nitrogen in the course of welding when fluxes with different bulk weight were used. The results of the experiments are shown in Figure 8. They prove that the nitrogen dissolution in the weld metal caused by fluxes treated with ammonium fluorides is small and less essential than its nitration by the air nitrogen.

**CONCLUSIONS**

1. The absence of a reliable slag «shelter» of the weld pool in submerged arc welding requires strengthening of gas shielding for the weld metal with the aim of preventing pore formation.
2. Increase of the fluorine content in the surface layer of grains of manganese-silicate fluxes to the level when its total content is within 0.5–1.5 % in terms of  $CaF_2$  facilitates  $SiF_4$  formation under heating in welding.
3. High-silica, fluorine-free and pumice-like fluxes exposed to fluorinating heat treatment at 500 °C in the mixture with 0.5 wt.%  $NH_4F$  or with the same quantity

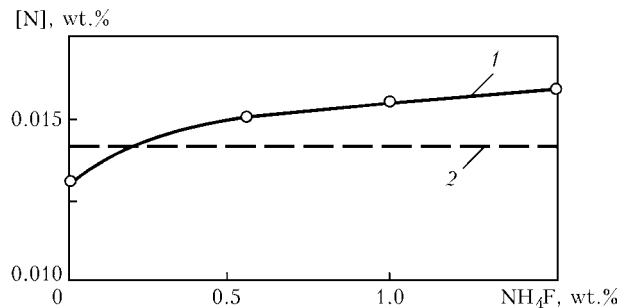


**Figure 7.** Nitrogen content in SF fluxes as a function of ammonium fluoride content (1, 2 — see Figure 6)

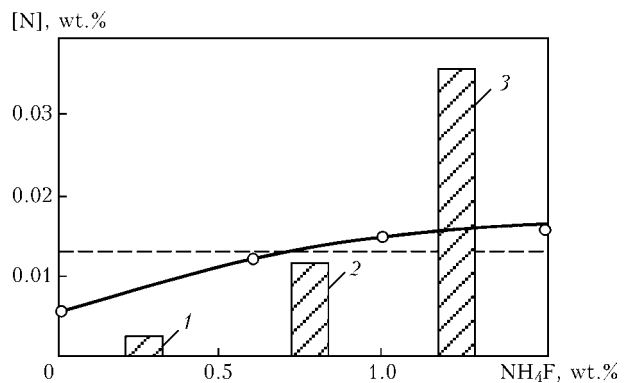


**Figure 8.** Dependence of the nitrogen content in the weld metal produced by using SF fluxes with bulk weight 1.3 (1), 1.0 (2), 0.7 (3) kg/dm³ on the content of  $NH_4F$ : solid curve — SF; dashed — AN-60 flux

of  $MgSiF_6$  are on par with standard flux AN-60 resistant against formation of rust porosity in welding.

1. Podgaetsky, V.V., Lyuborets, I.I. (1984) *Welding fluxes*. Kiev: Tekhnika.
2. Pokhodnya, I.K. (1972) *Gases in welds*. Moscow: Mashinostroenie.
3. Kuzmenko, V.G. (1998) About continuity of slag envelope in submerged arc welding. *Avtomatich. Svarka*, **3**, 14–19.
4. Lyubavsky, K.V. (1948) Metallurgy of automatic submerged arc welding of low-carbon steel. In: *Problems of theory of welding processes*. Moscow: Mashgiz.
5. Podgaetsky, V.V. (1953) Reactions in arc atmosphere in submerged arc welding. *Avtomatich. Svarka*, **1**, 10–12.
6. Podgaetsky, V.V., Novikova, T.P. (1960) About emission of silicon fluoride in heating of flux during welding and drying. *Ibid.*, **6**, 19–22.
7. Bratland, D., Fekri, A. et al. (1970) Vapour pressure of silicon tetrafluoride above mixtures of fluorides and silica. *Acta Chemica Scandinavica*, **24**, 846–870.
8. Kuzmenko, V.G. (1980) Peculiarities of reaction in mixtures of calcium fluoride and silica. *Avtomatich. Svarka*, **4**, 33–35.
9. Ryss, I.G. (1956) *Chemistry of fluorine and its inorganic compounds*. Moscow: Goskhimizdat.
10. Kuzmenko, V.G., Guzej, V.I. (2004) Hydration of fluxes with a locally-changed chemical composition of grains. *The Paton Welding J.*, **6**, 41–43.



# INFLUENCE OF THE DIMENSIONS OF A SPECIMEN OF ALUMINIUM ALLOY WELDED JOINT ON THE RESIDUAL STRESSED STATE AND FATIGUE RESISTANCE

V.A. SHONIN, O.I. GUSHCHA, V.S. MASHIN, V.S. KOVALCHUK and A.Z. KUZMENKO

E.O. Paton Electric Welding Institute, NASU, Kiev, Ukraine

The paper presents the results of evaluation of residual stresses in butt welded joints of aluminium alloy AD33 (6061) 6 mm thick on specimens of different width (70–600 mm) produced by TIG and MIG welding processes. Experiments are used to demonstrate the influence of longitudinal and transverse tensile residual stresses on the strength and fatigue life of welded joints with a transverse weld under axial load.

**Keywords:** *aluminium alloys, butt welded joints, fatigue resistance, strength, fatigue life, residual welding stresses, stress concentration, specimen dimensions*

Design fatigue resistance values of welded joints are determined mostly using the data of testing for axial cyclic load of one-type large-sized or laboratory specimens, in which the factors inherent in welded structures are taken into account to an utmost degree [1–9]. In a number of cases, also narrow samples are used (welded separately, or cut out of a large blank), which in the general form reproduce the shape and structural condition of the joints, typical for the used welding processes and modes. However, a certain degree of ambiguity is still present in selection of the dimensions of specimens for fatigue testing in terms of allowing for their residual stressed state.

**Problem analysis.** Presence of residual stresses in metal structures is the consequence [10–16] of a non-uniform thermal impact under the conditions of fusion welding. Residual stresses develop as a result of a longitudinal and transverse shortening of the metal at its cooling following the plastic thermal compression in the HAZ and weld shrinkage. The level of longitudinal and transverse residual stresses rises with reduction of the dimensions of an active temperature field relative to the length, width and thickness of the plates being welded [15, 16]. Therefore, the nature of distribution of the residual welding stresses depends not only on the dimensions of the parts being joined, but also on the welding process. Fatigue resistance is influenced by the surface residual stresses in the zone of the geometrical stress raiser, the nature of distribution of which is determined by the longitudinal and transverse components.

For welded joints of aluminium alloys it was earlier [5, 17–19] experimentally established that in combination with the geometrical stress raiser, the highest damaging action is produced by the residual stresses of the direction which coincides with the external loading stresses. Fatigue life of transverse joints with untreated welds is markedly reduced at increase of the level of tensile residual stresses, which are trans-

verse relatively to the weld. Their action is similar to the static component of cyclic stresses, which results in an increase of the effective coefficient of cycle asymmetry in the stress raiser zone [3].

In wide welded samples with continuous welds the high transverse tensile residual stresses (in the middle part of the specimen) are induced at higher heat input and low welding speed (for instance, manual TIG welding). They are balanced within the entire width of the plate in the longitudinal section of the weld. The level of these transverse residual stresses in the HAZ is up to the maximum value at plate size of more than  $500 \times 500$  mm [10, 13, 14]. Such conditions of development of high transverse tensile residual stresses are characteristic also for the case of making short welds, in which the length is much smaller than the plate width (for instance, welding of small-sized parts to the main element).

High level of transverse tensile residual stresses in the subsurface layers of the HAZ metal also develops when making multilayer welds (more than four passes) in thick-walled structural elements [5, 11]. However, in this case the residual stresses are equalized within the metal thickness and are little dependent on the width and length of the plates being welded.

With all the variants of fusion welding the longitudinal tensile residual stresses, balanced in the transverse section of the joint, have higher values than the transverse tensile residual stresses. They do not detract from the joint fatigue life with an unremoved weld convexity at cyclic load application along the weld, due to the minimum concentration of stresses in this direction. Damaging influence of the longitudinal tensile residual stresses is maximum in the joints with crossing welds [1], when the longitudinal weld was the last one to be made, which results in development of tensile residual stresses across the previous weld. Such cases are not typical for the welded structures. The role of the longitudinal component of the tensile residual stresses under the action of external stresses applied across the weld has not been completely clarified.



Incomplete data on the nature of distribution of the transverse and longitudinal residual stresses in specimens tested for fatigue and the actual structures, as well as ambiguous interpretation of experimental data on their influence on the fatigue life, have become reflected in the norms of steel structure strength analysis [7, 9]. These norms do not precisely specify the direction of the longitudinal and transverse components of the tensile residual stresses relative to the external loading stresses. Such a simplified approach based on the maximum damaging influence of the tensile residual stresses, is proposed for application also during development of the norms of aluminium structure design [20]. In this case, the possibilities of improvement of welded structure design by inducing in them a more favourable combination of residual stresses with external load stresses [15] are not taken into account. Application of highly-efficient processes of continuous welding, which lead to a considerable narrowing of the HAZ, is the main condition for a significant lowering of the transverse tensile residual stresses in the aluminium structure joints [6].

This created the need for assessment of the influence of the actual residual stresses, caused by a change of welded joint dimensions and the welding process, under the condition that the longitudinal component is much larger than the transverse component of the residual stress. This is required to establish such dimensions of specimens of aluminium alloy welded joints, made by high-efficient fusion welding processes, that would be sufficient for fatigue testing, and getting a reply to the question of the rationality of taking additional measures to induce transverse tensile residual stresses in the welded joint.

The purpose of this study was evaluation of the influence of a welded specimen dimensions on the fatigue resistance of butt welded joints of aluminium alloys in its interrelation with the transverse and longitudinal components of the tensile residual stresses for the case of application of high-efficient TIG and MIG welding processes.

**Materials and methods of investigation.** Investigations were performed on specimens of butt joints of AD33 T1 alloy (6061 T6) 6 mm thick. The appearance of the specimen for fatigue testing and its dimensions are shown in Figure 1. The specimen blanks were welded separately across the rolling direction without edge preparation in one pass in the downhand position. Specimens 200 and 500 mm wide were welded one blank at a time, and specimens 70 mm

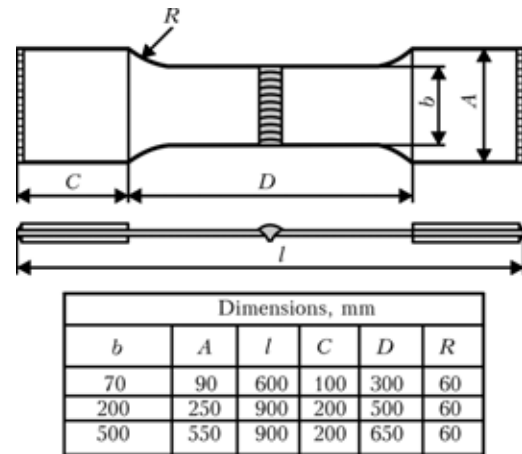


Figure 1. Welded specimens for fatigue testing

wide were welded as a packet of 3 to 6 blanks taking the weld start and finish sections to the run-on and run-off tabs. Two automatic welding processes were used, namely consumable electrode (MIG) in a mixture of inert gases (Ar + He) and nonconsumable electrode (TIG) in argon. The joints were made using 1.6 mm welding wire of alloys SvAMg5 and SvAK5.

MIG welding was performed with backward inclined electrode at an angle of 80° to the weld axis. Edge preparation for welding met the requirements of NFA 87010 standard. A steel backing was used to form the convexity on the reverse side of the weld (in keeping with the recommendations of NFA 89220 standard). Weld quality was not lower than that of the second class. MIG welding was performed using a DC power source VDU-506 (rated welding current of 500 A), pulsed current converter OI-122 and welding machine A-1431.

TIG welding was conducted using I-126 power source with automatic welding machine AS-TV-2M and 6 mm diameter tungsten electrode.

Welding modes are given in Table 1.

Residual longitudinal  $\sigma_{res}^x$  and transverse  $\sigma_{res}^y$  stresses in specimens of medium thickness were determined using a nondestructive acoustic measurement method, based on measurement of the velocity of ultrasound propagation in the metal, depending on its loading condition [14, 21]. Measurements were conducted using a portable device, developed at the E.O. Paton Electric Welding Institute. The error of the measured stress level was not higher than 10 % of the base metal yield point. Measurement base of the longitudinal and transverse residual stresses was determined by the transducer dimensions (7 × 7 mm),

Table 1. Welding modes

Welding process	Wire type	Welding current $I_w$ , A	Arc voltage $U_a$ , V	Wire feed rate $v_f$ , m/h	Welding speed $v_w$ , m/h	Gas flow rate, l/min	
						Ar	He
MIG	SvAMg5	300–320	24–25	350–360	38	20	20
	SvAK5	300–320	24–25	350–360	38	20	20
TIG	SvAMg5	430–440	10–11	85	8	20	--
	SvAK5	430–440	10–11	85	8	20	--



which was a square-shaped acoustic transducer. Values of residual stresses were measured in sections parallel to the weld axis, that ran through the HAZ and normal to the weld in the specimen central part. To bring the transducer as close as possible to the fusion zone, it was fastened on the specimen surface from the side of the weld root. In one section of the specimen, the measurements were taken in 7–15 points, depending on its width and anticipated stress gradient. Residual stresses were measured in welded blanks and initial specimens before testing; their results are presented in the generalized form in Figures 2–5. To determine the residual stresses in the immediate vi-

city of the fusion zone (at 2 mm distance from the weld boundary) a method of strain gauge measurement with gauges with a 5 mm base was also used. Residual stresses in the direction of the metal thickness (Figure 2) were not considered, as on the surface  $\sigma_{res}^z = 0$ .

Coefficient of stress concentration in the joints, which is due to the geometry of weld profile, was calculated by the known dependencies allowing for the recommendations given in [22]. Used for this purpose was the statistical data of measurement of the main parameters of weld profile, namely radius  $\rho$  and angle  $\theta$  of fillet surface on the weld boundary, as well

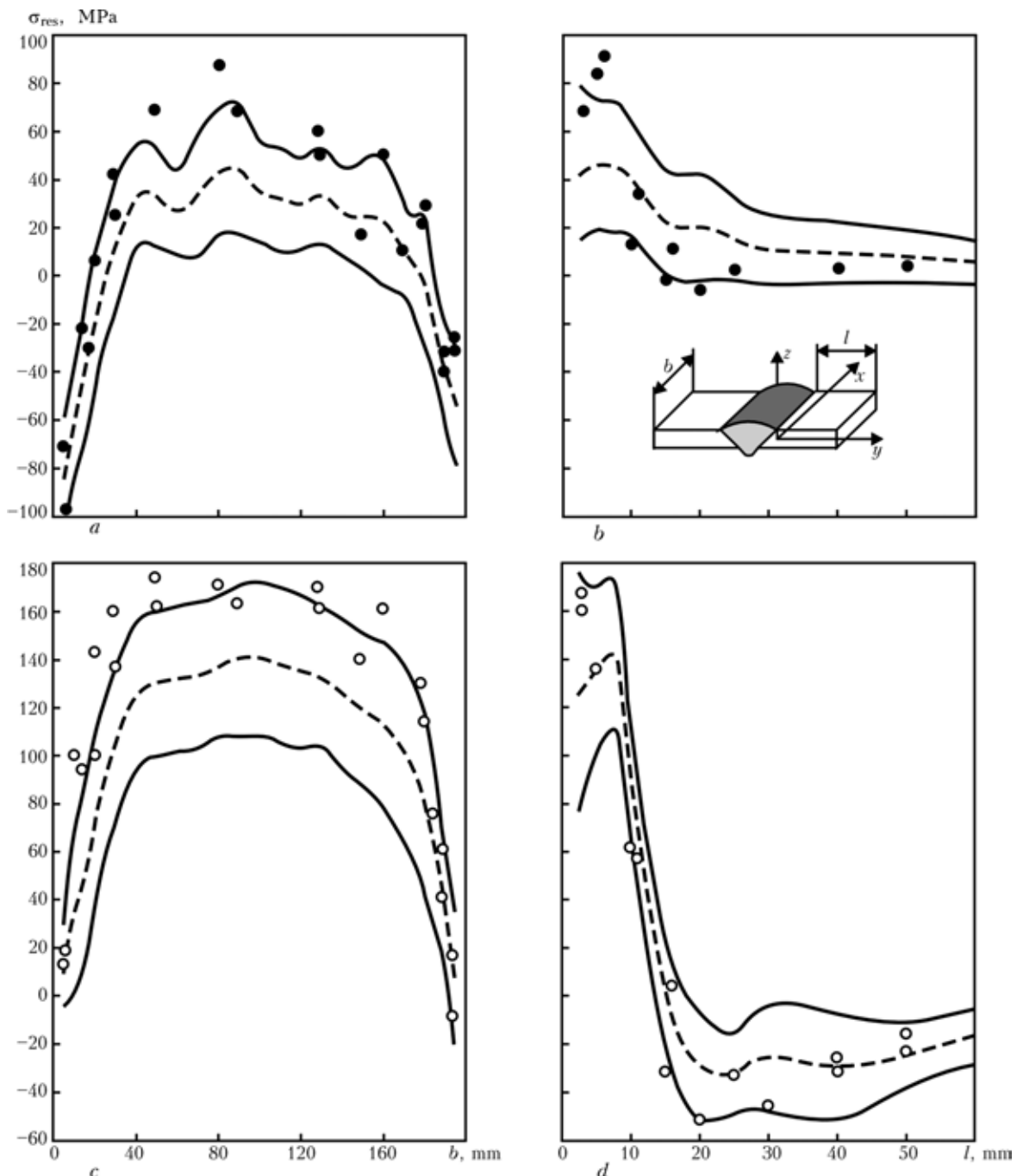


**Figure 2.** Transverse  $\sigma_{res}^y$  (a, b) and longitudinal  $\sigma_{res}^x$  (c, d) residual stresses in specimens 200 mm wide produced by MIG welding with application of SvAMg5 (curves) and SvAK5 (dots) wires: a, c --- section along the HAZ; b, d — section across the weld along the specimen axis; dashed curves --- average values of 12 measurements; solid curves — limits of measurement data scatter

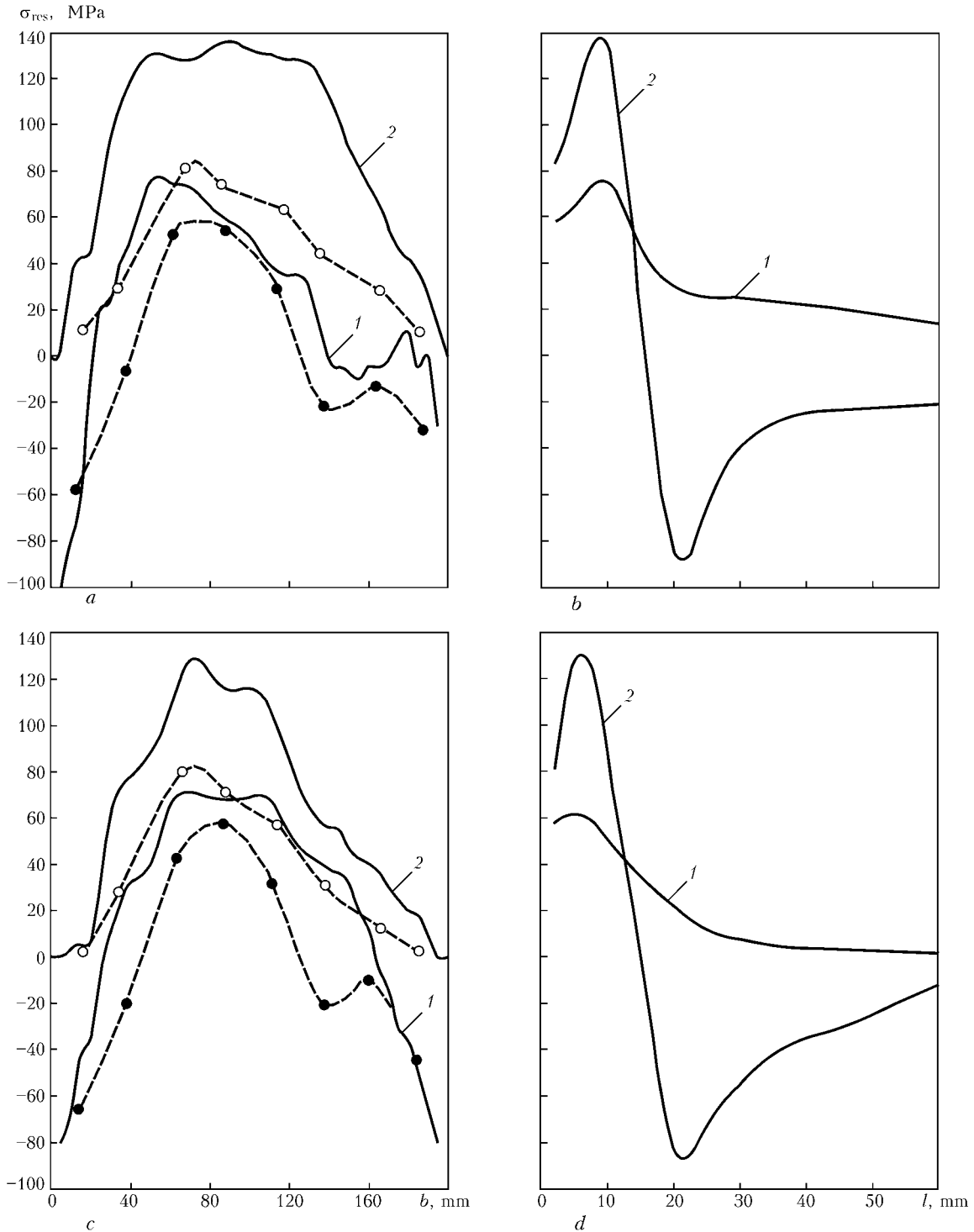


**Figure 3.** Transverse (1, ●) and longitudinal (2, ○) residual stresses in specimens 200 mm wide produced by TIG welding with application of SvAMg5 (a, b) and SvAK5 (c, d) wires: a, c — section along the HAZ; b, d — section across the weld along the specimen axis; 1, 2 --- average values from 3 measurements by acoustic method; dashed curves and points — data of strain gauge measurements

as weld height  $h$  and width  $b$ . These parameters were measured in blanks and specimens produced by different processes, and in different welding modes, namely by direct measurement method (profile measurement with the scale factor of 0.01 mm) and replica methods using plastic moulds and measurement in a tool microscope at 10-fold magnification of the cut mould profile. Obtained results are given in Table 2.

Fatigue testing of one-type of welded specimens of butt joints was conducted by applying axial cyclic

loading at a cycle asymmetry coefficient of a constant sign,  $R_\sigma = 0.1$  s with loading frequency of 4–7 Hz. Each test series included not less than eight specimens of one type. Considering the great range of their width (70–500 mm) their testing was performed using electrohydraulic machines URS-20 and Schenk-100 (RS-1.0) fitted with a dynamomeasuring device with load measurement error of  $\pm 1\%$ . Specimens of considerable width were tested using a hydraulic machine of pulsator type TsDM-200. The cyclic loading mode of this

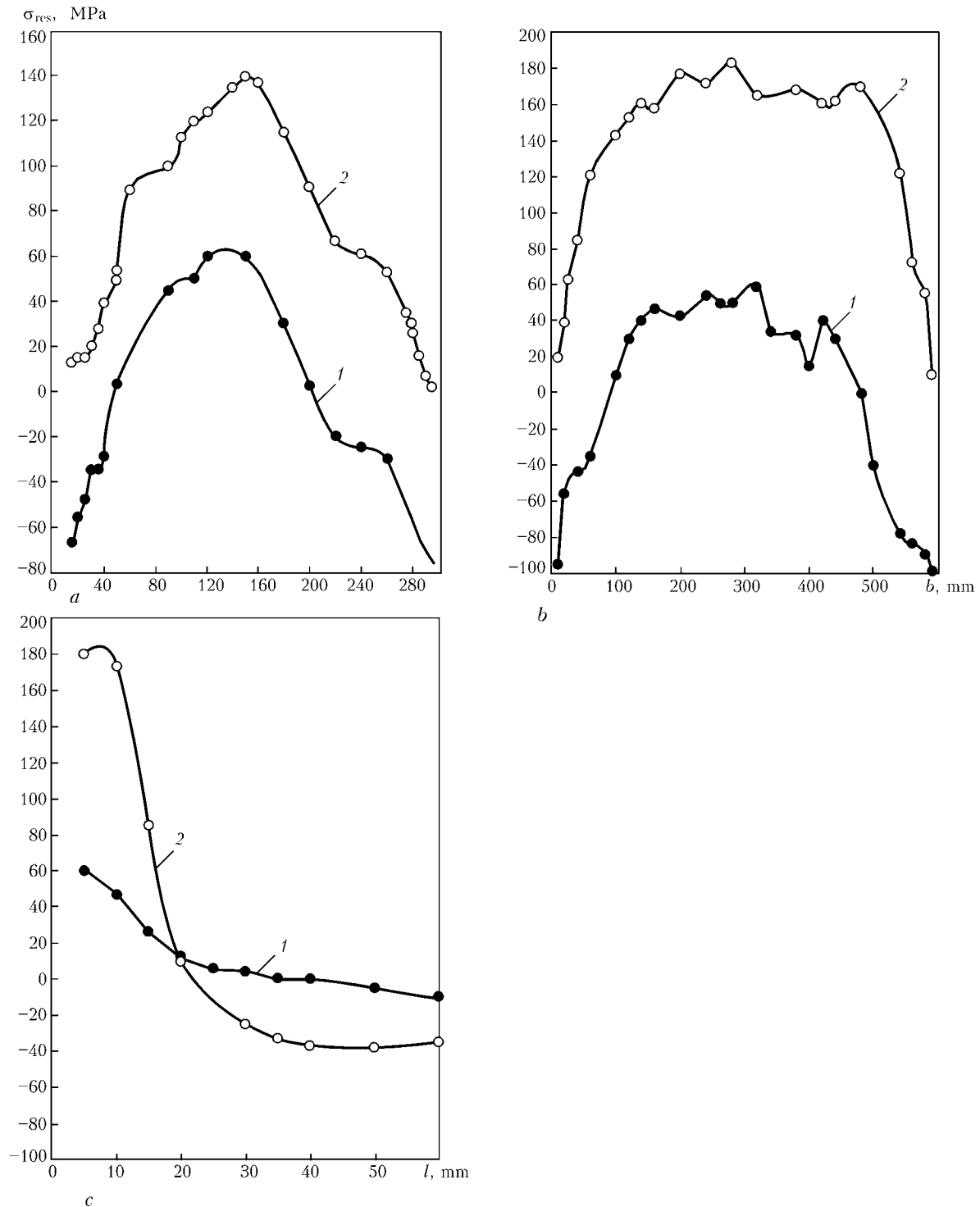


**Figure 4.** Longitudinal (1) and transverse (2) residual stresses in specimens 300 (a) and 600 (b, c) mm wide produced by MIG welding with application of SvAMg5 wire: a, b — section along the HAZ; c — section across the weld along specimen axis; dots — average values of 3 measurements

machine was set by the specimen stresses using strain gauges with 10 mm base. Gauges were symmetrically pasted in four points on the surface of the specimen working zone 10 mm from the weld boundary. To reduce a non-uniform distribution due to a concentrated application of the load, two-sided coverplates were used in the testing machine grips. The coverplates were cut out of the base metal to suit the dimensions of the specimen grip part. They were joined to the specimen end faces by transverse fillet welds.

Fatigue testing results were presented by values of the range of nominal stresses  $2\sigma_a$  and fatigue life to complete fracture of the welded joint.

A series of welded specimens 200 mm wide with artificially induced high tensile residual stresses in the HAZ located in the central part of the welded joint were also prepared. A point heating method was applied to induce in the HAZ transverse tensile stresses, comparable in their level to the longitudinal tensile stresses. Heating was performed with a gas

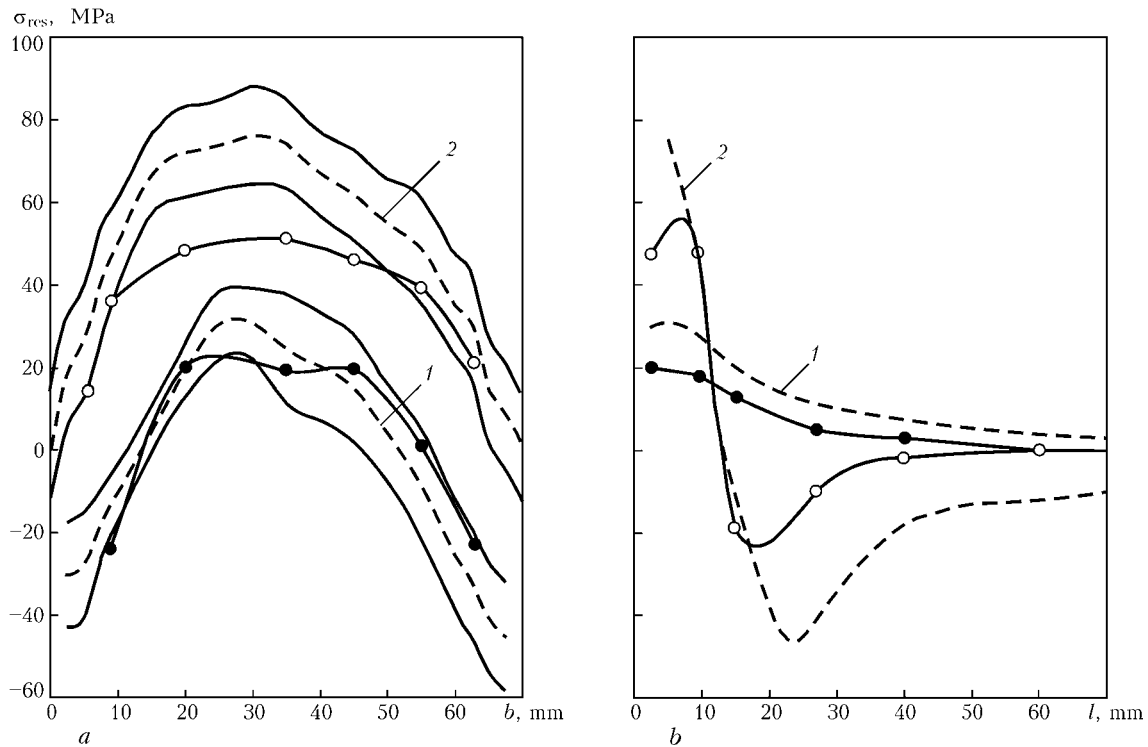


**Figure 5.** Transverse (1, ●) and longitudinal (2, ○) residual stresses in specimens 70 mm wide produced by MIG (curves) and TIG (dotted curves) welding with application of SvAMg5 wire: a — section along the HAZ; b — section across the weld along the specimen axis; dashed curves — average values from 6 measurements; solid curves — limits of measured data scatter; dots — results of isolated measurements

torch up to the temperature of about 250 °C at a certain distance from the weld with additional heat removal from the heating zone vicinity, using a circular copper coverplate, cooled by running water. Such a treatment did not cause an overall warping of the specimen, while the transverse residual tensile stresses in this case rose from 45 up to 130 MPa.

The main mechanical properties at testing by one-time static tension of the base metal and welded joints made by different welding processes, were determined on specimens of a standard width ( $b = 15$  mm). Tensile testing was also performed on wide specimens ( $b = 70$  and 200 mm). UME-10, UE-50 and Schenk-100 (RS-1.0) all-purpose machines were used. Yield point of specimens of width  $b = 70$  and 200 mm was evaluated using extensometer with base  $L_{E_0} = 100$  mm, and

for narrow ones ( $b = 15$  mm) —  $L_{E_0} = 25$  mm. At evaluation of standard relative deviation  $\delta_5$  for wide specimens the calculated measurement length ( $L_0 = 5.65\sqrt{Bt}$ ) was much greater than the width of the HAZ metal. Relative elongation  $\delta_{50\text{ mm}}$  on the base of  $L_0 = 50$  mm, which corresponded to the maximum HAZ width, was also determined. Average values obtained at testing three or more specimens are given in Table 3.

**Investigation results.** Mechanical properties of the welded joint. Testing of welded joint specimens by short-time tension demonstrated the following: ultimate strength  $\sigma_t$  is by 30 %, yield point  $\sigma_{0.2}$  by 50 %, relative elongation  $\delta_5$  by more than 2 times,  $\delta_{50\text{ mm}}$  by 21 % lower than the respective characteristics of the base metal (see Table 3). Such a lowering of the

**Table 2.** Parameters of weld convexity and design coefficient  $\alpha_\sigma$  of stress concentration in specimens

Welding process	Wire type	Weld side									
		Face					Root				
		$\rho, \text{ mm}$	$\theta, \text{ deg}$	$b, \text{ mm}$	$h, \text{ mm}$	$\alpha_\sigma$	$\rho, \text{ mm}$	$\theta, \text{ deg}$	$b, \text{ mm}$	$h, \text{ mm}$	$\alpha_\sigma$
TIG	SvAMg5	1.13	17.6	16.90	1.67	1.50	0.76	35.0	7.90	1.38	1.76
		0.22	2.2	2.60	0.18	0.06	0.30	7.4	0.36	0.16	0.16
	SvAK5	1.32	26.0	21.20	1.39	1.72	0.72	36.9	7.80	1.38	1.79
		0.91	6.4	6.45	0.19	0.39	0.24	5.5	0.52	0.13	0.14
MIG	SvAMg5	1.10	18.9	17.40	1.73	1.55	0.38	51.3	4.70	1.77	2.43
		0.32	3.2	0.46	0.27	0.09	0.21	9.7	0.65	0.31	0.67
	SvAK5	0.73	24.4	17.10	1.48	1.91	0.66	46.7	4.95	1.66	2.00
		0.65	6.9	0.88	0.25	0.34	0.53	7.3	1.90	0.31	0.40

Note. Numerator gives the average value, and denominator — the standard deviation.

**Table 3.** Mechanical properties obtained at tensile testing of the welded joint

Welding process	Wire type	Specimen shape	<i>b</i> , mm	$\sigma_t$ , MPa	$\sigma_{0.2}$ , MPa	$\delta_{50 \text{ mm}}$ , %	$\delta_5$ , %
TIG	SvAMg5	Without convexity	15	185	109*	7.6	6.9
		With convexity	70	199	137	9.2	4.0
	SvAK5	Without convexity	15	186	117*	8.0	7.3
		With convexity	15	178	119*	8.1	7.4
		Same	70	202	141	8.3	3.6
MIG	SvAMg5	Without convexity	15	203	102*	8.5	7.7
		Same	70	219	137	10.7	4.65
		With convexity	70	222	155	9.2	4.0
		Same	200	219	161	7.8	2.0
	SvAK5	Without convexity	15	200	117*	8.1	7.4
		Same	70	209	139	9.9	4.3
		With convexity	70	212	144	8.3	3.6
Without welding	Base metal	20	291	261*	--	13.0	

Note.  $\sigma_{0.2}$  values marked by an asterisk were determined by extensometer with 25 mm base, others — with 100 mm base.

mechanical properties is due to thermal softening of the base metal near the weld boundary. Welded specimens failed at 6–8 mm distance from the weld boundary. The fracture mode is practically independent on the used welding process and welding wire type. The base metal outside the HAZ practically did not accumulate any residual elongation deformations, when tested to fracture.

Increase of the width of welded specimen from 70 up to 200 mm leads to  $\sigma_{0.2}$  value rising by 5 % and  $\delta_{50 \text{ mm}}$  lowering by 15 %. Such an effect is produced by weld convexity (compared to specimens without a convexity), when it is cut off on narrow and wide specimens. The welding process practically does not influence  $\sigma_t$ ,  $\sigma_y$  and  $\delta_{50 \text{ mm}}$  of welded joints. However, in the case of a cut-off weld convexity, a noticeable increase of the conditional yield point is observed in specimens welded with SvAK5 wire instead of SvAMg5.

Increase of the conditional yield point and lowering of the relative elongation in wide specimens, is, probably, related to the influence of the longitudinal component of the tensile residual stresses in the welded joint. These stresses were directed normal to the external loading stresses and promoted a higher stressed state in the HAZ.

**Residual stresses.** In wide specimens ( $b = 200 \text{ mm}$ ) produced by MIG welding with application of SvAK5 wire, residual stresses have high values in the longitudinal direction  $\sigma_{\text{res}}^x = 140 \text{ MPa}$ , and low values in the transverse direction  $\sigma_{\text{res}}^y = 45 \text{ MPa}$  (see Figure 2). As is seen from the Figure, transverse tensile residual stresses are 3 times lower than the longitudinal stresses at steel specimen width recommended in [7]. Average values are given of the results of residual stress determination by the acoustic

method in 12 one-type specimens for sections running along the HAZ at 7.5 mm distance from the weld boundary, and across the weld along the specimen axis. In sections longitudinal relative to the weld, counting of the distance from the specimen edge across the width coincided with the welding direction, and in the sections transverse relative to the weld the counting started from the weld boundary, corresponding to the fusion zone. At unchanged MIG welding mode and application of SvAK5 wire, the tensile transverse ( $\sigma_{\text{res}}^y$ ) and longitudinal ( $\sigma_{\text{res}}^x$ ) residual stresses in the HAZ located in the specimen central part, are markedly higher than the average values of residual stresses in the specimens produced by MIG welding with SvAMg5 wire. The data for individual measurements of the residual stresses in the specimens, made with SvAK5 wire, are on the upper limit, corresponding to one standard deviation of the results of residual stress measurement in specimens welded with SvAMg5 wire.

In the section longitudinal relative to the weld (see Figure 2, c), the longitudinal tensile residual stresses of the same sign have maximum values in the specimen center and zero values along its edges. A similar nature of distribution of the transverse tensile residual stresses is observed in the section normal to the weld at their maximum value near the weld and lowering to zero value at a distance from the weld of more than 60 mm (see Figure 2, b). Similar to longitudinal residual stresses in the section transverse relative to the weld (see Figure 2, d), transverse tensile residual stresses in the section longitudinal relative to the weld (see Figure 2, a), are equalized by compressive stresses along the specimen edge (in the longitudinal section) and base metal adjacent to the HAZ (in the transverse section). However, the



nature of distribution (epure) of the transverse tensile residual stresses in the section longitudinal relative to the weld, unlike the classical epure in the form of a regular parabola with an extremum in the specimen center, has a somewhat more complicated form with several extremums across the entire width of the specimen. Alternation of the stress maximum and minimum markedly affects the lowering of the maximum tensile stress and increase of the scatter of measurement results (see Figure 2, a).

More than one extremum of the transverse tensile stresses is also observed on specimens 200 mm wide (see Figure 3, a, c) made by TIG welding with filler wires SvAMg5 and SvAK5. The first peak forms at the start of the weld at 80 mm distance from the specimen edge and has a higher average tensile residual stress ( $\sigma_{res}^y = 80$  MPa) than in MIG welding. The second low level peak is observed at 160 mm distance from the specimen edge.

At thermal cycle of TIG welding of specimens 200 mm wide the same zone with tensile residual stresses forms along the weld as in the case of MIG welding; it is equal to 15 mm from the weld face side. However, lowering of the maximum longitudinal tensile stresses  $\sigma_{res}^x$  is more pronounced, particularly in the direct vicinity of the weld boundary (see Figure 3, b, d). Application of strain gauging method of residual stress measurement at 2 mm distance from the weld boundary showed that the longitudinal and transverse residual stresses and mode of their distribution do not depend on the type of the used welding wire, and the values of the maximum transverse residual stresses are close to the values obtained by the acoustic method. As is seen from Figure 3, a, c, the longitudinal residual stresses at 2 mm distance from the weld boundary (measured by strain gauging) are essentially lower than the longitudinal residual stresses at 7.5 mm distance from the weld boundary.

At increase of the width of the specimen made by MIG welding with SvAMg5 wire to 300 mm, the residual stresses remain practically on the same level ---  $\sigma_{res}^x = 140$  and  $\sigma_{res}^y = 60$  MPa (see Figure 4, a). Further increase of the width to 600 mm for a specimen made by MIG welding with SvAMg5 wire, promotes increase of average longitudinal residual stresses to  $\sigma_{res}^x = 180$  MPa, the values of the transverse tensile residual stresses being on the same level ( $\sigma_{res}^y = 50$ –60 MPa) or becoming 3 times smaller than the maximum longitudinal residual stresses (see Figure 4, b, c). With increase of specimen width, that of the HAZ with longitudinal residual stresses increases up to 18 mm.

In specimens 70 mm wide made by MIG welding with SvAMg5 wire, the mode of distribution of the transverse residual stresses in the HAZ section also depends on the welding direction (see Figure 5). The first maximum is as the distance of 20–25 mm from the specimen edge in the welding direction. The level of the average maximum transverse tensile stress in

the HAZ is  $\sigma_{res}^y = 30$  MPa by the results of six measurements. Results of measurement of the transverse residual stresses in the specimens, produced by TIG welding with SvAMg5 wire, do not go beyond the standard deviation of residual stresses in specimens made by MIG welding. However, the longitudinal tensile residual stresses in individual specimens markedly depend on the welding process. The average maximum tensile stresses in the specimens in MIG welding are equal to  $\sigma_{res}^x = 75$  MPa, and in TIG welding  $\sigma_{res}^x = 50$  MPa. Irrespective of the welding process, the zone with the longitudinal tensile residual stresses extends for 13 mm from the weld boundary, and the ratio of the longitudinal residual stresses to the transverse stresses in the HAZ of the specimen central part is equal to about 2.6.

Thus, in specimens of the same width, MIG welding ensures higher tensile longitudinal residual stresses and lower tensile transverse residual stresses, compared to the residual stresses  $\sigma_{res}^x$  and  $\sigma_{res}^y$  developing in TIG welding in the direct vicinity of weld boundary (see Figures 2--5). At increase of specimen width from 70 to 600 mm the longitudinal residual stresses, developing in MIG welding, rise from 0.25 to 0.80 of the value of ultimate tensile strength  $\sigma_t$  of the welded joint (see Table 3). In TIG welding the longitudinal residual stresses are 1.8 times lower than  $\sigma_{res}^x$  in specimens of the same size ( $b = 200$  mm) produced by MIG welding. With increase of specimen width, the transverse component of the tensile residual stresses also rises practically proportionally with preservation of the ratio of  $\sigma_{res}^x / \sigma_{res}^y = 2.8$  (in MIG welding) and 1.4 (in TIG welding).

Thus, the biaxial residual tension due to welding, propagates in the specimen central part in the HAZ over 13 to 18 mm width from the weld boundary (in specimens with  $b = 70$ –600 mm), and over a length of approximately 0.7 of the overall weld length or specimen width. In MIG welding the stable maximum values of the tensile residual stresses  $\sigma_{res}^x = 0.8\sigma_t$ , and  $\sigma_{res}^y = 0.3\sigma_t$  are achieved at specimen with  $b = 300$  mm.  $\sigma_{res}^x / \sigma_{res}^y$  suggests that a higher stressed state is found in the joints produced by MIG welding. As  $\sigma_{res}^x$  are directed normal to the specimen axis, at tensile testing they are not added up to the external loading stresses.

A characteristic feature of distribution of the transverse residual stresses in the HAZ is formation of several extreme peaks along the weld. In MIG welding the number of peak values of the transverse tensile residual stresses is higher, and their level is 2 times lower than in TIG welding. In specimens of the most widely accepted width (70 mm) produced by MIG welding, values of the transverse residual stresses are a just as low, as in the wide specimens. Transverse tensile residual stresses in the central part of the specimens, starting with the width of 200 mm, drop to zero value in some cases. In this case, the epure of

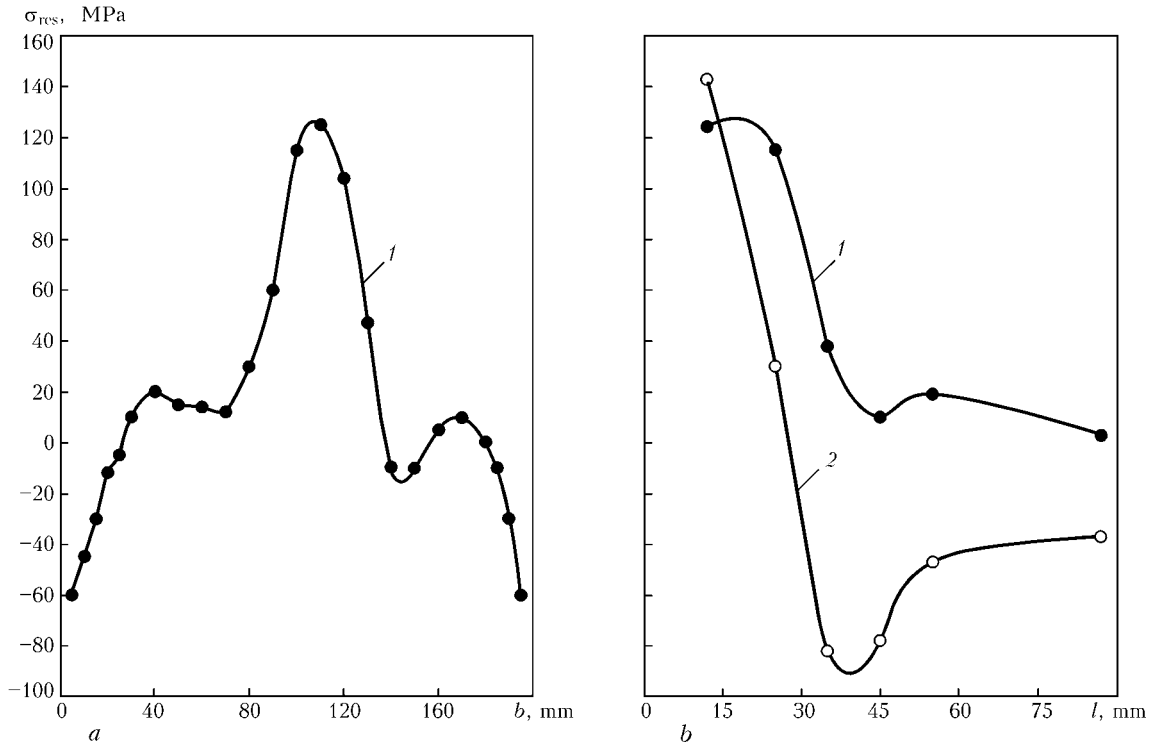


**Figure 6.** Transverse (1) and longitudinal (2) residual stresses after point heating in the center of welded specimen 200 mm wide: a — section along the HAZ; b — section across the weld along specimen axis (distance is counted from heating center)

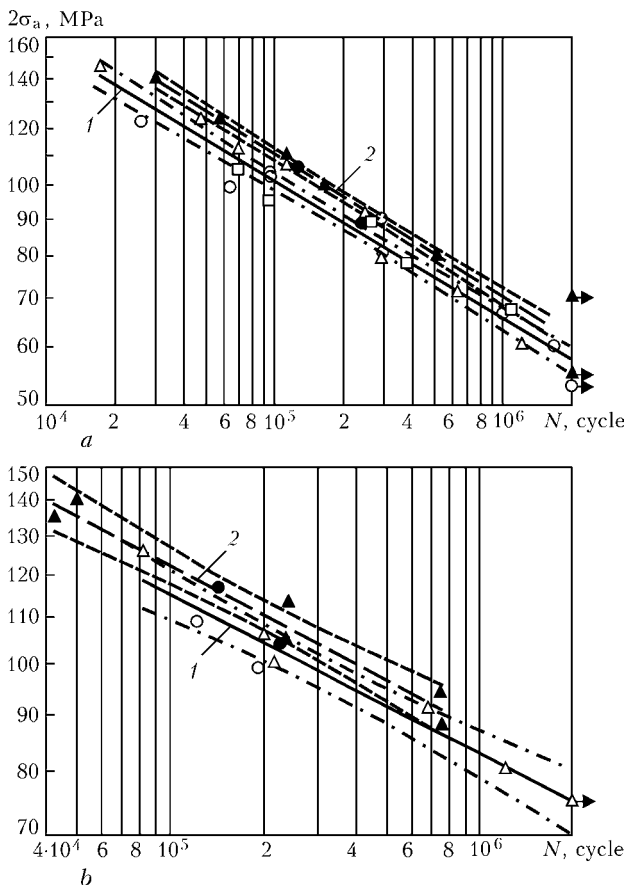


**Figure 7.** S-N curves and their 95 % confidence interval for joints produced by MIG (1) and TIG (2) welding with SvAMg5 (a) and SvAK5 (b) wires:  $\Delta$ ,  $\blacktriangle$  — specimens 70 mm wide;  $\circ$ ,  $\bullet$  — 200;  $\square$  — 500; light dots — MIG welding; dark dots — TIG welding

transverse stresses across the specimen width can take a «two-hump» form (see, for instance, Figure 3).

Use of point heating for an additional increase of the tensile residual stresses in the HAZ showed that the high transverse residual stresses are only localized near the zone of active heating at 35 to 40 mm distance from the heating point (Figure 6, b). The resulting values of the transverse residual stresses in the HAZ section rise considerably only in the narrow central zone of the specimen (Figure 6, a) up to  $\sigma_{res}^y = 125$  MPa or  $0.6\sigma_t$ , corresponding by the level to the longitudinal component of the tensile residual stresses in large-sized welded specimens.

**Fatigue resistance.** Fatigue testing of welded joint specimens demonstrated that for the considered welding processes, specimen width and the corresponding residual stresses, do not have a substantial influence on the fatigue life (Figure 7). Average statistical S-N curve of 70 mm wide specimens produced by MIG welding with SvAMg5 wire, and that generalized for all specimens of 70, 200 and 500 mm width, made by MIG welding with SvAMg5 wire, practically coincide within 95 % of confidence interval (Figure 7, a). The average statistical S-N curve for specimens 70 and 200 mm wide, produced by TIG welding with SvAMg5 wire, is shifted upwards and coincides with the upper limit of the region of scatter of the results of testing all the specimens made by MIG welding with the same wire. Specimen width (70 and 200 mm) does not cause any noticeable changes in the fatigue resistance also in the joints produced by MIG and



TIG welding with SvAK5 wire (Figure 7, b). Average statistical S-N curve of the joints made by TIG welding, is above the S-N curve of the joints made by MIG welding. It is obvious that the lower transverse and higher longitudinal tensile residual stresses in high-efficient MIG welding process are not the determinant factor in increasing the fatigue resistance of welded joints, compared to less favourable residual stresses developing in TIG welding. Increase of the levels of longitudinal and transverse residual stresses with greater specimen dimensions, does not lead to any noticeable reduction of the joint fatigue life.

In the presented welding processes, a higher fatigue resistance of the joints made by TIG welding, compared to that of the joints made by MIG welding, is due to lower average values of the stress concentration factor  $\alpha_\sigma$  (by 11–28 %) and 3 to 4 times lower scatter of  $\alpha_\sigma$  values, particularly from the side of the weld root (see Table 2). The obtained testing results show that stress concentration is the main cause for a fatigue crack initiation practically over the entire width of the specimens along the welded joint. Use of various types of welding wires does not cause any significant deviation in the stress concentration factor in the weld root part. However, the fatigue crack, while initiating in the fusion zone on the boundary of the root convexity, propagates in-depth of the weld metal across its thickness, the crack having an essential influence on the fatigue resistance of the specimens due to a change in the composition and mechanical properties of weld metal. The fatigue life of the joints produced using SvAK5 wire, is increased more than 4 times in the high-cycle region, compared to the fatigue life of the joints produced by TIG and MIG welding using SvAMg5 wire (Figure 8). Removing the convexities without a thermal impact or change of the residual stresses in the weld metal leads to an essential increase of the fatigue life and level of the limit stress range in the joints 70 mm wide, made by MIG welding with SvAMg5 and SvAK5 wires. Limit stress ranges rise by more than 50 %. Therefore, fatigue resistance of the joints produced with application of the considered welding processes, is determined primarily by the coefficient of stress concentration and mechanical properties of the metal in the zone, where the fatigue fracture initiates. Specimen dimensions and the natural residual stress level in them are less significant factors than the geometry of welds, welding wire composition or applied welding process.

Artificial inducing of additional transverse tensile residual stresses at the concentrator zone in the central part of a 200 mm wide specimen to the level comparable with the longitudinal tensile residual stresses in the joint, causes a lowering of the fatigue life more than 2 times, and of the limit stress by 10 MPa (14 %), compared to the respective characteristics of specimens with a natural residual stress level (Figure 8).

Fatigue testing of large-sized welded specimens up to 500 mm wide provided proof of the fact that

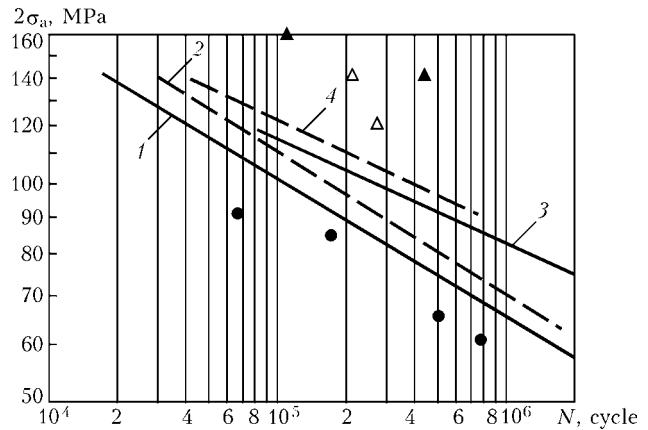


**Figure 8.** Generalized average statistical S-N curves of specimens made by MIG (1, 3) and TIG (2, 4) welding with SvAMg5 (1, 2) and SvAK5 (3, 4) wire and results of testing specimens made by MIG welding and after additional treatment: ● --- specimens 200 mm wide with artificially induced transverse tensile residual stresses ( $\sigma_{res} = 125$  MPa), weld made by SvAMg5 wire; ▲, ▲ --- 70 mm wide with removed convexity, weld made with SvAMg5 and SvAK5 wires, respectively

the transverse and longitudinal tensile residual stresses differ in their detrimental effect. Increase of the longitudinal tensile residual stresses in the butt joint HAZ from  $\sigma_{res}^x = 50$ –70 (at  $b = 70$  mm) up to  $\sigma_{res}^x = 130$ –140 MPa (at  $b = 200$  mm) and even to  $\sigma_{res}^x = 160$ –180 MPa (at  $b = 500$  mm) does not lead to any significant changes in the fatigue life, if their values are 3 times lower than the transverse tensile stresses (in the case of MIG welding). These stresses in the joints are directed normal to the external tensile stresses. Combined with the external tensile stresses, they induce a biaxial tension in the HAZ metal. As is known [23], transition from uni- to biaxial stress is the main condition for restraining plastic deformation of the metal, which may be the cause for a higher yield point and lowering of the stress concentration coefficient.

A noticeable (more than 2 times) lowering of the fatigue life at an increased value of the transverse component of the tensile residual stresses to  $\sigma_{res}^y = 125$  MPa in specimens of welded joints, produced using point heating, compared to the initial specimens ( $\sigma_{res}^y = 60$ –70 MPa) at a constant value of the longitudinal residual stresses, is due to interaction of these stresses with the external load stresses. The main condition providing a longer fatigue life of welded joints, is application of the high welding speeds at a minimum heat input, as well as making continuous welds, thus promoting an essential reduction of the transverse component of the tensile residual stresses. In this case, high values of the longitudinal component of the tensile residual stresses can be acceptable, that not only does not have any detrimental effect under the conditions of welded joint fatigue, but can also compensate the influence of the transverse component of the tensile residual stresses under the conditions that  $\sigma_{res}^y \leq 1/3 \sigma_{res}^x$ , and small-sized welded specimens ac-



cepted in practice can be used for conducting fatigue tests.

## CONCLUSIONS

1. It is found that application of automated processes of arc welding of butt joints of alloy AD33 T1 6 mm thick on individual specimens 70 to 600 mm wide with a transverse continuous weld promotes development of tensile residual stresses in the HAZ central part with the ratio of the level of longitudinal stresses to transverse stresses of 3:1 (in MIG welding) and 1.4:1.0 (in TIG welding). In the case of MIG welding the longitudinal tensile stresses reach their maximum stable level ( $0.8\sigma_T$ ) in the HAZ at specimen width of more than 300 mm. At the same width of the specimens ( $b = 200$  mm) the transverse tensile residual stresses are 1.8 times lower in MIG welding than in TIG welding.

2. Under the impact of a cyclic load across the weld section, the role of tensile residual stresses longitudinal and transverse relative to the weld is not identical at fatigue damage. Increase of longitudinal residual stresses from 40 up to 160 MPa due to increase of specimen width in MIG welding practically does not detract from the joint fatigue life. However, increase of transverse tensile residual stresses from 40 up to 125 MPa through additional measures with unchanged level of the longitudinal residual stresses reduces the fatigue life of the specimens more than 2 times.

3. It is not rational to apply large-sized specimens for conducting fatigue tests of aluminium alloy joints made by the MIG processes by a continuous weld, as increase of the specimen width above 70 mm does not lead to any significant increase of the transverse component of the tensile residual stresses. There is no need for additional measures to increase the transverse residual stresses in narrow specimens, as the stress concentration, due to the convex shape of the weld, is the main damaging factor under cyclic load.

1. Trufyakov, V.I. (1973) *Fatigue of welded joints*. Kiev: Naukova Dumka.
2. Shonin, V.A. (1982) Analysis of results of fatigue tests of AMg6 alloy welded joints. *Avtomatich. Svarka*, **3**, 71–73.
3. Sanders, W.W., Day, R.H. (1983) Fatigue behavior of aluminum alloy weldments. *WRS Bull.*, **266**.
4. Dvoretzkii, V.I., Mikheev, P.P., Shonin, V.A. (1984) A procedure of fatigue analysis of aluminum structure welded joints. *IIW Doc. XIII-1138-84*.
5. Kelsy, R.A., Nordmark, G.E. (1984) Effect of residual stresses on fatigue resistance of aluminium alloy butt joints. In: *Proc. of Soviet-American Seminar on Welding of Aluminium Alloys of Cryogenic and General Purposes*, Kiev, June 1981. Kiev: Naukova Dumka.
6. Shonin, V.A. (1984) *Fatigue resistance of aluminium alloy welded joints taking into account the effect of residual stresses*. Syn. of Thesis for Cand. of Techn. Sci. Degree. Kiev.
7. RD 50-551-85. Calculations and strength tests. Computational-experimental methods of evaluation of welded joint fatigue resistance: Proc. Guidelines. Moscow: Standart.
8. Shonin, V.A. (1990) Fatigue limit of AMg6 alloy welded joints. *Avtomatich. Svarka*, **4**, 12–18.
9. RD 50-694-90. Reliability in engineering. Probabilistic method of calculation of welded joint fatigue. In: Proc. Guidelines. Moscow: Standart.
10. Kazimirov, A.A., Nedoseka, A.Ya. (1962) About residual stresses and strains arising in welding of AMg5V alloy. *Avtomatich. Svarka*, **10**, 16–21.
11. Kiselyov, S.N., Khavanov, V.A., Skornyakov, L.M. et al. (1966) Special features of distribution of surface residual stresses in welded plates of avial alloy. *Svarochn. Proizvodstvo*, **12**, 6–8.
12. Tanaka, E., Hirata, K., Takeuchi, K. (1970) Residual stress in butt-welded 5083 aluminum alloys. Studies on residual stresses in welded joints of aluminum alloys. *Light Metals*, **1**, 7–15.
13. Nedoseka, A.Ya. (1974) Residual stresses in plates during welding of butt joint. *Avtomatich. Svarka*, **11**, 32–38.
14. Guz, A.N., Makhort, F.G., Gushcha, O.I. et al. (1974) *Principles of ultrasonic non-destructive method of stress determination in solids*. Kiev: Naukova Dumka.
15. Okerblom, N.O. (1950) *Welding stresses in metal structures*. Moscow-Leningrad: Mashgiz.
16. Makhnenko, V.I. (1976) *Calculation methods of study of weld stress and strain kinetics*. Kiev: Naukova Dumka.
17. Trufyakov, V.I., Mikheev, P.P., Shonin, V.A. et al. (1976) Effect of residual stresses on fatigue resistance of aluminium alloy welded joints. *Avtomatich. Svarka*, **5**, 37–39.
18. Shonin, V.A. (1978) Effect of residual stresses on fatigue resistance of load-carrying element of AMg6 alloy in the point of welding-up transverse stiffeners. *Ibid.*, **1**, 70–71.
19. Mikheev, P.P., Shonin, V.A. (1981) Fatigue resistance of aluminium alloy welded joints allowing for the stressed state. In: *Proc. of Soviet-American Seminar on Welding of Aluminium Alloys of Cryogenic and General Purposes*, Kiev, June 1981. Kiev: Naukova Dumka.
20. Maddox, S.J. (2003) Review of fatigue design rules for welded structures. *The Paton Welding J.*, **10/11**, 94–99.
21. Guz, A.N., Makhort, F.G., Gushcha, O.I. (1977) *Introduction to acousto-elasticity*. Kiev: Naukova Dumka.
22. Makhnenko, V.I., Mosenkis, R.Yu. (1985) Calculation of coefficients of stress concentration in welded joints with butt and fillet welds. *Avtomatich. Svarka*, **8**, 7–18.
23. Osaulenko, L.L., Kotenko, E.V. (1981) Biaxial tension and sensitivity of material to stress concentration. *Problemy Prochnosti*, **3**, 21–25.



# OPTIMIZATION OF PARAMETERS OF DETONATION-GAS SPRAYING USING A GENETIC ALGORITHM

V.A. ULSHIN and M.Yu. KHARLAMOV

V. Dal East-Ukrainian National University, Lugansk, Ukraine

A method is proposed to determine the optimum process parameters of detonation-gas spraying of coatings by the criterion of energy characteristics of the spray powder particles, which is based on the use of a genetic algorithm. Advantages of this approach are demonstrated compared to other methods of solving the optimization problems, and computer simulation is used to demonstrate its effectiveness.

**Keywords:** *detonation-gas spraying, simulation, optimization, particle velocity, particle temperature, genetic algorithm*

Conditions of coating formation are strongly affected by the velocity and temperature of the spray particles. In their turn, the energy characteristics of the particles at detonation-gas spraying of coatings (DGSC) depend on many process parameters. Therefore, in order to produce coatings with the specified properties, it is necessary to establish the optimum parameters. The large number of these parameters, as well as impossibility of separating the process, which determines the final results, make search for optimized spraying conditions more difficult. In practice, conducting a great variety of expensive experiments solves the problem of finding the optimum parameters of DGSC process. Analytical procedures of finding optimized spraying conditions do not provide any precise recommendations. These procedures consist either in finding a partial optimum by variation of process factors by one of the possible optimization parameters [1], or a tentative algorithm of process construction (depending on the used particle material), which is eventually also reduced to variation of the some process parameters with the others being constant [2]. As a result, when solving a specific problem of producing coatings with the specified properties, the above methods can only provide estimated values of process parameters, and imply conducting full-scale experiments.

This study was aimed at development of the method of optimizing the process modes of DGSC, allowing for all the parameters, which affect the energy characteristics of the spraying particles, and, thus also the coating formation. These include [1, 3, 4] powder composition; gas mixture composition; powder particle size; powder sample; initial arrangement of particles in the D-gun (DG) channel; geometrical parameters of DG channel; and shooting distance.

Let us consider selection of optimization parameters and criteria in greater detail. During calculations the geometrical parameters of DG channel and powder

composition were assumed to be preset, and the other parameters were optimized for a number of causes. Selection of the spray powder composition is mainly determined by the operating conditions of the item to be sprayed, which excludes this parameter from the number of the variable ones.

An urgent problem is development of detonation combustion chambers (DG channels) optimum as to their design for spraying the coatings. However, in view of the diversity of the possible variants of channel design (use of DG with composite parts, which change the shape of longitudinal and transverse section of the channel, use of various fillers, etc.), the space of searching for the optimum parameters is greatly increased, and the problem becomes practically unsolvable.

From the theory of thermal spraying it follows that the velocity and temperature of the sprayed particles are the determinant parameters in coating formation. Space-time distribution of the above values in the zone of coating formation has a very important role here. On the other hand, the data on the required mode of distribution of particle parameters in time and space to produce coatings with the specified properties, are absent in publications. The cause for that is insufficient understanding of physico-chemical processes of coating formation in thermal spraying. As a result, when solving specific problems simplified mathematical models are applied, which only indirectly reflect the structural features of the sprayed coatings. Therefore, in a number of cases averaged values of velocity and temperature of powder particles at interaction with the sprayed surface can be used.

These characteristics were used also at optimization of DGSC process in this work. In the future with the advance of the theory of interaction of a pulsed two-phase jet and base at DGSC, the optimization criteria can be widened, which will promote selection of optimum spraying modes, providing coatings with the specified structure and properties.

Such an optimized parameter as powder particle size should be considered separately. The known studies on detonation spraying usually consider either the

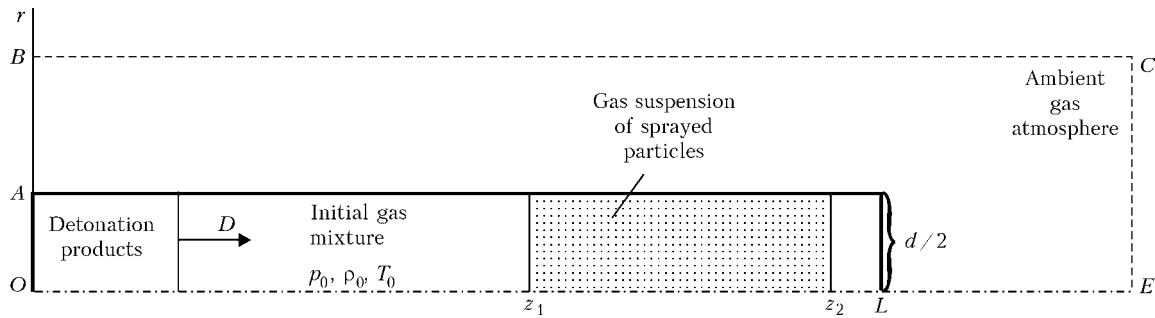


Figure 1. Schematic of a DG channel and design area (for designations see the text)

dynamics of individual particle behaviour in the flow of detonation products (DP), or a flow of monodisperse gas suspension. In selection of spraying process parameters, use of the latter approach is preferable, as it allows for such a factor as influence of the powder sample on two-phase flow parameters. In [1, 5, etc.] the dynamics of behaviour of polydisperse flows is studied, using several simplifications (several clusters of particles of different diameter are considered, the particles in one cluster having one co-ordinate and velocity, etc.), this not allowing particle distribution by size to be regarded as a continuous process. Greater accuracy and validity of simulation results can be achieved at simultaneous description of the dynamics of behaviour of a large number of particles. This was done in [6], where the motion of powder particle in a plasma jet was simulated for 3000 particles. Much more time required to solve the problems should be regarded as one of the disadvantages of the models describing the behaviour of polydisperse powders. At the current level of development of computer systems, this is not acceptable for solving the optimization problems, requiring calculation of a large number of possible variants of the optimized parameter values. For these purposes, it is rational to use mathematical models, describing the behaviour of a monodisperse powder at DGSC, while considering the average particle diameter in the spray fraction.

Thus, the researchers have the task of selecting the composition of the used gas mixture, average diameter of the powder particles, powder sample, initial arrangement of the particles in the DG channel and the shooting distance at the set geometrical parameters of DG channel and powder composition, in order to give the spray particles the specified values of average velocity and temperature at interaction with the surface being treated.

In this work a model from [7] was used that allows determination of the space-time parameters of the sprayed particle flow, both inside DG channel, and in the space between the channel edge and the treated item, also when using DG channels of a variable cross-section. Simulation was conducted under the following conditions. DG channel of length  $L$ , having a cylindrical shape of inner diameter  $d$ , or a channel of a variable section, having output diameter  $d$ , is partially or completely filled with a mixture of gases at

their initial pressure  $p_0$ , density  $\rho_0$  and temperature  $T_0$ . A gas suspension of solid spherical particles is inside the channel in region  $(z_1, z_2)$  at  $0 \leq z_1 < z_2 \leq L$ . At initiation a stationary detonation wave (DW) forms at the left closed end of the channel, which propagates to the right at detonation velocity  $D$  (Figure 1). At partial filling of the channel by a detonation mixture, unreacted gas takes up the remaining part of the channel. In this case, after DW has reached the contact boundary of gas mixture–unreacted gas (GM–UG), DW decomposes into a shock wave moving along UG and rarefaction wave moving in the opposite direction through DP. After the shock or detonation wave has reached the open end of the channel, DP and disperse particles start outflowing into the surrounding gas atmosphere.

Boundary conditions were defined as follows. Conditions of non-flowing of the gas and disperse particles were assumed on the axis of symmetry and walls of DG channel. As long as DW has not reached GM–UG contact boundary, its parameters are found by the formulas for the front of the stationary DW (right boundary condition). After DW has reached the contact boundary, conditions of free flow of the phases are set on the open boundaries of calculation region  $AB$  and  $BC$ , and the condition of non-flow for the gas phase and free penetration for the disperse phase is specified on right boundary  $CE$  according to [8], i.e. the powder which has reached the barrier, is sprayed on it.

The following assumptions were used: pressure is only induced by gas; influence of powder particles is ignored; viscosity and heat conductivity of the phases is only taken into account in the processes of inter-phase interaction; distances over which the flow parameters change, are much greater than the dimensions of the particles or distances between them; particles are spherical monodisperse ones and do not react with DP; fragmentation or collision of particles are absent; before the start of the flow DP are considered as the reacting medium, having an equilibrium composition in each point, and after the outflow start — as an inert gas with a constant adiabatic index; particle influence on DW characteristics is ignored.

A system of equations of a two-dimensional axisymmetric nonstationary motion of the gas suspension has the following form [9]:



$$\begin{aligned} & \frac{\partial \rho_i}{\partial t} + \frac{1}{r} \frac{\partial (r \rho_i v_i)}{\partial r} + \frac{\partial (\rho_i u_i)}{\partial z} = 0; \\ & \frac{\partial (\rho_i v_i)}{\partial t} + \frac{1}{r} \frac{\partial (r \rho_i v_i^2)}{\partial r} + \frac{\partial (\rho_i v_i u_i)}{\partial z} + \alpha_i \frac{\partial p}{\partial r} = (-1)^i f_r n, \\ & \frac{\partial (\rho_i u_i)}{\partial t} + \frac{1}{r} \frac{\partial (r \rho_i v_i u_i)}{\partial r} + \frac{\partial (\rho_i u_i^2)}{\partial z} + \alpha_i \frac{\partial p}{\partial r} = (-1)^i f_z n, \\ & \frac{\partial (\rho_2 e_2)}{\partial t} + \frac{1}{r} \frac{\partial (r \rho_2 e_2 v_2)}{\partial r} + \frac{\partial (\rho_2 e_2 u_2)}{\partial z} = qn, \\ & \sum_{i=1}^2 \left[ \frac{\partial (\rho_i E_i)}{\partial t} + \frac{1}{r} \frac{\partial (r \rho_i v_i E_i)}{\partial r} + \frac{1}{r} \frac{\partial (r \alpha_i p v_i)}{\partial r} + \right. \\ & \quad \left. + \frac{\partial (\rho_i u_i E_i)}{\partial z} + \frac{\partial (\alpha_i p u_i)}{\partial z} \right] = 0; \\ & \rho_i = \alpha_i \rho_i^0, \quad E_i = e_i + (v_i^2 + u_i^2)/2, \\ & n = 6\alpha_2/(\pi\delta^3), \quad \alpha_1 + \alpha_2 = 1, \quad \rho_2^0 = \text{const}, \quad i = 1, 2, \end{aligned}$$

where  $v_i$  and  $u_i$  are the velocity components in radial  $r$  and axial  $z$  directions, respectively;  $e_i$ ,  $E_i$  are the specific internal and full energy of  $i$ -th phase;  $p$  is the gas pressure;  $f_z$ ,  $f_r$  are the components of force interaction from the side of the gas on the disperse particle in cylindrical co-ordinates;  $q$  is the intensity of heat input into the individual particle surface;  $n$  is the number of disperse particles in a unit of mixture volume. Share of mixture volume taken up by  $i$ -th phase, is characterized by its bulk content  $\alpha_i$ . Each point of mixture volume is correlated with average phase density  $\rho_i$ , characterizing phase mass in a unit of volume, and true phase density  $\rho_i^0$ , characterizing the density of substances, making up the mixture. Indices  $i = 1$  are for the gas; and  $i = 2$  are for disperse phases.

Equations of state of an ideal gas were used ---  $p = \rho_1^0 R T_1 / \mu_1$ ,  $e_1 = e_1(T_1)$ , where  $R$  is the absolute gas constant;  $\mu_1$  is the DP molecular mass;  $T_1$  is the gas phase temperature. Equation of the total inner energy of the gas  $e_1(T_1, \mu_1)$  and equation of chemical equilibrium  $\mu_1(\rho_1, T_1)$  [10, 11] were used for the reacting gas flow before the outflow start. Equation for the inner energy of the disperse phase, having the form  $e_2 = e_2(T_2)$ , where  $T_2$  is the disperse phase temperature, was written, allowing for the possible phase transition (particle melting).

Assigning the laws of interphase force and thermal interaction of the gas and disperse phases  $f_z$ ,  $f_r$ ,  $q$ , closed derived system of equations. Numerical integration was performed by the method of «coarse particles» [8]. The difference scheme was constructed allowing for conducting the calculations for DG channels of a variable cross-section.

DW parameters required for calculations (detonation velocity, temperature, pressure, density, gas velocity in Champen--Juge point, etc.), were calculated for a mixture with the conditional formula  $C_a H_b O_c N_d$  with addition of inert gases based on balance equations of material, chemical equilibrium, gas dynamics and equation of state, using the model of [12].

In order to solve the optimization problem, one of the representatives of the class of evolutionary methods of calculation, namely a genetic algorithm (GA), was selected [13, 14]. Application of this algorithm allows generation of efficient algorithms for a broad class of optimization problems [15]. This does not require any additional information on the nature of the studied function, its properties (differentiability, continuity, etc.), and no restrictions are applied to the search region, which may be non-convex or multiply connected. Features of other methods of solving the global optimization problems, the main of which are the enumeration and local-gradient approaches, do not allow their use in optimization of DGSC process modes. Enumeration algorithm is the simplest to implement, but searching for an optimum solution requires calculation of all the possible variants of variable values, which is unrealistic for multiparametric multiextremal problems. Gradient methods are very fast, but do not ensure the optimality of the derived solution. They are ideal for solving the problems, where the criterion function has one extremum. In terms of the speed and accuracy of calculation GA is superior also to random search methods (Monte-Carlo method, etc.), as it allows accumulating successful solutions during the calculation process.

The main idea of a GA consists in a collective search for an optimum through a multitude of independent sets of values (vectors) of variables, which are the potential solutions. At the initial stage, the variable vectors are generated in a random manner. Furtheron, each new multitude of sets of variable values is formed on the basis of the previous one by certain rules, taking into account the criterion function. During iterating, the criterion function value average over the set, verges towards the extremum. GA usually uses the terminology taken from biology. So one combination of a set of variable values is an individual, and a set of individuals for each iteration of the algorithm, is a population. Individual adaptation is a quantitative characteristic, showing how successful is the individual in solving the posed problem, i.e. adaptation is the value of criterion function for a given variant of variable set. Let us consider GA functioning in greater detail for the case of optimization of DGSC process parameters.

In GA the variable vectors are coded into a chromosome, which is a chain of symbols written using two, three or four letters of the alphabet. In the algorithm version for establishing the optimum parameters of DGSC process, a binary coding variant was used, which is the most natural in the algorithm implementation on a computer, where all the information is a sequence of zeros and units. In addition, this version demonstrated faster convergence at algorithm testing. Each variable is coded by a certain fragment of the chromosome, consisting of a fixed number of genes (digits). Adjacent fragments are not separated from each other in any way, but at backward decoding of the chromosome into a variable vector one and the

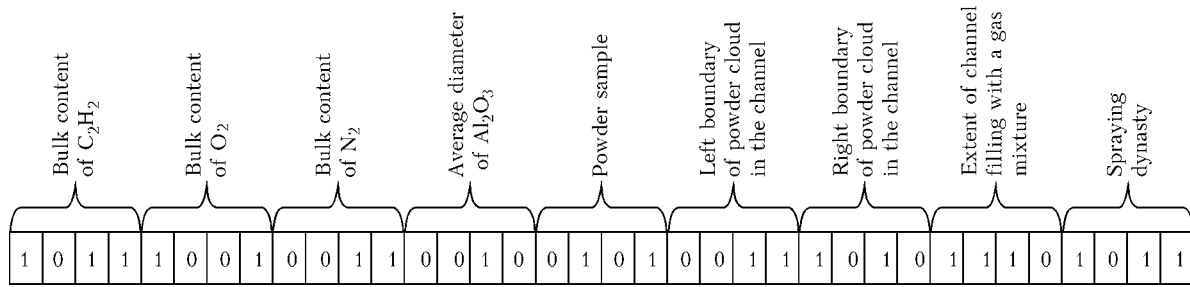


Figure 2. Example of a chromosome mapping mask

same mapping mask is used over the entire simulation period. Chromosome dimension is determined proceeding from the number of optimization parameters and bit number, required for each parameter coding. The interval of possible values of parameter  $k_i[a_i, b_i]$  and accuracy of its discrete variation  $\epsilon_i$ , are taken into account. Allowing for the set conditions, bit number  $t_i$ , required for coding  $k_i$  is found from relationship:

$$t_i = \frac{\ln \left( \frac{b_i - a_i}{\epsilon_i} + 1 \right)}{\ln 2}$$

As an example, Figure 2 shows chromosome mapping for the most often used in DGSC gas mixture of acetylene, oxygen and nitrogen and aluminium powder.

The direct operation of variable vector coding into a chromosome is not used in GA. The chromosomes are generated at random, all subsequent population changes affect the genetic level first, and only after that the chromosomes are decoded and consequences of these changes are analyzed.

During calculations the new population is produced by acting on the genotype of the parent individuals of genetic operators: crossover, mutation and inversion, the action of which is described in detail

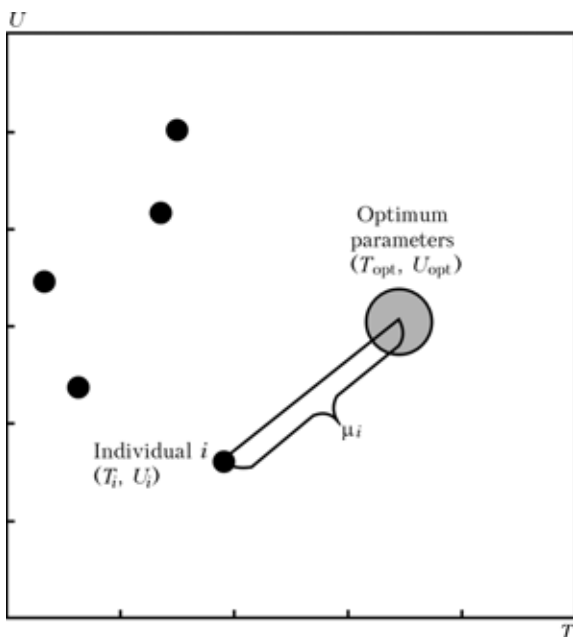


Figure 3. Criteria space for the problem of finding the optimum DGSC process parameters

in [14]. To produce a new chromosome, crossover operator performs exchange of parts into which two parent chromosomes are divided in any point. Mutation operator randomly reverses the state of chromosome genes. Inversion disturbs the gene sequence in the offspring chromosome, compared to the parent chromosome. When searching for a global extremum, the most significant is the crossover operator, as it allows selection of variables, corresponding to the most suitable solution variant for the specified criterion function (unsuitable variants will not be included into the new generation). Inversion operator is also designed for global search, while mutation is identified with the means of local adjustment of the solution.

GA assumes that the number of individuals remains unchanged from generation to generation. Under such conditions, selection of parent individuals for producing a new population is important. Therefore, the probability of any individual in the current population becoming a parent individual is determined in proportion to its adaptation.

At optimization of DGSC process, individual adaptation was determined as follows. Process parameters, produced at chromosome decoding, were used to model the movement of a two-phase flow in DG channel, its outflow into the surrounding gas atmosphere, and average values of velocity  $U_i$  and temperature  $T_i$  of particles on the substrate are calculated. If data on the average values of particle velocity and temperature at interaction with the sprayed surface are available, the individual can be conveniently represented as a point in the criteria space with axes  $U$  and  $T$  (Figure 3). Then adaptation  $\mu_i(t)$  of individual  $A_i$  can be defined as the distance between this individual parameters and the optimum parameters for producing the specified coating, and the optimum values of velocity  $U_{opt}$  and temperature  $T_{opt}$  can be calculated by the following formula:

$$\mu_i(t) = \sqrt{(T_{opt} - T_i)^2 + (U_{opt} - U_i)^2} \rightarrow \min,$$

where  $t$  is the generation number.

After determination of the adaptation of all the individuals in the population, the average adaptation for the population  $\hat{\mu}(t) = \sum_{i=1}^M \mu_i(t)/M$  is found, where  $M$

is the number of individuals in the population. Parent individuals are selected from the individuals with ra-

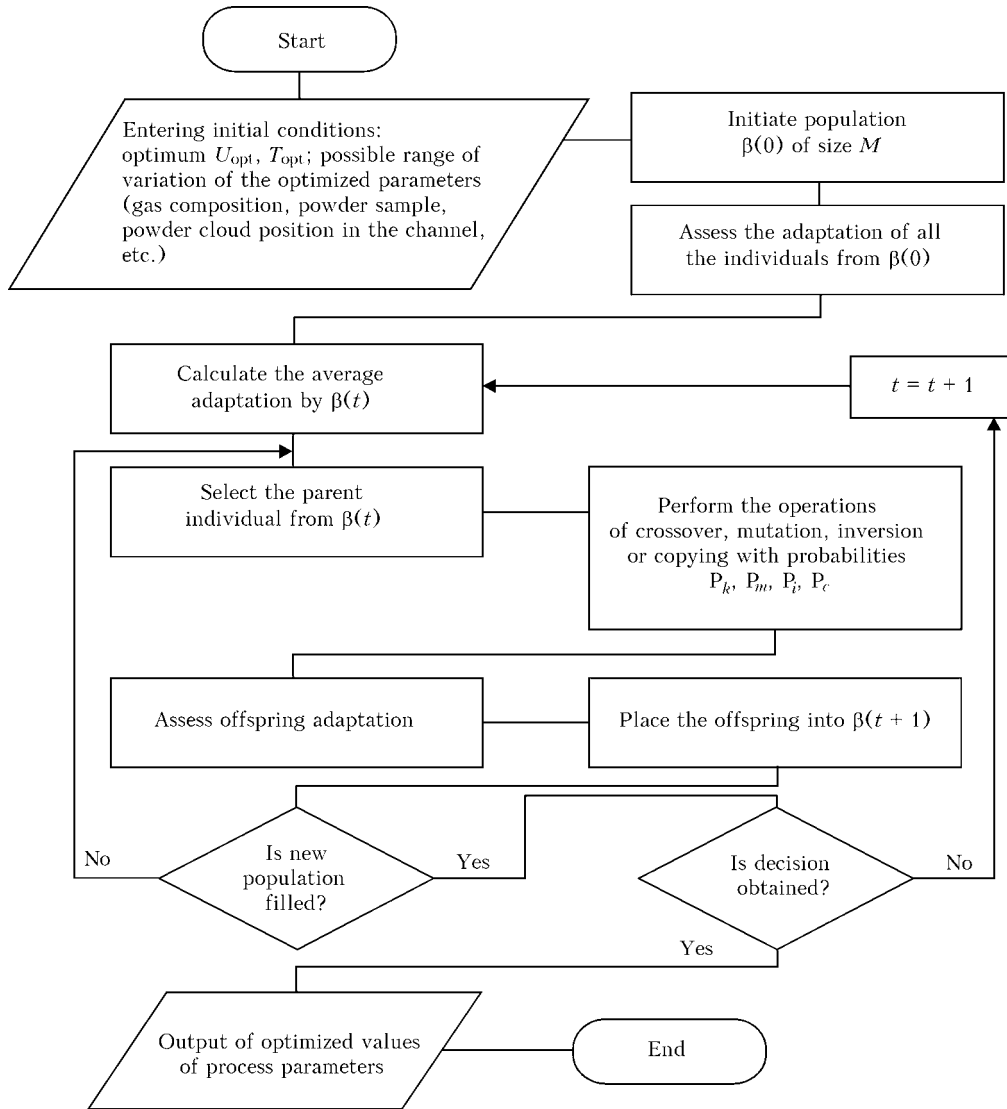


Figure 4. Block-diagram of genetic algorithm functioning

tio  $\mu_1(t) / \mu(t) < 1$  with probabilities in proportion to their adaptation.

Algorithm of searching for optimum process parameters of DGSC is shown in Figure 4. Genetic operators, namely crossover, inversion, mutation and copying procedure (when the individual was transferred to the next generation unchanged) were selected at each stage at random with probabilities of 0.75, 0.05, 0.15, 0.05, respectively. GA functioning was tested when searching for a minimum of Rosenbrok function.

The results of a numeric experiment on determination of optimum parameters of DGSC process for aluminium oxide powder and gas mixture of acetylene, oxygen and nitrogen are given below to illustrate the application of the above algorithm. Initial conditions were as follows: DG channel 1.6 m long and 0.24 m in diameter;  $C_2H_2$  volume fraction was selected to be equal to 1; volume fraction of  $O_2$  1.0–2.5; volume fraction of  $N_2$  0–1; possible particle diameter 20–90  $\mu m$ ; powder sample 0.05–1.00 g; possible position

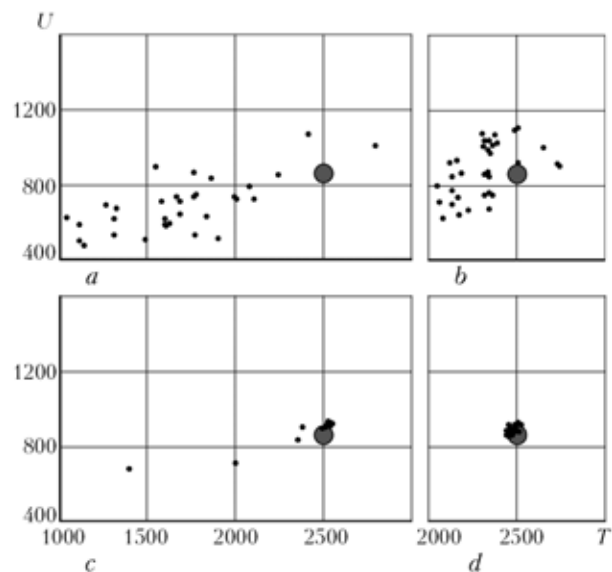


Figure 5. Search for optimum process parameters of DGSC of coatings for aluminium oxide particles: a --- generation number  $t = 0$ ; b --- 4;  $\circ$  --- 16;  $\bullet$  — 25



of left boundary of powder cloud 0.8–1.2 m; right one 1.1–1.6 m from the closed end of DG channel; shooting distance 0.10–0.25 m. Velocity  $U = 850$  m/s and temperature  $T = 2500$  K were selected as the optimum particle parameters. Population consisted of 30 individuals. Searching for optimum process parameters is shown in Figure 5.

As is seen from Figure 5, GA converges rather quickly, and by 25th generation all the individuals are grouped around the extremum. The following parameters were obtained: gas mixture  $C_2H_2 + 1.7O_2 + 0.88N_2$ ; particle diameter 20  $\mu m$ ; powder sample 0.05 g; left boundary of powder cloud 0.8 m from the closed end of DG channel; right boundary 1.28 m; shooting distance 0.1 m. Calculation time in a PC with Pentium 4 processor was equal to approximately 1 h.

Thus, software developed on the basis of a genetic algorithm, essentially simplifies machine experiments on optimization of DGSC process parameters and shortens the time required. This is achieved by complete automation of the process of searching for optimum solutions, so that operator actions are reduced to just entering the initial conditions. Further on this program will be integrated into a system of supporting decision taking, when designing DGSC technologies.

1. Bartenev, S.S., Fedko, Yu.P., Grigorov, A.I. (1982) *Detonation coatings in machine-building*. Leningrad: Mashinostroenie.
2. Boguslaev, V.A., Dolmatov, A.I., Zhemanyuk, P.D. et al. (1996) *Detonation coating deposition on parts of aircraft engines and process fixtures with magneto-abrasive post-treatment*. Zaporozhie: Deko.
3. Shorshorov, M.Kh., Kharlamov, Yu.A. (1978) *Physico-chemical principles of detonation-gas spraying of coatings*. Moscow: Nauka.
4. Zverev, A.I., Sharivker, S.Yu., Astakhov, E.A. (1979) *Detonation spraying of coatings*. Leningrad: Sudostroenie.
5. Karamysheva, S.A., Prokhorov, E.S. (1986) Influence of the shape and degree of channel filling by explosive mixture on parameters of particle acceleration in detonation spraying units. In: *Transact. on Problems of Detonation Application in Technological Processes*. Novosibirsk: IGSO AN SSSR.
6. Lugscheider, E., Papenfub-Janzen, N. (2002) Simulation of the influence of spray parameters on particle properties in APS. In: *Proc. of ITSC'2002*, Essen.
7. Kharlamov, M.Yu. (2003) Dynamics of acceleration and heating of powder by detonation-gas jet. In: *Transact. on Resource-Saving Technologies for Manufacturing and Pressure Treatment of Materials in Machine-Building*. Part 1. Lugansk: V. Dal SNU.
8. Belotserkovsky, O.M., Davydov, Yu.M. (1982) *Method of coarse particles in gas dynamics*. Moscow: Nauka.
9. Nigmatulin, R.I. (1978) *Principles of mechanics of heterogeneous media*. Moscow: Nauka.
10. Zhdan, S.A., Fedenyuk, V.I. (1982) Parameters of equilibrium gas flow in the detonation unit channel. *Fizika Goreniya i Vzryva*, **6**, 103–107.
11. Nikolaev, Yu.A. (1978) Model of kinetics of chemical reactions at high temperatures. *Ibid.*, **4**, 73–76.
12. Kharlamov, M.Yu. (2002) Calculation of product composition and parameters of gas mixture detonation in spraying of coatings. *Visnyk V. Dal SNU*, **11**, 254–262.
13. Kruglov, V.V., Borisov, V.V. (2002) *Artificial neural networks. Theory and practice*. Moscow: Gor. Liniya–Telecom.
14. Voronovsky, G.K., Makhotilo, K.V., Petrashev, S.N. et al. (1997) *Genetic algorithms, artificial neural networks and problems of virtual reality*. Kharkov: Osnova.
15. Batishchev, D.I., Isaev, S.A. (1997) Optimisation of multiextremal functions using genetic algorithms. In: *Transact. on High Technologies in Engineering, Medicine and Education*. Voronezh: VGTU.

# FUSION WELDING OF TITANIUM AND ITS ALLOYS (REVIEW)

V.E. BLASHCHUK<sup>1</sup> and G.M. SHELENKOV<sup>2</sup>

<sup>1</sup>E.O. Paton Electric Welding Institute, NASU, Kiev, Ukraine

<sup>2</sup>Open Joint Stock Company «M.V. Frunze Sumy Research and Production Machine-Building Factory», Sumy, Ukraine

Practical applications of different methods for fusion welding of titanium and its alloys are reviewed. Recommendations on the use of these welding methods are given, and their advantages and disadvantages are considered.

**Keywords:** beam welding methods, metal- and tungsten-arc welding in shielding gases and vacuum, submerged-arc metal-electrode welding, electroslag welding, plasma arc and microplasma welding, titanium, titanium alloys, technological capabilities, base metal thickness

Titanium and its alloys are characterised by special physical-mechanical properties, such as high specific strength and corrosion resistance under atmospheric conditions, in sea water and in a number of aggressive environments, where many traditional materials exhibit low or insufficient strength [1].

The scopes of commercial application of titanium and its alloys depend in many respects upon the technological capabilities of a welding process. Substantial difficulties in welding of titanium arise, first of all, because of its high reactivity at increased temperatures. Titanium alloys lose ductility and acquire sensitivity to delayed fracture as a result of interaction with atmospheric gases. Defects (e.g. pores) are formed in the welds, resulting in a considerable decrease in fatigue resistance and leading to fracture of a welded structure. Welding of thermally unstable alloys is hampered by peculiar structural changes and phase transformations in the weld and HAZ metal during the thermal-deformation welding cycle, which may lead to formation of brittle and unstable phases. However, selection of appropriate welding methods and utilisation of optimal conditions of welding and postweld heat treatment can help to provide sound welded joints.

The majority of the existing fusion welding methods (except for manual arc welding using stick electrodes) are applied now for joining titanium and titanium alloys [1–7].

The purpose of this study is to systematise information on technological capabilities of processes for fusion welding of titanium and its alloys of different thickness.

The main difficulty arising in fusion welding of titanium is to ensure reliable protection of the weld pool, weld root and cooling regions of the welded joints from contact with air.

Regions of a welded joint heated to a temperature above which a marked interaction of titanium with atmospheric gases begins require shielding. As indi-

cated in home literature and standards, this temperature is equal to 400 °C [2–4], while according to the AWS standards it is equal to 500 °F (250 °C) [7]. Vacuum and inert gases, such as argon, helium and their mixtures, are used for shielding. As the quality of the welded joint depends upon the purity of inert gas, argon of the first (volume content of argon is not less than 99.987 %) and highest grade (GOST 10157–79), as well as high-purity helium (TU 51-940–80) are used for shielding. In western countries argon (EN439, class 11) and helium (EN439, class 12), as well as their mixtures (EN439, class 13) are used, according to EN439:1994. Selection of a shielding gas is based on ANSI/AWS C5.6-94R [7].

The following versions of shielding of the welding zone with an inert gas are used, depending upon the sizes of parts welded and requirements to their quality:

- general shielding of a part in chamber with a controllable atmosphere. This is the case of the most reliable shielding of the welding zone and cooling regions of the weld, its root and HAZ. It is reasonable to use this type of shielding in mass production and manufacture of parts of complex configuration;

- local shielding of a welded joint using local micro chambers, which finds application primarily in welding of circumferential position and roll butt joints. In this case the back side of the weld is shielded through filling the workpiece cavity with an inert gas;

- jet-type shielding of the welding zone and cooling regions of the joint, provided through their continuous blowing using a nozzle with a larger orifice diameter and longer extension, compared with welding other metals and alloys. Blowing of the weld root is provided using an additional device, which feeds inert gas from below [2–9]. Therefore, in this case the shielding gas is fed into three channels: into a nozzle and shielding devices, i.e. elongated extension and forming protective backing.

Welding of titanium alloys in vacuum is performed under a pressure of residual gases equal to  $1 \cdot 10^{-2}$  Pa. Welding in low (about 1–10 Pa) vacuum also finds application. This atmosphere is much cleaner as to the oxygen and nitrogen content than argon of class 1. Welding in vacuum eliminates any contamination of

metal of the welded joints with harmful impurities (gases) and provides ductility and toughness of the welded joints as close as possible to those of the base metal (BM) [3–5, 8].

Quality of the titanium welded joints is determined in many respects by the technology used for preparation of edges for welding, as well as by the grade of a titanium welding wire. Preparation of edges for welding is performed only by machining. Roughness of the edge surfaces should be not worse than  $R_z = 40$  (GOST 2789). The surfaces of parts adjoining the edges on both sides at a distance of not less than 20 mm are cleaned with a scraper or electrocorundum wheel, or with a rotating metal brush or vulcanite wheel. No overheating of metal is permitted in cleaning with abrasive wheels, as it causes formation of temper colours on the welded joint surfaces. Immediately before tack welding and welding, the cleaned surfaces of the welded joint and welding wire are degreased, and then moisture is removed using a clean cotton cloth wetted with acetone or commercial ethyl alcohol.

Arc welding methods have received the widest acceptance for welding titanium. Among them the most widespread method is tungsten-electrode inert-gas (TIG) welding. This welding method is most versatile, as it allows a joint to be welded in different spatial positions and under restrained conditions, and requires no re-adjustment of equipment when thickness of a metal welded or type of a joint is changed.

TIG welding is performed at direct current of straight polarity. The tungsten electrode is a cathode, and its life, shape of a pointed tip and constancy of emissive ability determine in many respects the welding process stability, quality of weld formation and penetration depth. The Table gives data on correspondence of tungsten electrodes to a number of national and international standards. Electrodes of pure (un-alloyed) tungsten are not applied for welding titanium, as they are characterised by an insufficient life [3, 4, 7]. Diameter of a non-consumable electrode is selected depending upon the amperage, allowing for a permissible current load.

Automatic, mechanised and manual welding can be performed using a continuous or pulsed arc. Plates of titanium alloys with thickness  $b \leq 5$  mm can be joined in single pass by TIG welding using the surface arc without groove preparation (maximal welding current  $I_w \leq 500$  A). Titanium butt joints of large thickness are made by multipass welding with groove

preparation or with a narrow gap using filler wire. Titanium welding wires are used as filler materials for welding titanium and its alloys. Composition of a welding wire depends upon the type of the materials joined and postweld heat treatment of the weldments [1–4, 7].

Pulsed-arc TIG welding using straight polarity current pulses is used to join sheets 0.5–2.0 mm thick. Size of the weld can be changed through regulating the welding current and speed, as well as duration of the current pulses and pauses. With this welding method the level of deformation of titanium structures is 15–30% lower than in welding using the continuous arc, the level of residual stresses and sensitivity of the welds to porosity, which is the main defect in welding using the surface arc, are decreased. In addition, the HAZ and crystalline grains are decreased in size, which leads to improvement of mechanical properties of the welded joints [3, 4].

Some improvements in the TIG welding method were made to increase the penetrating power of the arc. The following modifications of TIG welding are available for joining titanium and its alloys: immersed arc welding with or without electromagnetic stirring of the weld pool, welding with through penetration, welding over the flux layer, welding using flux-cored filler wire, narrow-gap (slot) welding, twin-arc welding, etc. [2–12].

In immersed-arc welding the tungsten electrode tip is located below the surface of the metal welded. This leads to a substantial rise in the efficiency of utilisation of thermal power of the arc and allows metal plates with  $b \leq 15$  mm to be welded in one pass without groove preparation. In the case of two-sided welding the titanium plates with thickness  $b \leq 36$  mm can be welded by this method. The welds on each side of a plate are made in two passes without filler wire: the first pass is made by the immersed arc to ensure the required penetration depth, and the second pass is made by the surface arc to smooth the weld and impart it the required geometric sizes.

The arc is immersed manually (at small thickness of the metal plates —  $b \approx 8$ –10 mm) or using a special forcing automatic system that controls the arc voltage. The drawbacks of this method include large width of the weld and coarse-crystalline structure of the weld metal, as well as impossibility to regulate chemical composition of metal and high sensitivity to porosity (Figure 1) [2–4, 10].

In immersed-arc welding the controlled movements of molten metal in the pool, excited by the axial magnetic field, provide the possibility of rationally affecting the thermal-concentration processes that determine the solidification processes. This leads to improvement of structure of the weld metal and dramatic decrease in its porosity [2–3, 11].

Twin-arc welding, where the arcs are burning at tungsten electrodes in the axial magnetic field, allows a 1.5–2 times increase in the permissible speed of the welding process without the risk of formation of such

Correspondence of tungsten electrodes to standards

ISO 6848 EN26848NF EN26848 JIS Z3233 AWS A5.12-98	ANSI/AWS A5.12	Types of tungsten electrodes	GOST 23949-80	Nominal content of activating addition
WC20	EWCe-2	R 07932	---	2 % CeO <sub>2</sub>
WL10	EWLa-1	R 07941	EVL	1 % La <sub>2</sub> O <sub>3</sub>
WT20	EWTh-2	R 07912	EVT-12	2 % ThO <sub>2</sub>

specific defects of the welds that accompany the forced conditions as elongated gas cavities. Electromagnetic stirring of the weld pool brings the level of mechanical properties and electrochemical characteristics of a welded joint close to those of BM, and favours decrease in defectiveness of the welds, porosity in particular [2–3, 11].

Welding with two tungsten electrodes located in plane normal to the weld axis was developed to increase the deposition efficiency in multilayer one-sided TIG welding of titanium plates  $b \leq 50$  mm thick with groove preparation. Welding of metal plates  $b = 50$  mm thick by this method is performed in 6–8 passes using filler wire with diameter  $D_w = 5$ –7 mm. This method is applied in the cases where the weld metal differs in composition from the base metal, as well as for cladding. The resulting welded joints are characterised by high quality (Figure 2). This welding method and the equipment used to implement it were developed by the E.O. Paton Electric Welding Institute [3–5, 12].

TIG welding with through penetration allows metal plates with  $b \leq 12$  mm to be welded in one pass, the set arc length being 0.5–1.0 mm. To provide the «keyhole» type penetration, the welding parameters are set so that a hole is formed in metal beneath the arc, and as the arc advances this hole is filled with liquid metal. To form the weld reinforcement with this welding method, it is necessary to make the second pass using a filler wire. However, application of this welding process is limited by difficulties associated with regulation of chemical composition of the weld metal over the entire weld section [3, 4].

Argon-arc welding over the flux layer (A-TIG) is an efficient method for affecting the penetrating power of the arc, as well as the weld formation and weld metal structure. With this welding method halides of alkali and alkali-earth metals leading to a change in character of metal penetration and weld formation through arc contraction are added to the arc atmosphere. A-TIG welding over the flux layer deposited on the surfaces of the weld edges allows the one-pass welds to be made without groove preparation on titanium plates with  $b \leq 6$ –7 mm. In this case the current and heat input required for welding can be substantially decreased owing to an increased concentration of thermal energy in the anode spot. Flux leads not only to increase in the penetration depth, but also to change in the penetration shape. Width of the back bead in A-TIG welding grows faster with increase in the welding current than width of the weld. Conditions of the back bead formation are improved, and the probability of burns-through in welding without backing is reduced [3–5].

Low heat input and small width of the weld and HAZ allow application of A-TIG welding not only for making butt joints, but also fillet, T-, overlap, plug and other types of joints in titanium plates with  $b \leq 3$  mm, which are hard or impossible to weld without the application of flux. Welding of overlap and

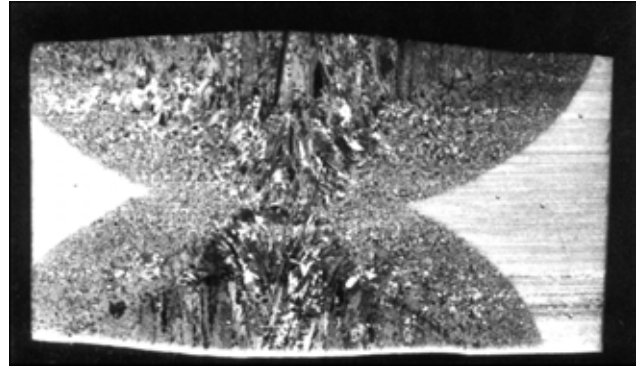


Figure 1. Macrosection of butt welded joint 24 mm thick made by immersed-arc welding

plug joints can be done either with through or incomplete penetration of the lower plate. Small volume of the weld pool makes it possible to employ A-TIG welding for making welds in different spatial positions on a vertical plane in titanium plates with  $b \leq 6$  mm. Distortion of welded structures is reduced by 15–20 %, and porosity is eliminated as a result of the application of fluxes. This welding method is especially suitable for joining heat-hardenable and high alloys. However, A-TIG welding requires an increased accuracy of fit-up for welding, compared with TIG welding. Special fluxes of the ANT-A and FAN-1 grades were developed for this welding method [3–5].

To feed the required amount of the flux in welding titanium plates with  $b > 4$ –5 mm, it is added to the arc from the core of a flux-cored filler wire with a titanium sheath. This makes it possible to perform one-pass welding of titanium plates with  $b \leq 16$  mm. A layer of solidified slag, which provides additional shielding for the cooling metal, remains on the weld surface after A-TIG welding and welding using flux-cored filler wire. It should be removed by machining or by a chemical method, which adds to labour consumption in welding operations.

Narrow-gap welding is employed to join titanium plates of medium and large thickness. This welding method allows the volume of deposited metal to be decreased by about 30 %, the process productivity to be raised and labour consumption in performing op-

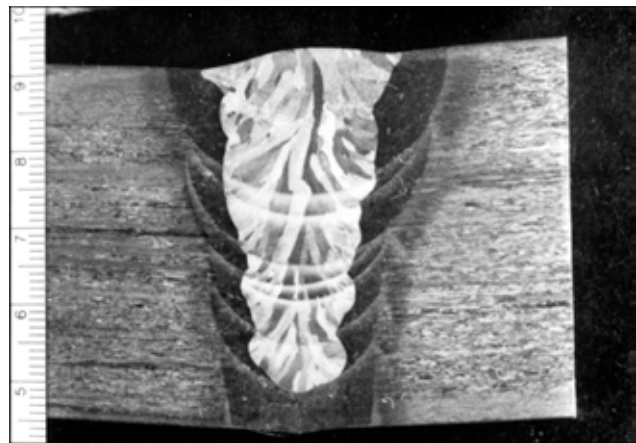
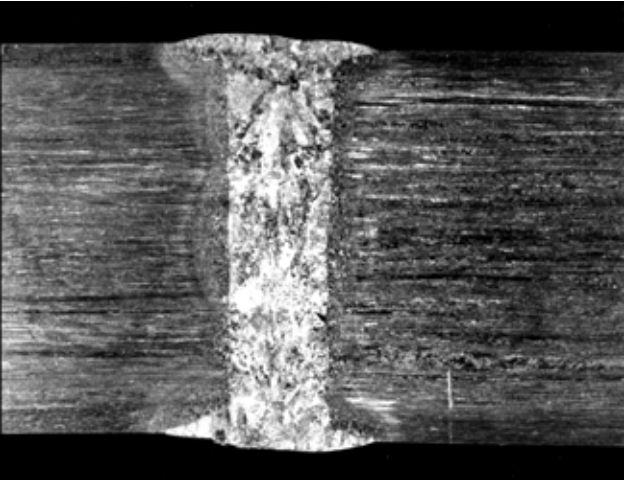


Figure 2. Macrosection of butt welded joint 30 mm thick made by twin-arc welding using a filler



**Figure 3.** Macrosection of butt welded joint 24 mm thick made by manual narrow-gap welding in axial magnetic field

erations associated with edge preparation for welding to be reduced. The torch with a special device providing welding in reversible axial magnetic field (Figure 3) is used to ensure reliable fusion of the weld metal with the groove walls in manual tungsten-electrode welding [1–3, 11, 13].

The method of automatic narrow-gap magnetically-impelled arc tungsten-electrode welding is applied to weld metal plates with  $b \leq 110$  mm. This welding method allows reduction in utilisation of welding consumables, 1.5–2 times increase in process productivity and decrease in defectiveness of welded joints in titanium alloys [3, 4, 13, 14]. This welding method provides the weld metal with a homogeneous structure and welded joints with high values of mechanical and corrosion properties.

TIG welding with the surface arc is applied for position and roll but welding of pipes and welding

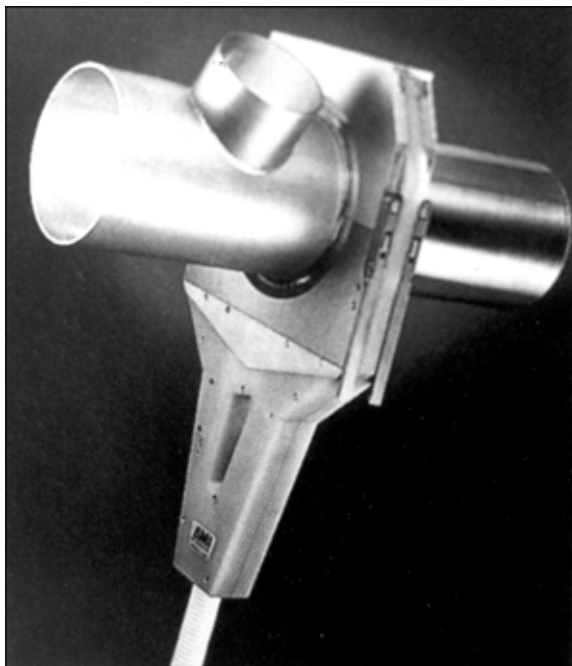


**Figure 4.** Chamber with built-in electric motor to drive tungsten electrode under field conditions (manufactured by Arc Machines, USA)

of tubes to tube plates. In this case the use is made of a specialised equipment, which cannot be employed with other welding methods. These processes are considered in more details in studies [2–4, 7, 15–17].

The E.O. Paton Electric Welding Institute developed and manufactured a range of specialised equipment with captive protective micro chambers, in which the required purity of inert gases is achieved owing to argon purging. This equipment is intended for position butt welding of titanium pipes 10 to 200 mm in diameter ( $b = 0.5$ – $2.0$  mm) under field conditions. Such chambers are located around a mill, the tungsten electrode is moved using an electric motor, which is set both at a distance from a chamber and in one unit with it. Welding can be performed in a continuous or pulsed mode. Figure 4 shows the general view of a modern welding micro chamber made as one unit with the electric motor.

TIG welding of tubes to tube plates in heat exchangers of titanium alloys can be performed in two positions, i.e. in flat position and on a vertical plane. A deep shaft for vertical location of a heat exchanger is arranged in a workshop to perform flat welding. With this welding method a tube plate is located in a horizontal plane. At the absence of shafts, the tube plate is placed on a vertical plane and tubes are placed on a horizontal plane. The appropriate welding methods, i.e. manual or automatic TIG welding, are applied depending upon the size of heat exchangers and spatial location of the welds. These operations are performed by using special equipment of a domestic (Open Joints Stock Company «M.V. Frunze Sumy Research and Production Machine-Building Factory» in Sumy, Ukraine) or foreign production (ESAB, Sweden; Astro Arc Polysoude, France; etc.) [15–18].

Along with TIG welding, also plasma (PW) and microplasma (MPW) welding performed in inert gases are applied for making permanent joints in titanium and its alloys. These processes are intended for welding titanium plates with thickness  $b \leq 1.5$  mm. The shielding methods used in these cases are similar to those used with TIG welding. PW is a high-speed and high-productivity process. It is performed with the constricted arc of a cylindrical shape, which is formed through its constriction by the nozzle walls. The PW equipment is of the following types: for welding titanium plates ( $b \leq 4$  mm) at a high or low current, and for metal-electrode welding with the arc burning in the plasma flow [1–4, 19–21].

The constricted transferred arc burning between the electrode and workpiece is used as a heat source for MPW of titanium. A stable arc burning and spatial consistency of microplasma at low currents ( $I_w \geq 0.1$  A) are achieved owing to a high degree of constriction of the arc column, which is provided by using a nozzle with a small-diameter (up to 1 mm) channel and pilot arc continuously burning from the second power source. MPW of titanium is performed at a direct current of straight polarity using the arc burning in a continuous or pulsed mode. Argon is used as



a plasma gas, and helium or Ar + (50–70 %) He mixture is used as a shielding gas. The mean working length of the arc in MPW is almost by an order of magnitude larger than in tungsten-electrode welding in argon. Therefore, comparatively large deviations of the arc length from an assigned value are permitted with this welding method, as this has no substantial effect on the weld parameters. In a case of welding titanium parts with  $b \leq 0.3$  mm, the joints are made by flanging the edges, and at  $b = 0.1$ – $0.2$  mm the workpieces are assembled for welding using precision devices. Butt joints can be made with or without backing. The E.O. Paton Electric Welding Institute developed corresponding designs of plasmatrons and power supplies. Mechanical properties of the MPW joints are practically identical to those of BM. Any ingress of tungsten to the weld is eliminated with this welding method.

PW provides deeper penetration than TIG welding. Therefore, PW of parts with  $b > 10$  mm can be performed without groove preparation. In a case of PW of thick plates of titanium with the «keyhole» type penetration, the maximal thickness of the plates welded by the one-pass method is determined primarily by width of the back bead, the formation of which is affected by surface tension forces. Filler wire can be fed to the leading part of the weld pool. In this case the requirements to its diameter and feed speed are as stringent as in TIG welding. The groove in this case is one- or two-sided V-shaped. The use of a filler wire widens the range of welding parameters (gap, edge displacement, welding speed), and it is possible to control chemical and structural composition of the weld metal, thus preventing the formation of cracks, undercuts, pores and enabling a substantial increase in volume of the deposited metal.

The special heat source for welding processes was developed to combine advantages of vacuum shielding and technological merits of TIG welding. This source provides an arc discharge between the tungsten or titanium hollow non-consumable cathode (ADHC) and a workpiece in vacuum, and it is inferior in energy parameters only to the beam energy sources. Argon is fed at a low flow rate through the hollow cathode during welding. Realisation of this process is 3–5 times less expensive, compared with the beam welding processes, due to a low cost of equipment and less stringent requirements to edge preparation and safety measures (corresponding to the level of safety in arc welding performed in a controlled atmosphere). Arc welding in vacuum allows joining of titanium parts with  $b = 8$ – $12$  mm without groove preparation in one pass without backing in the through penetration mode with a smooth transition to BM on the face and back side of the weld. Joining of titanium plates with  $b = 12$ – $20$  mm is performed without groove preparation by the two-sided welding method using a small-diameter filler wire. The latter should pass through the ADHC plasma and touch the tailing part of the weld pool. This welding method is applied to make a closing

weld on titanium spherical tanks. Performance of welded joints made by the ADHC method is at a level of or even higher than that of the joints made by TIG welding.

Welding with a 1.6–5.0 mm diameter consumable electrode in inert gases (MIG) finds application for making butt, T- and overlap joints in titanium plates with  $b \leq 3$  mm in flat position. Welding is performed at a direct current of reverse polarity. MIG welding of titanium can provide optimal properties of the welded joints by choosing composition of the weld metal through changing the metal electrode chemical composition or adjusting the BM content of the welded joints. Diameter of the wire used for automatic welding is 1.6–5.0 mm, and that used for mechanised semi-automatic welding is 1.6–2.0 mm [1–4].

In MIG welding of titanium, the size of the weld and quality of its formation depend upon the shielding gas fed to the torch. The welds made in the helium atmosphere are characterised by a smoother transition from reinforcement to BM, compared with the argon atmosphere, while penetration in this case is wider and shallower, other conditions being equal. The use of helium allows the thermal power of the arc and melting process productivity to be increased, which is especially important for welding of titanium plates with medium or large thickness. However, MIG welding performed in argon causes smaller spattering of the molten metal than welding in helium. The flow rate of argon is 2–3 times lower than that of helium. In addition, the arc voltage is lower when welding is performed in argon. Therefore, it is recommended that welding of titanium be performed in a mixture of He + 0.2 Ar, which provides good weld formation and process stability. Welding of butt joints in titanium alloy plates of medium and large thickness is performed with groove preparation, the optimal value of the included angle being  $60^\circ$  (Figure 5).

The method of welding with metal electrode preheated through ohmic resistance from a separate low-voltage source was suggested to increase the deposition efficiency of automatic MIG welding with the stable arc and increased process speed. In this case the deposition efficiency grows and the penetrating power of the arc decreases. Pulsed-arc MIG welding allows the joints to be made in different spatial positions under field conditions, penetration of BM to be stabilised and spattering to be avoided. This is provided by superimposing the high-power short-time current pulses on the direct-current arc, and enables the process of formation of a droplet at the electrode tip to be regulated. Automatic MIG welding ensures high ductility, strength and impact toughness of the weld metal.

Mechanised MIG welding, unlike the automatic one, is applied primarily for making T-joints (e.g. welding-in of connecting pipes) in thin-sheet titanium structures. This can be explained by an increased weight of the torch equipped with protective devices and difficulty to ensure a reliable shielding of the

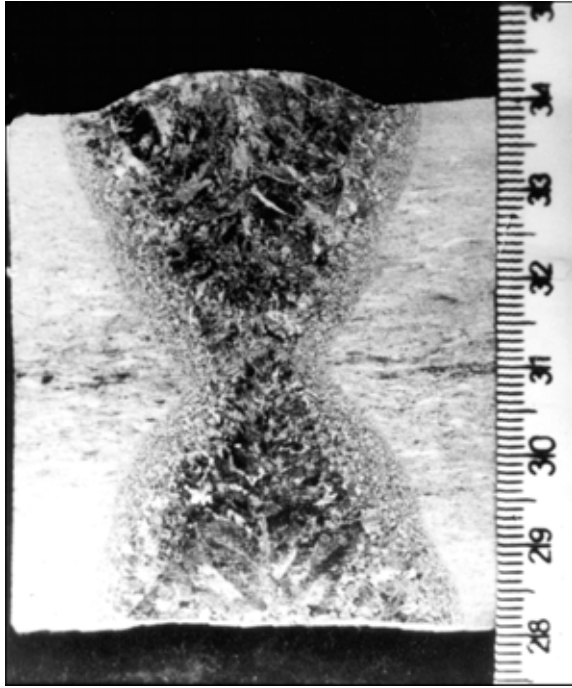


**Figure 5.** Macrosection of butt welded joint 60 mm thick made in titanium alloy VT1 by two-sided MIG welding with groove preparation

welding zone and cooling weld regions. Welding with metal electrode 1.6–5.0 mm in diameter at a direct current of reverse polarity was suggested for welding titanium parts with  $b = 2\text{--}50$  mm in vacuum. This welding method provides considerable ductility of the weld metal owing to its high purity as to the content of harmful impurities (gases). This method was initially developed for welding in space and verified under the zero-gravity conditions [3].

The technology of vertical narrow-gap welding using metal electrode in argon with a horizontal location of the weld pool and equipment for its realisation were developed for automatic welding of radial joints on spheres of titanium alloy plates with  $b = 30\text{--}130$  mm. In this case the gap is filled in one pass by weaving the welding nozzle through thickness of a workpiece. The technology and equipment provide high quality of the welds, decrease in labour

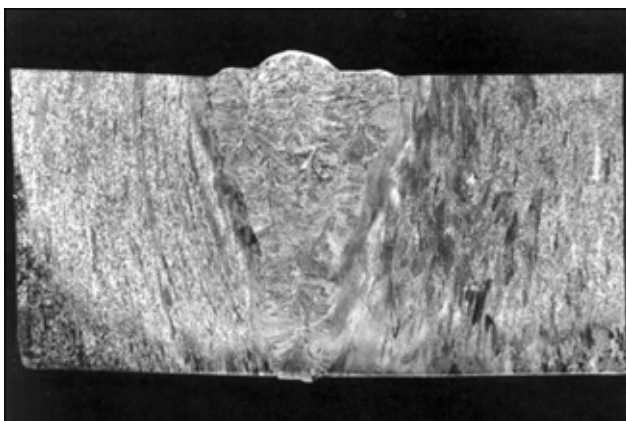


**Figure 6.** Macrosection of welded joint 60 mm thick made by multipass submerged-arc metal-electrode welding

consumption during welding and reduction in consumption of welding wire by 10–15 % [22].

The E.O. Paton Electric Welding Institute developed the technology for submerged-arc welding with metal electrode using the air-stream granulation oxygen-free halide fluxes of the ANT series to join plates of titanium alloys with  $b = 2.5\text{--}40.0$  mm. Submerged-arc welding of butt, fillet and overlap joints is performed at a direct current of reverse polarity. Welding of butt joints in titanium plates is carried out on a copper backing, flux pad or permanent backing with  $b \leq 3$  mm. The metal plates with  $b \leq 10\text{--}12$  mm are welded in one pass without groove preparation, and those with  $b \geq 20\text{--}25$  mm are welded with multipass welds. To improve weld formation, welding is performed in a groove with an included angle of  $90^\circ$  and root face of 3–5 mm (Figure 6) [3, 4]. The procedure of automatic submerged-arc welding of titanium hardly differs from that used for welding of steels. The weld is cleaned from the slag crust after all its regions are cooled down to  $300\text{--}350^\circ\text{C}$ . Metal of the welds made by the submerged-arc method with metal electrode is characterised by satisfactory mechanical properties, high density and absence of pores.

The E.O. Paton Electric Welding Institute developed the electroslog welding (ESW) method for joining titanium plates with thickness  $b \geq 40$  mm. Because of a high electrical resistance of titanium, welding by this method is performed using electrodes of a large cross section ( $D_w \leq 5$  mm), i.e. plate and wire electrodes, as well as consumable nozzles. Refractory oxygen-free fluxes (of the ANT-2 type) are utilised for ESW, and surface of the slag pool is shielded with argon [3, 4, 23, 24].

In welding with a plate electrode ( $b \leq 350$  mm) the weld formation is provided using split copper water-cooled moulds. ESW with one or two electrode wires is employed to join titanium plates with  $b = 30\text{--}110$  mm. The consumable-nozzle ESW process and appropriate equipment were developed for joining large-size parts of titanium alloys. Selection of optimal welding parameters providing the permissible process energy allows production of the welds with good formation (Figure 7).

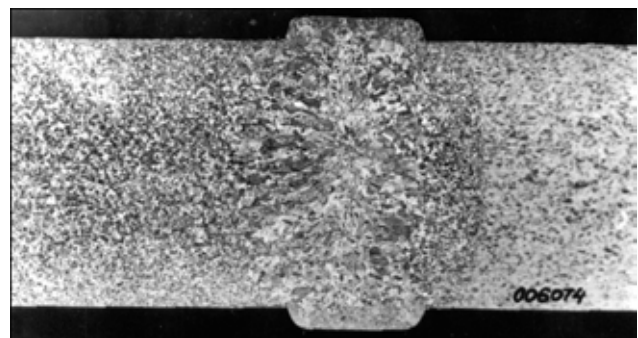


**Figure 7.** Macrosection of butt welded joint 60 mm thick made in titanium alloy VT1-0 by ESW using plate electrode

ESW of  $\alpha$ - and pseudo  $\alpha$ -alloys, as well as low ( $\alpha + \beta$ ) titanium alloys provides welded joints with satisfactory mechanical properties in a case of using electrodes (plates, consumable nozzles, electrode wires) with a composition identical to that of BM, despite a coarse-crystalline martensite-like structure of the weld metal. In ESW of high-strength two-phase ( $\alpha + \beta$ ) titanium alloys using electrodes close in composition to BM it is not always possible to provide required mechanical properties of welded joints, especially if it is necessary to subject the welded joints to heat hardening. In this case it is recommended to find an optimal composition of the weld metal, differing from that of BM. The most promising method for refining a coarse-crystalline structure of the deposited metal is to affect the weld pool by the external magnetic field.

Among the fusion welding methods the beam methods find an increasingly wide application. Electron beam welding (EBW) received the widest acceptance for joining titanium [3–5, 8]. EBW of titanium is performed in vacuum (under a pressure of residual gases ranging from  $1 \cdot 10^{-3}$  to 1 Pa), this providing environmentally clean production conditions and a high level of comfort in operation of the equipment. However, it requires a high degree of mechanisation and automation of all operations. A high energy concentration in the electron beam (the maximum power density is  $5 \cdot 10^7$  W/cm<sup>2</sup>), locality of metal heating (the lowest density in a cross section is  $1 \cdot 10^{-4}$  cm<sup>2</sup>), minimal distortion of metal welded, vacuum protection of the welding zone and cooling weld regions, remote control of the technological process, precise controllability of space-energy parameters of the electron beam, high efficiency and low operational costs (with substantial initial capital investments), as well as good mechanical properties of the welded joints made by EBW predetermine its competitiveness and high prospects. To produce sound welds in EBW of titanium, a higher accuracy of fit-up for welding, compared with fusion arc welding processes, and strict keeping to a permissible size of the gap between the weld edges are required. Therefore, in a number of cases EBW is performed with the thickened edges, which are removed by machining after completion of the welding process.

EBW of titanium is characterised by deep penetration at low values of heat input. The minimal melting zone in EBW leads to a substantial decrease in distortion of workpieces, compared with other fusion welding methods. EBW of titanium can be used to make the fundamentally new types of the welds, e.g. joining of structural members located at different height, welding in narrow gaps, as well as making of slot welds, where the lower element is accessible for a direct impact by the heat source. EBW of titanium parts is performed in flat position or with a horizontal beam and through penetration. The weld can be made on a horizontal or vertical plane. Horizontal location of the weld pool provides quality formation of the

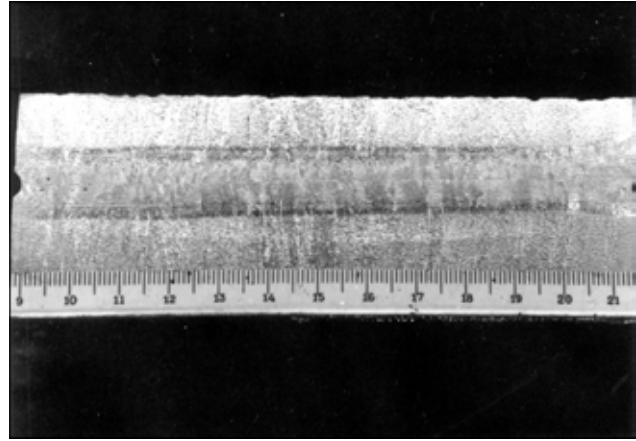


**Figure 8.** Macrosection of butt welded joint 120 mm thick made in titanium alloy VT6 by EBW using a horizontal beam

welds with almost parallel boundaries on the titanium alloy plates with  $b \geq 100$ –150 mm (Figure 8).

$\alpha$ - and pseudo  $\alpha$ -alloys of titanium, as well as alloys with a stable  $\beta$ -structure are characterised by good weldability when joined by the EBW method. The thermal cycle of EBW provides welded joints with high ductility and toughness. The EB welded joints in ( $\alpha + \beta$ ) titanium alloys have satisfactory mechanical properties. The most common defect of the EB welded joints in titanium alloys is porosity, which is the main cause of fatigue fracture of the weldments.

Laser welding (LW) has found application for joining titanium and its alloys [25–28]. Laser radiation provides a high energy concentration. In this respect it is much superior to other energy sources used for welding (the minimal cross section area of the laser beam is  $1 \cdot 10^{-6}$  cm<sup>2</sup>, the highest power density is  $1 \cdot 10^9$  W/cm<sup>2</sup>). In contrast to EBW, LW of titanium requires no vacuum chambers. The LW process is carried out in shielding gases, i.e. argon or helium. That is why it can be employed to join structural members of any dimensions. A distinctive feature of laser radiation is simplicity of its transportation. It can be directed using optical mirror systems to hard-to-reach locations, fed to substantial distances without energy losses, and used simultaneously or sequentially in several work places. These peculiarities of laser radiation make it possible to easily and promptly control the LW process. In addition, the laser beam is insensitive to the effect of magnetic fields generated by the process fixture. This provides quality formation of the welds over their entire length.

Solid-state and gas lasers generating the periodic-pulse or continuous waves are applied for welding titanium plates from 0.2 to 25.0 mm thick. The processes of automatic and manual LW of small sections can be carried out both in the CW and pulsed modes (seam and spot welding). LW with deep penetration is performed only in the automatic mode. Advantages of LW with deep penetration are especially pronounced in welding of titanium. Comparison of EBW and LW as to their technological and economical parameters shows that LW is indicated for welding of



metal plates with  $b \leq 5$  mm (the beam power is up to 4 kW), and EBW is more economically advantageous for welding of titanium plates with  $b \geq 10$  mm (the beam power is more than 10 kW). LW requires that the laser beam be precisely guided and exert a stable effect. The laser welds are characterised by a high quality, which in the majority of cases allows avoidance of their subsequent treatment. Mechanical properties of laser welded joints in titanium are at a level of properties of BM. Drawbacks of LW include a high cost of laser radiation sources. A serious problem in LW of titanium is formation of pores in the root part of the welds, which is caused by a drastic change in solubility of gases during rapid cooling and solidification of metal.

Ion-beam welding of titanium in vacuum with a controlled evolution of gases (oxygen, nitrogen) from the welds involves the use of high-density ion flows. Electron-ion welding can be used to alloy the weld metal. However, at present these welding processes [29, 30], as well as the light beam welding process [31], find no practical application.

Fabrication of welded structures with high technological and economical indicators always involves the need to select a welding method, which has to correspond to the maximal possible degree to specific production and service conditions. The proper choice of a welding method provides the required quality and efficiency of specific welding joints, which eventually affects the technical level of production of the weldments, as well as their performance and life. Modern fusion welding methods allow successful joining of titanium plates with thickness ranging from fractions of a millimetre (laser and microplasma welding) to tens of centimetres and more (EBW and ESW).

Several versions of value analysis (VA) were developed and found commercial application for selection of a welding technology or its improvement. VA is a method for system examination of an object (workpiece, process, structure), which is intended for revealing and utilisation of the improvement reserves. The main initial condition of VA is that each object has functionally excessive costs, which can be revealed, eliminated or utilised in a more efficient way [32].

- Gorynin, I.V., Gechulin, B.B. (1990) *Titanium in machine-building*. Moscow: Mashinostroenie.
- Shelenkov, G.M., Blashchuk, V.E., Melekhov, R.K. et al. (1984) *Manufacture and operation of titanium equipment*. Kiev: Tekhnika.
- Gurevich, S.M., Zamkov, V.N., Blashchuk, V.E. et al. (1986) *Metallurgy and technology of welding titanium and its alloys*. Kiev: Naukova Dumka.
- Gurevich, S.M. (1990) *Reference book on welding of non-ferrous metals*. Kiev: Naukova Dumka.
- Zamkov, V.N., Prilutsky, V.P., Shevelev, A.D. (1992) *Metallurgy and technology of welding titanium alloys*. In: *Welding and Surfacing Rev.* Vol. 2.
- (1997) *Forming, welding, brazing and heat treatment of titanium and its alloys in aircraft engineering*. Ed. by A.G. Bratukhin. Moscow: Mashinostroenie.
- (1998) *AWS Welding Handbook*. Vol. 4.
- Nazarenko, O.K., Kajdalov, A.A., Kovbasenko, S.N. et al. (1987) *Electron beam welding*. Ed. by B.E. Paton. Kiev: Naukova Dumka.
- (2000) Specialized gas shielding for titanium. *Welding J.*, **3**, 56.
- Dolotov, B.I., Muraviov, V.I., Ivanov, Yu.L. et al. (1997) Immersed tungsten electrode welding of VT20 alloy on non-treated edges. *Svarochn. Proizvodstvo*, **7**, 25–27.
- Chernysh, V.P., Kuznetsov, V.D., Briskman, A.N. et al. (1983) *Welding with electromagnetic stirring*. Kiev: Tekhnika.
- Zamkov, V.N., Topolsky, V.F., Kushnirenko, N.A. (1978) Twin-arc tungsten-electrode welding of thick titanium plates. *Avtomatich. Svarka*, **2**, 44–47.
- Belous, V.Yu. (2002) Narrow-gap arc welding of titanium alloys (Review). *The Paton Welding J.*, **9**, 35–39.
- Paton, B.E., Zamkov, V.N., Prilutsky, V.P. (1996) Narrow-groove welding proves its worth on thick titanium. *Welding J.*, **5**, 37–41.
- Tsaryuk, A.K. (1998) Welding of tubes to tube plates (Review) *Avtomatich. Svarka*, **4**, 25–29.
- Nikitin, V.B., Stepanov, V.I. (2001) Manufacture of heat exchanging apparatuses using titanium alloys for the «Alkholma» heat power plant. *Tekhnologiya Mashinostroeniya*, **2**, 53–57.
- (1996) Customized orbital welding meets the challenge of titanium welding. *Welding J.*, **12**, 39–41.
- Tsaryuk, A.K. (2000) Equipment for welding of tubes to tube plates. *Svarshchik*, **4**, 12–13.
- Blashchuk, V.E., Onoprienko, L.M., Shelenkov, G.M. et al. (1993) Plasma welding of titanium alloys. *Avtomatich. Svarka*, **3**, 31–33.
- (1979) *Microplasma welding*. Ed. by B.E. Paton. Kiev: Naukova Dumka.
- Nerovny, V.M. (2001) Vacuum arc welding of titanium alloys. *Tekhnologiya Mashinostroeniya*, **2**, 27–30.
- Gorbach, V.D., Khvalynsky, V.N. (2002) New technologies for manufacture of marine engineering load-carrying spherical structures. *Svarochn. Proizvodstvo*, **7**, 28–33.
- Zamkov, V.N., Lychko, I.I., Topolsky, V.F. (1999) ESW of plates of grade 5 titanium alloy. *Avtomatich. Svarka*, **9**, 73–75.
- Yushchenko, K.A., Lychko, I.I., Sushchuk-Slyusarenko, I.I. (1999) Effective techniques of electroslag welding and prospects for their application in welding production. In: *Welding and Surfacing Rev.* Vol. 12.
- Gedopt, J., Delarbre, E. (2003) Pulsed Nd:YAG laser welding of titanium EAR implants. In: *Proc. of Int. Conf. on Laser Technologies in Welding and Materials Processing*, Katsiveli, Ukraine, May 19–23, 2003. Kiev: PWI.
- Gavrilyuk, V.S., Zhilkin, A.M., Ivanov, N.L. (2000) Laser treatment of materials. *Tekhnologiya Metallov*, **5**, 32–44.
- Abbott, D.H., Arcella, F.G. (1998) Laser forming of titanium components. *Advanced Materials and Processes*, **153**(5), 29–30.
- Pronin, M.M., Startsev, V.N., Popov, V.O. et al. (1999) Laser treatment of materials. *Voprosy Materialovedeniya*, **3**, 375–393.
- Gabovich, M.D., Protsenko, M.D., Poritsky, V.Ya. et al. (1980) Ion-beam welding of titanium alloy VT6. *Avtomatich. Svarka*, **2**, 69–70.
- Gabovich, M.D., Khomich, V.A., Nazarenko, O.K. (1993) Electron beam welding with weld alloying. *Ibid.*, **10**, 49–50.
- Frolov, V.A., Pronin, N.S., Fyodorov, S.A. et al. (2003) Development and advancement of technology for light beam welding, brazing and heat treatment. *Svarochn. Proizvodstvo*, **11**, 19–21.
- Demchishev, P.G., Mariin, S.B. (2004) Express-VA immersed tungsten-electrode welding process. *Svarka v Sibiri*, **1**, 31–34.

# CO<sub>2</sub>-LASER CUTTING OF DISK SAW BODIES

V.D. SHELYAGIN, V.Yu. KHASKIN and A.G. LUKASHENKO  
E.O. Paton Electric Welding Institute, NASU, Kiev, Ukraine

It is shown that laser cutting is a good choice for manufacture of disk saw bodies made from steel 65G sheets 2 to 6 mm thick. This cutting method provides high quality and small width of a cut, minimum HAZ and low manufacturing costs. Good prospects for development of a hybrid laser-plasma cutting technology are noted. The technology is characterised by stabilisation of the arc plasma by the laser beam and its additional contraction, thus making plasma penetrate into the keyhole formed in cutting.

**Keywords:** laser cutting, disk saws, tool steels, parameters, cutting facility, laser upgrading, three-axis manipulator, cutter, computer control

Pattern cutting of metal sheets is one of the main processes used in current engineering blanking production, the preference being given to automatic cutting following an arbitrary trajectory [1]. Often it is necessary to make holes in finished parts. In these cases no buckling or distortion is permitted, cutting forces characteristic of mechanical cutting methods are also undesirable [2]. There are industrial sectors, e.g. ship building, where it is required to cut thick (up to 100 mm thick) steel plates at a very high productivity [3]. The best process for this case, allowing a high quality of cutting of almost any material within a wide range of thickness to be combined with high productivity, is laser cutting.

Transition to a short-run production characteristic of the current industry of Ukraine makes it unpractical to use dies, while this urges enterprises to use mechanical, plasma or laser cutting of metal. The latter has the following advantages [4]: wide range of materials to be cut, ensuring a thin cut owing to sharp focusing of the laser beam, small heat-affected zone, minimal mechanical effect on a blank, chemical cleanliness of the cutting process, possibility of automating the process, high productivity, possibility of cutting of complex profiles with 2D or 3D configurations. As a result, this method can provide the net-shape blanks with a high-quality cut, requiring no subsequent machining. The method is characterised by the absence of mechanical deformation of the blanks, while the process of location and spacing of the blanks is free from human factor.

One of the hot problems for Ukraine is manufacture of disk saws used to cut wood, stone and metals. Disk saws applied in blanking production have complex configurations (Figure 1), which is caused by decrease in mechanical and dynamic loads on a disk during cutting. Such saws can operate at an increased (up to 3000 min<sup>-1</sup>) rotation frequency. Manufacture of the saws includes the following operations: laying-out of a tool steel sheet allowing for its subsequent treatment, finish cutting of the tool steel sheet following a trajectory corresponding to the saw profile,

heat treatment of a type of normalising (if necessary), surface grinding of a disk saw blank, and brazing (welding) of hard-alloy segments. One of the most labour-consuming and critical operations is finish cutting of a saw blank profile from a tool steel sheet (usually steel 65G). In this case thickness of a steel sheet is selected from a range of 2 to 6 mm, depending upon the saw diameter (300–900 mm).

We suggested using CO<sub>2</sub>-lasers with a radiation power of up to 1 kW for cutting of disk saw blanks. This cutting method has sufficient productivity (cutting speed may amount to 1–5 m/min) and can provide low roughness of the cut edges (approximately  $R_a = 2.5 \mu\text{m}$ ).

We conducted comparative experiments on optimisation of the laser and microplasma cutting technologies, showing that higher cutting speeds could be achieved with microplasma cutting. However, microplasma cutting has substantial drawbacks: the angle of taper of a cut is up to 30° to vertical, and width is 2.5–3.5 mm. The latter is especially undesirable in terms of ecology, as a large amount of metal goes to slime and harmful fumes, which are then ejected into the atmosphere. Besides, in making disk saw blanks, in addition to producing vertical edges (at an angle as close as possible to 90° to the saw plane) and thin (up to 1 mm wide) cuts, in locations of subsequent brazing of hard-alloy segments it is necessary to provide cut profile radii of no more than 0.5 mm.

Considering the above-said, the laser cutting technology providing a cut width of 0.5 mm was chosen

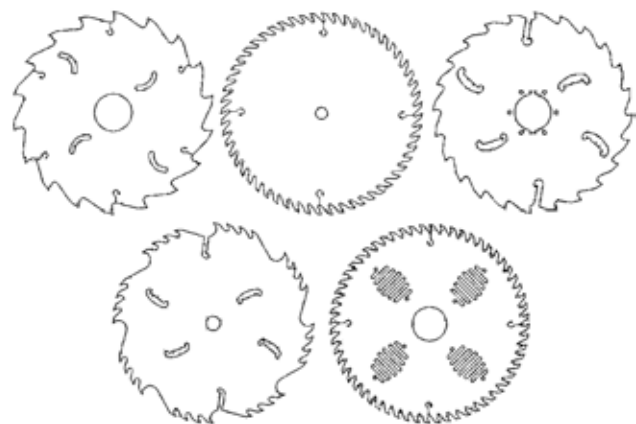
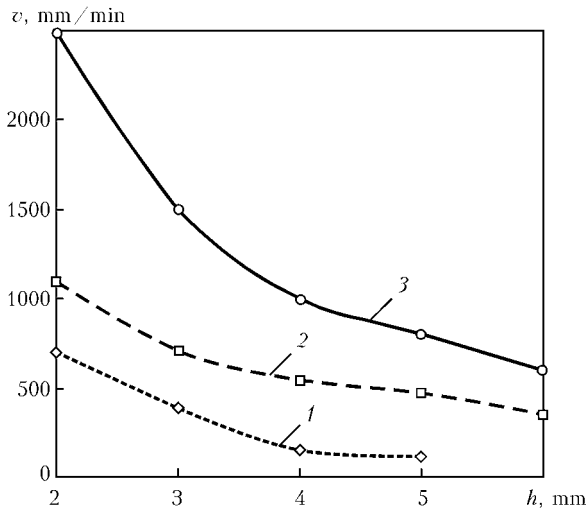


Figure 1. Types of bodies of disk saws used in current blanking production



**Figure 2.** Dependence of speed  $v$  of 700 W CO<sub>2</sub>-laser cutting upon thickness  $h$  of steel 65G sheet cut with compressed air (1), air-oxygen mixture with a component ratio of 3:1 (2) and oxygen (3) used as a cutting gas

for the given application. It meets the above requirements to the manufacture of disk saw blanks. Figure 2 shows dependence of the cutting speed upon the thickness of a cut sheet of steel 65G. The dependence was derived in optimisation of the laser cutting technology using CO<sub>2</sub>-laser with mode TEM<sub>10</sub>. To implement this technology, the E.O. Paton Electric Welding Institute developed the special computer-controlled automated facility (Figure 3). The Bulgarian 1.3 kW laser «Hebr-1A», produced in 1989, which we upgraded, is used as a technological laser in the facility [5]. To ensure consistent operation of the laser, the water-cooling system of ballast resistors is replaced by resistors with air cooling. Lining of the gas-discharge chamber and composition of a working gas mixture are also changed. The latter is important in terms of economic operation of the laser. According to certificate data, gas mixture CO<sub>2</sub>:N<sub>2</sub>:He should be in a ratio of 1:10:30, but in this case one bottle of helium (the most expensive gas) is sufficient only for 40 h of operation. So, we changed this proportion to 1:6:4, which allowed us to extend the time of using a helium bottle to 200 h at a laser radiation power of 1 kW. Therefore, the cost of 1 h operation of the laser was decreased 5 times.



**Figure 3.** Computer-controlled automated technological facility for laser cutting based on upgraded CO<sub>2</sub>-laser «Hebr-1A»

In the developed facility the three-axis manipulator «Granit-1600» of an ingenious design is used to move the «flying» optics. Compressed air under a pressure of more than 0.3 MPa and electric motors with a linearly flared-out stator are used to move the beam (axis  $y$ ) and carriage (axis  $x$ ) along the polished granite guides. Movement of a cutting head (axis  $z$ ) is carried out from the electric motor with a rotating rotor. The values of movement of the tool (cutting head) along the axes are as follows:  $x:y:z = 1500:1000:50$  mm, the speed of operation in the automatic mode ranging from 0.01 to 22 m/min. Precision of positioning of the tool is not lower than  $\pm 3 \mu\text{m/m}$ .

The circular variable-capacitance transducer located about a cutting nozzle is applied to stabilise position of the focus with respect to a metal sheet being cut. Two water-cooled rotating mirrors of gold-plated silicon and focusing lenses of potassium chloride single crystal with a focal distance of 150, 200 and 300 mm are employed in the optical tract. To

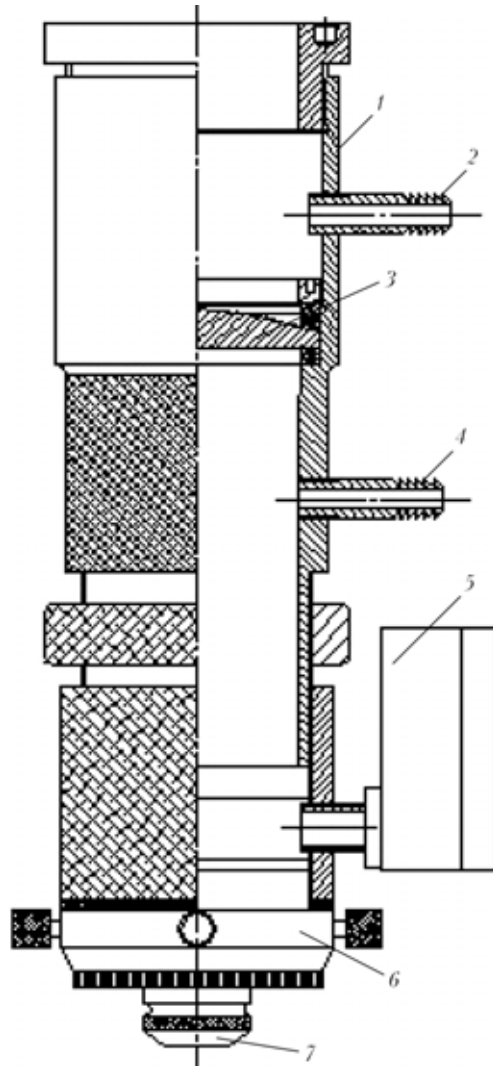


**Figure 4.** Schematic diagram of laser cutter used in the technological facility for laser cutting of disk saw bodies: 1 --- casing; 2 --- connection for air cooling of lens; 3 --- focusing lens; 4 --- connection for feeding of cutting gas; 5 --- manometer; 6 --- cutting nozzle alignment system; 7 --- cutting nozzle

extend the life of the lenses, their air cooling is provided for in our design of the laser cutter (Figure 4).

Computer based on a processor operating at a frequency of not lower than 300 MHz and CNC system are used to control the laser facility. The control software developed for OS Windows makes it possible to automatically convert the files of drawings stored in AutoCAD 2000 and higher into its format. Therefore, there is no need to convert design documents into machine codes.

One of the key points of adaptation of the technological process of laser cutting of steel 65G sheets to peculiarities of the developed facility is selection of shape and diameter of a cutting nozzle, as well as composition of a cutting gas. Air, air-oxygen mixture (in different proportions) and pure oxygen were used as a cutting gas (see Figure 2).

As established experimentally, it is reasonable to reduce diameter of the cutting nozzle approximately to a diameter of the focused laser beam passing through it (to 0.6 mm in our case) and make it as close as possible in shape to the Laval nozzle [6]. Cutting should be performed in pure oxygen.

This approach does not only lead to rise in productivity, but also allows the cut to be narrowed, the size of flash at the cut edges to be minimised and, hence, wastes and harmful fumes formed in cutting to be reduced, the flow rates of oxygen being comparatively low (150–200 l/h). Continuous air cooling of the upper part of a lens with periodic (corresponding to laser radiation) feed of oxygen makes it possible to avoid thermal cracking of the lens, and the lens location seal prevents mixing of air with oxygen. The experiments proved high prospects of the hybrid laser-plasma cutting technology, in which plasma penetrates into the keyhole. A practical example of application of laser cutting is a disk saw body (Figure 5), which was cut using our automatic facility.

## CONCLUSIONS

1. Laser cutting, providing an improved quality and decreased (4–6 times) width of a cut, is a good choice for manufacture of bodies of saw disks made from 2–6 mm thick sheets of steel 65G, despite a higher cost of laser equipment. The use of laser cutting allows

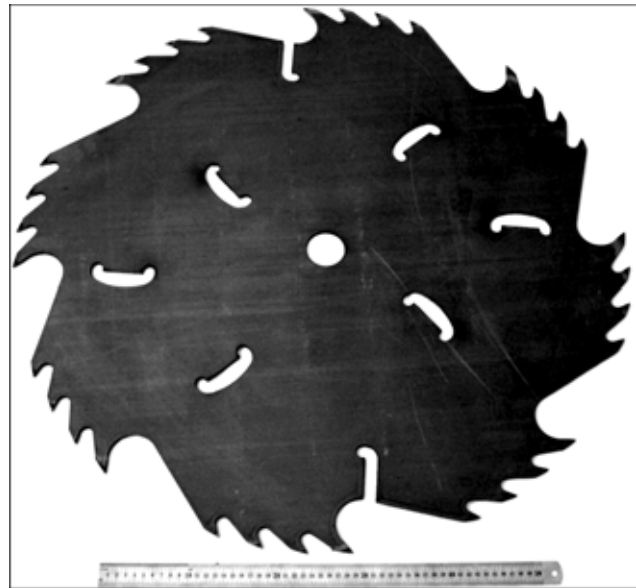


Figure 5. Body of a disk saw 800 mm in diameter made from steel 65G sheet 5 mm thick

the size of HAZ to be decreased and some finishing operations to be eliminated, which decreases the costs of manufacture of disk saws.

2. Decrease in the cut width leads to a substantial decrease in the amount of slime and harmful fumes ejected into the atmosphere. This factor is important for mass production in terms of ecology, and it should be taken into account in selection of technology and development of equipment.

1. Aichele, G., Nickenig, L. (2003) Laserstrahlschneiden — Maschinenbauarten und zu trennende Werkstoffe. *Praktiker*, **10**, 302, 304–306.
2. Muraviov, V.I., Matvienko, D.V., Mariin, B.N. (2003) Effect of gas-laser cutting in commercial nitrogen atmosphere on properties of titanium alloy welded joints. *Svarka v Sibiri*, **2(10)**, 33–35.
3. Hencock, R. (2003) Laser-oxygen cutting of steel sheets up to 75 mm thick. *Svarshchik*, **6**, 18–19.
4. Grigoriants, A.G., Sokolov, A.A. (1988) Laser technique and technology. In: *Laser cutting of metals*. Manual for institutes for higher education. Book 7. Ed. by A.G. Grigoriants. Moscow: Vysshaya Shkola.
5. Abilsiitov, G.A., Golubev, V.S., Gontar, V.G. et al. (1991) *Technological lasers*. Refer. Book. Vol. 1: Calculation, design and service. Ed. by G.A. Abilsiitov. Moscow: Mashinostroenie.
6. (1973) *Large Soviet Encyclopedia*. 3rd ed. Vol. 14, 242. Moscow: Sov. Entsiklopediya.

# TECHNOLOGICAL PECULIARITIES OF HIGH-ALLOY STEEL WELDING BY ELECTRODES WITH RUTILE COATING

I.N. VORNOVITSKY<sup>1</sup>, N.V. ZAKHAROVA<sup>1</sup>, O.V. SHISHKOVA<sup>1</sup>, A.A. VILISOV<sup>2</sup> and A.V. ZINCHENKO<sup>2</sup>

<sup>1</sup>Closed Joint Stock Company «Elektrod», Zheleznogorsk, Russia

<sup>2</sup>Personnel Upgrading Center, Perm, Russia

The paper presents the technological advantages of rutile type electrodes for high-alloy steel welding, compared to electrodes with a basic coating type. Information is given on the new grades of electrodes, developed at CJSC «Elektrod».

**Keywords:** arc welding, stainless steels, coated electrodes, rutile type coating, technological properties

Specialists of Company «Elektrod» developed a series of grades of electrodes with rutile coating for welding of high-alloy steels. These electrodes are branded with a letter-digit designation ZhZL (ZhZ stands for Zheleznogorsk Plant, L --- for welding of high-alloy steels). Table 1 presents certain characteristics of the electrodes. The «Elektrod» continues developing and improving electrodes with rutile and other coating types for welding of high-alloy steels and alloys. Such known electrode grades as OZL-17U, ANZhR-1, ANZhR-2 and others are their prototypes.

In the last twenty-three years the way of using the electrodes with rutile coating for welding of high-alloy steels has changed as against electrodes with a basic coating for the same purpose. Analysis of the information [1–3] allows a statement that a share of rutile-coated electrodes in the total volume of the electrodes produced for welding of high-alloy steels is about 80 %, the rest are the electrodes with the basic and other coatings.

A share of electrodes with rutile coating for welding of high-alloy steels makes up in the post-soviet territory only 10 %, though during several decades

the Moscow Experimental Welding Plant, the E.O. Paton Electric Welding Institute and a number of other organizations [4, 5] have been actively involved into their development and improvement.

Advantage of the electrodes with rutile coating is in their high technological maneuvering ability, which essentially facilitates the work of the welder, decreases labor intensity and provides high quality of welded joints.

The rutile electrodes are characterized with an easy striking and a repeated striking of arc, a possibility to weld with AC and DC, spray metal transfer and formation of a smooth fine-ripple weld surface facilitating easy and often spontaneous detachment of the slag whose thermal expansion coefficient is 1.5 times higher than in the basic slag. It is though necessary to emphasize a small sputtering of the electrode metal. All mentioned properties are provided by a thorough selection of the coating composition, which contains a considerable fraction of rutile or its products.

Other functional advantages of rutile electrodes (a possibility of welding of thin-plate structure and vertical down welding, increased productivity of the process) is determined by the diameter of the electrode and thickness (weight coefficient) of the coating. In this case the weld formation and a number of the

**Table 1**

New grades of electrodes with rutile coating	Type of electrode (GOST 10052–75)	Grades of welded steels	Grades of prototype electrodes with basic coating
ZhZL-1	E-08Kh17N8M2	10Kh17N13M2T, 08Kh17N5M3, 08Kh16N13M2B	NIAT-1
ZhZL-6	E-10Kh25N13G2	10Kh23N18, 20Kh23N18, 08Kh21N6M2T, 08Kh23N6	OZL-6, TsL-25
ZhZL-8	E-07Kh20N9	08Kh18N10, 12Kh18N10T, 08Kh18N12B	OZL-8
ZhZL-11	E-08Kh20N9G2B	08Kh18N12B, 08Kh18N12T	TsL-11
ZhZL-15	E-08Kh19N10G2B	12Kh18N12T	TsT-15
ZhZL-400	E-07Kh19N11M3G2F	08Kh17N13M2T	EA-400/10U
ZhZL-NZh/13	E-04Kh20N9	06Kh18N11, 04Kh18N10	UONI-13/NZh-2, OZL-6
ZhZL-395	E-11Kh15N25M6AG2	KhN35VT, Kh15N25AM6	EA-395/9



above mentioned factors of the electrodes depend on the behavior of the molten metal and slag. Specifically, viscosity of rutile slags of both non-alloyed and alloyed electrodes is higher than in other types of commercial electrode slags. Many skillful welders learnt how to properly use this property of the slag in welding in different spatial positions.

A higher arc voltage of the electrodes with rutile coating is another advantage in comparison with electrodes with basic coating at practically similar welding current (Table 2).

It is believed that the arc temperature of the electrodes with rutile coating is higher than of electrodes with basic coating while melting rate of the electrodes with rutile coating is known to be higher than of the electrodes with the basic coating. These factors suggest a necessity to correct the groove shape, for example, size of the root gap and root face for welding of butt welds.

With the aim of developing practical guidelines for welding with new electrodes special tests were carried out, their results being presented below.

Due to a very easy striking of the arc the weld pool is formed almost immediately. Its shape, volume and weight are well exposed to regulation due to the welding current and electrode displacement velocity. In addition, the weld pool fluidity is regulated, the metal outflow from the weld pool is prevented and the weld is easily formed in all spatial positions. Rather viscous slag formed under melting of electrodes also facilitates this process. It is the slag viscosity that prevents outflow of the molten metal from the gap during welding of penetration beads, which enables a skillful welder to form a reverse bead or other shape prescribed in the specifications.

Additional tests permit establishing that with an excessive thickness of the coating a part of the formed slag leaks in front of the weld pool making it difficult to control the formation of the weld. This may lead to disturbance of its rectilinearity and shape.

It is also established that a stable easily controlled arc is formed during welding with new electrodes allowing for manipulation with the electrode face in most inconvenient positions for the welder and in all positions of the weld.

An easy repeated striking of the arc makes it possible to make vertical and overhead welds in the continuous and pulse conditions, i.e. with short-term arc brake providing a symmetrical formation of the weld of the prescribed size (width and thickness). This technique (a short brake of the arc) allows welding

**Table 2**

Diameter of electrode, mm	Recommended welding current for electrodes with coatings, A		Arc voltage in welding using electrodes with coating, V	
	Basic	Rutile	Basic	Rutile
2.00	40–65	45–65	22	29
2.50	50–85	60–90	22	29
3.25	85–115	80–120	21	30
4.00	105–160	120–170	21	32

of the thin-plate metal and thin-walled pipes, formation of the penetration layer of the weld with excessive or variable clearance by the perimeter of the pipe (because of incorrect assembling and preparation of pipe butts to the welding).

A possibility to weld with alternating current allows using (especially for assembling and repair) simple and available equipment.

Easy and spontaneous detachment of the slag essentially decreases the labor intensity of welding operations and a probability of formation of slag impurities. However, the welder should remember about a certain danger of getting eye trauma (especially) if the slag detachment is too active.

Tests of ZhZL electrodes reveal a somewhat increased sensitivity of the electrodes to overheating. Therefore, the welding should be performed within the range of currents recommended for every diameter of the electrode under controlled indications of the ammeter.

It has been earlier mentioned that a wide use of electrodes with rutile coating for welding of high-alloy steels has been retarded in this country. Probably one of the reasons is a poor knowledge of the consumers and welders about technological peculiarities of electrodes with rutile coating recognized in many countries of the world. The authors hope that this article will play a positive role in successful mastering of high-alloy electrodes with rutile coating, which is as a new progressive material.

1. (2001) *Schweissgeraete und Schweisszusatzze*. Lincoln Smitweld GmbH. Katalog. Netherlande.
2. (2001) *Consumable for manual and automatic welding*. Welding handbook. Goeteborg: ESAB.
3. (2001) *Welding consumable guide*. Zika. Israel.
4. Sidlin, Z.A. (1985) High-alloy welding electrodes. *Svarochn. Proizvodstvo*, 2, 3–5.
5. Lipodaev, V.N., Kakhovsky, Yu.N. (1976) Development of electrodes for welding of stable-austenite alloys EP943 and EP516. In: *Abstr. of All-Union Conf. on Welding Consumables*, Kiev, Oct. 5-7, 1976.

# INCREASE OF CORROSION RESISTANCE OF WELDED JOINTS OF HIGH-STRENGTH ALUMINIUM ALLOYS BY EXPLOSION CLADDING

S.Yu. ILLARIONOV, L.D. DOBRUSHIN, S.G. POLYAKOV and G.E. BOEVA  
E.O. Paton Electric Welding Institute, NASU, Kiev, Ukraine

Evaluation of explosion welding application was conducted for the case of cladding welded joints of aluminium alloys 7010 and 2024 with pure aluminium. It is shown that such a protection of welds prevents stress corrosion cracking or intercrystalline corrosion.

**Keywords:** explosion welding, explosion cladding, friction stir welding, high-strength aluminium alloys, welded joints, stress-corrosion cracking, intercrystalline corrosion.

Welded joints of aluminium alloys are characterized with a lower corrosion resistance as against basic metal, which is specified by their physical-mechanical and electromechanical heterogeneity. The latter is very typical for welded joints of high-strength aluminium alloys.

Studies of local explosion cladding of welded joints produced by friction stir welding (FSW) using technically pure aluminium were conducted as requested by the Airbus Industries Company to prevent the contact of the corrosion medium with weld surface as well as thermal and thermomechanical effect. This is a relatively new welding method patented in 1991 by the Welding Institute, Great Britain. The essence of this method is that a special rotating tool is penetrated into the butt of the workpiece. As a result of friction, which leads to plasticization of metal around the tool, a heat is evolved subsequently imparting linear motion to the tool and the workpieces. The metal passes over the tool pin and moving from heating to cooling zone forms a joint. This method has high technological potential and permits producing joints of a wide range of aluminium alloys including thermally strengthened ones, as well as steel and copper joints [1].

Previously, anticorrosion explosion cladding of welded joints of the autoclave reaction cups for producing concentrated nitric acid was studied at the E.O. Paton Electric Welding Institute [2]. The apparatuses were produced of technically pure aluminium of grade A85 by fusion welding. Cladding was performed by alloy A85. As a result the durability of the autoclave reaction cups increased about 6 times, which proves a correctness of the chosen approach.

The purpose of this work is to evaluate the efficiency of using explosion welding (EW) for cladding of FSW joints of high-strength aluminium alloys with technically pure aluminium for increasing of their corrosion resistance.

Explosion cladding and subsequent tests were carried out for the following objects:

- butt joints of 7010 T7651 aluminium alloy plates 65 mm thick ( $\sigma_t = 520\text{--}525$  MPa;  $\sigma_{0.2} = 455\text{--}465$  MPa;  $\delta = 12\text{--}12.5$  %) produced by FSW into the depth of down to 13 mm;
- butt joints of sheets of aluminium alloy 2024 T351 4 mm thick ( $\sigma_t = 435$  MPa;  $\sigma_{0.2} = 280$  MPa;  $\delta = 15$  %) produced by FSW through all thickness of the sheets.

Cladding was performed by sheets of alloy 1050 (analog AD0) 2 mm thick. Preliminary metallographic analysis of welded specimens showed that there were sites with grains at a depth of 5 mm oriented perpendicular to the sheet surface in the zone of thermomechanical effect of FSW joints of alloy 7010. Such location of grains most of all facilitates the development of intercrystalline corrosion (ICC), so a layer of metal 5 mm thick was removed from the surface to expose these sites. Besides, a recess was made from the side of the FSW weld root for removal of the acute concentrator caused by an incomplete joint penetration.

Considering the necessity to weld the extended FSW joints a parallel EW scheme was employed when the cladding sheet before welding was located parallel to the surface subject to cladding. As against commonly used angular scheme it is simpler in assembling and is characterized by an equality of the detonation rate of the explosive  $D$  and the rate of the contact point  $V_c$  of the welded surfaces. Since the quality joint for the given pair of metals is achieved at  $V_c \approx 2$  km/s, then a mixture of ammonite # 6ZhV with ammonium nitrate was selected as an explosive. A collision velocity of two sheets determined by the dependencies from the work [3] was about 500 m/s. Criteria of quality of the obtained joint were its equal strength with the metal of the cladding layer (alloy 1050) and the absence of cast metal inclusions on the joint boundary. Microstructures of the joints of the cladding layer and the FSW weld of alloy 7010, respectively, in the longitudinal direction relative to the EW process and cladding layer, and FSW weld of alloy 2024 are shown in Figure 1.

It is noteworthy that a more ductile metal is advisable to use as a cladding layer, therefore alloy 1050 was subjected to annealing before EW. Besides, this

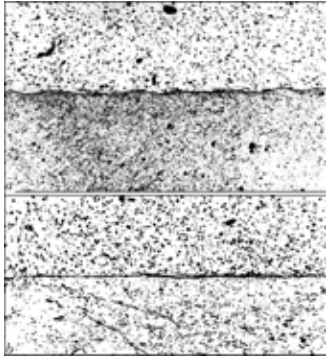


**Figure 1.** Microstructures of the joint zone of cladding layer and FS weld on alloy 7010 (a) and 2024 (b) ( $\times 100$ )

contributed to a smaller deformation of the clad sheets, which is especially important for alloy 2024 with its thickness about 4 mm. Specimens of the FSW joints produced by explosion cladding are presented in Figure 2. Tests on resistance to stress corrosion cracking (SCC) and ICC are carried out to compare corrosion resistance of clad and non-clad (initial) FSW joints. Tests of the FSW joints of aluminium alloy 7010 were carried out by the ASTM G 39 [4] and ASTM G 44 standards [5]. The specimens were tested under loading by a four-point scheme (Figure 3). The load in this case was preset by a value of a maximal deviation of  $y$  determined by the formula

$$y = \frac{\sigma(3H^2 - 4A^2)}{12Et},$$

where  $\sigma$  is the preset load assumed as  $0.75\sigma_y$  for non-clad FSW joints, MPa;  $E$  is the elasticity module, MPa;  $t$  is the specimen thickness, mm;  $H$  is the distance between external supports, mm;  $A$  is the distance between internal and external supports, mm.

The specimens were periodically submerged into chemical solution of 3.5 % NaCl (pH 6.4–7.2) and tested according to the following cycle: 10 min in the solution, 50 min in the air. The tests lasted 40 days. The specimens were cut so that their length was 120 mm (transverse to FSW joint and cladding direction), width — 15 mm (along the joint) and thickness — 4 mm. The enamel EP-5147 (TU U 6.24514086-044–98 «A») was used to protect the specimens from the action of the corrosion medium from the edge and lower surfaces of the FSW joints.

The SCC tests of the FSW joints of aluminium alloy 2024 were carried out by the standards ASTM G 49 [6] and ASTM G 44, the ICC tests — by the standards ASTM G 110–92 [7] and QVA-Z10-59–03 [8].

The SCC-tested specimens were under permanent tensile load, which (like for the specimens with the FSW joints of alloy 7010) was preset equal to  $0.75\sigma_y$  for initial non-clad joints. Testing regime of clad and non-clad FSW joints of alloy 2024 was the same as for the FSW joints of alloy 7010 with the exception of their holding under stress and in corrosion medium being 30 days. Specimens for the ICC tests were carried out so that their length was 70 mm (transverse to FSW joint and cladding direction), width — 50 mm (along the joint). The specimens were placed

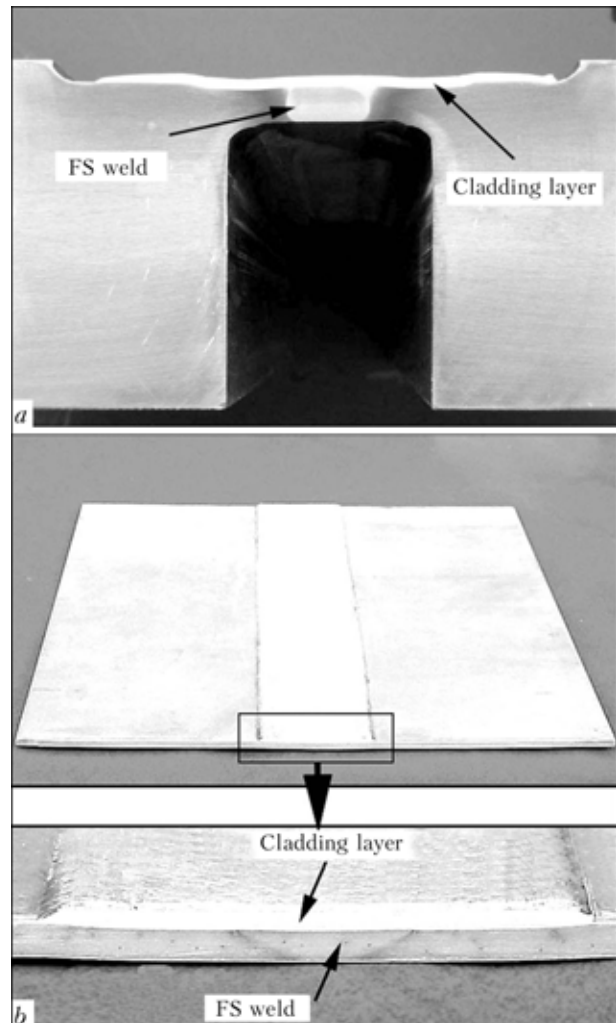


**Figure 2.** Explosion clad of FSW joints of alloys 7010 (a) and 2024 (b)

into the corrosion solution (57 g NaCl + 10 ml  $H_2O_2$  (30 %) + 1000 ml  $H_2O$ ) and held there 6 h at the temperature 30 °C.

The specimens of alloy 7010 (initial and clad) were not destroyed completely during SCC tests. Initial FSW joints of alloy 7010 were fully covered with corrosion products. No corrosion traces were observed on the surface of the cladding layer of alloy 1050 while on the unprotected part of the clad specimens (parent metal) there were the same corrosion traces as on the initial specimens. The metallographic analysis of the initial specimens after tests showed that all of them are subject to ICC. A typical depth of the ICC penetration in the most dangerous thermomechanically affected zone is 150–160  $\mu\text{m}$  (Figure 4, a) while in one case out of all series of speci-

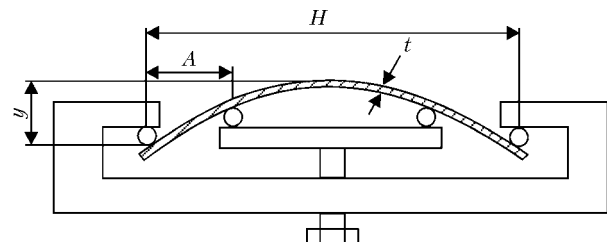


**Figure 3.** Scheme of fixation of the alloy 7010 specimen for SCC tests (for designations see the text)

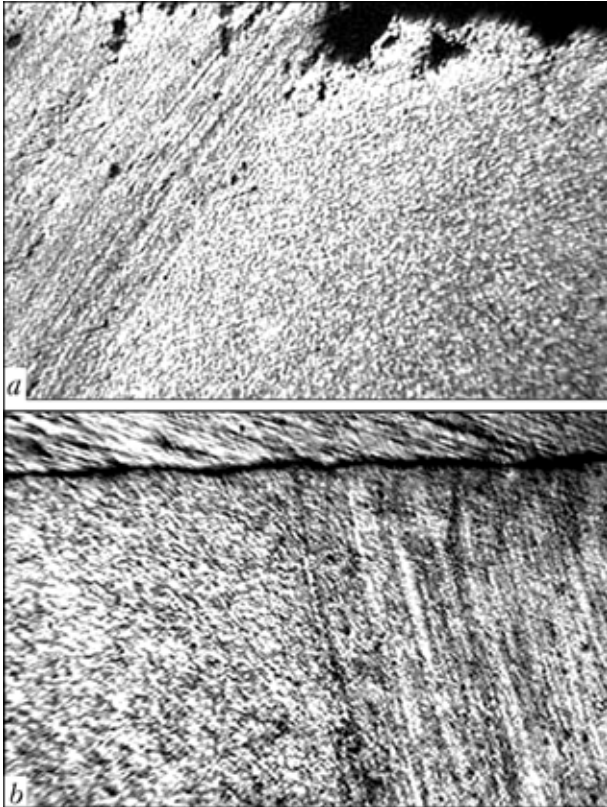


**Figure 4.** Microstructure of thermomechanically affected zone in initial (a) and clad (b) FSW joint of alloy 7010 after SCC test ( $\times 100$ )

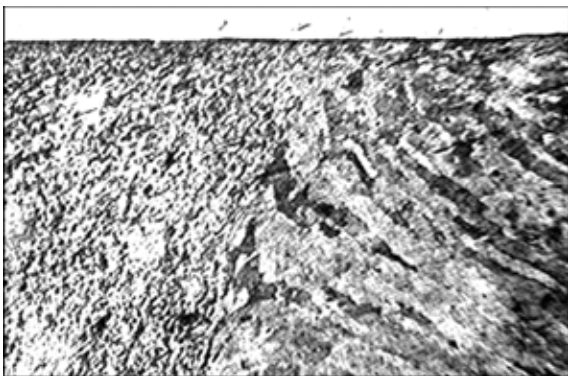


**Figure 5.** Microstructure of thermomechanically affected zone in the clad FSW joint of alloy 2024 after SCC tests ( $\times 100$ )

mens it was  $720 \mu\text{m}$ . No corrosion traces of the FSW joints were observed in the clad specimens (Figure 4, b). Therefore, a cladding layer of technically pure aluminium completely excludes any action of the corrosion medium on the protected weld.

During the SCC tests under uniaxial tensile load of the alloy 2024 joint specimens, the initial specimens were destroyed during the testing period. The presence of pitting corrosion was observed on the surface of the cladding layer but without load it was not at all observed. The metallographic analysis showed the absence of corrosion of the FSW joint under cladding layer (Figure 5). Therefore, disregarding the surface pitting corrosion of the cladding layer, the latter performed its function.

The ICC tests showed that there are no corrosion traces in the clad specimens (Figure 6). A depth of

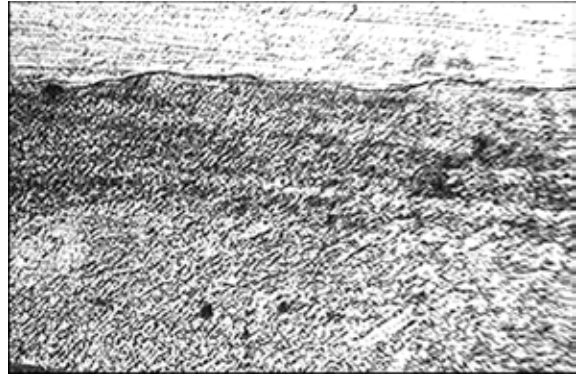


**Figure 6.** Microstructure of clad FSW joint of alloy 2024 after ICC test ( $\times 100$ )

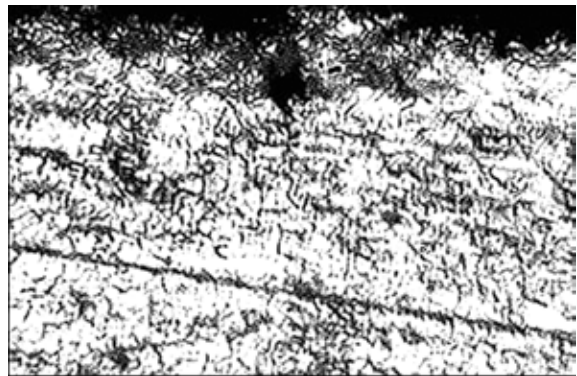


**Figure 7.** Microstructure of initial FSW joint of alloy 2024 after ICC test ( $\times 100$ )

corrosion penetration in the near-weld zone is  $43 \mu\text{m}$  (Figure 7) and in the thermomechanically affected zone is  $72 \mu\text{m}$ .

In conclusion it is worth noting that the corrosion traces were absent in the explosion-clad FSW joints of alloys 7010 and 2024 after SCC tests, the depth of ICC penetration in the non-clad joints of alloy 7010 was  $150\text{--}160 \mu\text{m}$  while the joints of alloy 2024 were destroyed. Besides, a depth of corrosion penetration in the FSW joints of alloy 2024 achieved  $72 \mu\text{m}$  under ICC tests even without loading.

The performed studies have shown a high efficiency of the proposed method for protection of the FSW joints of high-strength aluminium alloys against corrosion, which allows recommending this method for practical application.

1. Tretyak, N.G. (2002) Friction stir welding of aluminium alloys (Review). *The Paton Welding J.*, 7, 10–18.
2. Petushkov, V.G., Zotov, M.I., Polyakov, S.G. et al. (1989) Corrosion resistance of aluminium welded joints after explosion cladding. *Avtomatich. Svarka*, 1, 21–24.
3. Kudinov, V.M., Koroteev, A.Ya. (1978) *Explosion welding in metallurgy*. Moscow: Metallurgiya.
4. ASTM G 39: Standard practice for preparation and use of bent-beam stress-corrosion test specimens.
5. ASTM G 44: Standard practice for evaluating stress-corrosion cracking resistance of metals and alloys by alternate immersion in 3.5 % sodium chloride solution.
6. ASTM G 49: Standard practice for preparation and use of direct tension stress-corrosion test specimens.
7. ASTM G 110: Standard practice for evaluating intergranular corrosion resistance of heat-treatable aluminium alloys by immersion in sodium chloride + hydrogen peroxide solution.
8. QVA-Z10-59-03: Intergranular corrosion test for age-hardenable aluminium alloys.

# SOURCES OF BEAM HEATING FOR BRAZING (REVIEW)

A.M. ZHADKEVICH

E.O. Paton Electric Welding Institute, NASU, Kiev, Ukraine

The paper deals with the features of development of the design and application of technologies using the electron beam, laser, quartz lamps, as well as solar energy. It is shown that the inertialess heat sources enable controlling the heat input in a broad range, which allows considerable widening of the scope of brazed materials. Intensive development of the technique of brazing using concentrated heat sources is noted.

**Keywords:** *brazing, electron beam, laser, infrared radiation, heat source, quartz lamp, history of engineering.*

In the history of the development of joining processes the second half of the 20th century was marked by the beginning of the transition period, which implied a transition to a wide application of the intensive brazing processes. This was conditioned by the appearance of new materials and more complex conditions of their exploitation. Often a quality of the joints of new materials can be insured only by brazing. However, at the same time it was discovered that chemical erosion of the base material was the main disadvantage of main brazing processes. Besides, among other factors influencing the intensity and depth of erosion much significance is attached to a period of stay of the brazing filler alloy in the liquid state, the interval between the liquidus and solidus of the brazed metal–filler alloys [1, 2]. Therefore, the necessity arose to develop the brazing technologies based on the concentrated heating sources.

Since 1960s the designers of products of different purposes became interested in technological peculiarities of brazing. Specific requirements to heating developed from micro-miniaturization of the electronic devices and minimization of their weight in the large-scale structures of aviation-space engineering, nuclear power engineering etc. A number of organizations in the USSR launched comprehensive researches whose ultimate objective was to provide quality of the brazed articles for critical use employing the newest materials. These researches took into consideration the temperature conditions, design feasibility of the article, peculiarities of the metallurgical correlation of the brazed metal, technological nature of the structure, endurance of joints, their corrosion resistance and aging tendency, requirements to durability and reliability [3, 4].

The results obtained in the 1960s allowed the USSR to become the leader in development and application of the technology of brazing of special articles including the brazing of non-organic dielectrics, cermets and other materials with metals. High temperature resistance, mechanical strength were achieved and a number of other stringent requirements

to the super-powerful electronic, electric-vacuum SHF devices, power nuclear energy units, articles for thermonuclear synthesis and acceleration engineering etc. were met [5].

Even though the brazing with beam energy sources has been already used for several decades no attempts have been made so far to generalize the results of the studies on the brazing techniques, history of the development of technologies and equipment. So, in fundamental work [6] nothing is said in the overview section about brazing by beam sources. In this and other works [1, 2, 4–6] the data are not systematized and no comparison is made on peculiarities and potentialities of different sources of beam heating, the range of their optimal application is not established.

The aim of this work is to conduct a retrospective analysis of beam brazing methods, comparison of schemes and principles of heating, analysis of possibilities and peculiarities of the brazing techniques on specific examples and the results of applications in manufacturing of modern articles.

High concentration of energy, inertialessness of heating sources of articles, a possibility to accurately regulate the regime parameters are the most important properties of the basic beam technologies (welding, brazing, heat treatment, cutting etc.). Electron beam with its universal possibilities is widely applied. During the last two decades the researchers and producers paid much attention to the development of laser technologies. Creation of artificial beam energy sources was conditioned by a wide scope of the works in the sphere of electricity in the early 19th century while in the mid of the 19th --- by intensive studies of physical phenomena on the molecular-electronic level. Particularly, heat action of electron beams and infrared radiation were discovered and practically applied for the first time. Devices for different technologies of material treatment were designed in the first half of the 20th century, in the second half of the 20th century the electron beam welding and in the end of the 20th century the laser welding were developed and found extensive application. At the same time brazing technologies with the same heating sources were developed in a number of countries.

Electron beam treatment is based on heating the article with a heat evolved under moderation of the flow of electrons accelerated to high energies. The English physicist W. Crooks (1869) was the first to observe electron beams as a blue glowing along gas-discharge tube. Ten years after he discovered that the cathode beams may fuse metals including refractory platinum. Even earlier in 1852 V.G. Grove made similar presentation in the London Royal Society. However, only after discovery of electrons by G.G. Thomson in 1897 the American physicist R. Milliken associated the beams with the flow of electrons. Formation, focusing and deviation of electron beams attracted attention of scientists from many countries. As early as in the end of the 19th century the electron beams were applied in practice initiating thereby a scientific direction called electronic and ionic optics. The idea of deviation of the electron beam was practically implemented in 1897 by the German physicist K.F. Braun (by magnetic field) and by the English physicist G.G. Thomson (by electrostatic field).

Experiments and attempts to apply the electron beams for melting metals continued in the 20th century. However, a level of development of vacuum and electronic engineering was still insufficient for development of industrial technologies based on transformation of kinetic energy of electron flows into heating one during interaction with the surface of the heated body. Electron beam units for melting of niobium and tantalum ingots were created only in the beginning of the 1950s. Creation of high-production vacuum pumping systems, EB guns capable to provide a stable

technological process and reliable systems of power supply and control of the guns accelerated introduction of EB units in the metallurgy of pure metals and alloys [7].

The first technologies and units for EBW were developed in the 1950s by J. A. Stohr, G. Briola (France), W.L. Wyman (USA) [8, 9], N.A. Olshansky, B.A. Movchan, D.M. Rabkin, S.M. Gurevich, O.K. Nazarenko, S.D. Zagrebnyuk (USSR) [10, 11]. For a short period of time the methods of formation of electron beam, constructions of EB units with vacuum chambers up to several dozens of cubic meters in volume, cap chambers for local treatment are developed as well as advantages and a range of rational application of the EBW are determined and production of the equipment is organized. As to brazing technology, then electron beam heating (EBH) came into use for different experiments of brazing of high-accuracy articles assembled of thin-walled elements different in thickness and for manufacturing of units and structures of active and refractory metals.

V.F. Khorunov, Yu.B. Malevsky and others from the E.O. Paton Electric Welding Institute studied deformations, structural transformation and other characteristics of certain methods of brazing conducted in the vacuum unit with circular EBH [12]. In this case cyclic heating in different temperature and time intervals was achieved with sufficiently high accuracy. A.N. Kabanov, A.A. Kafarov and others from the Research Institute of Aviation Engineering developed several models of EB units ELURO for precision welding, brazing and size treatment with a possibility to regulate total and specific power in the beam within a wide range both in the pulse and continuous regimes (Figure 1) [13, 14]. The achieved specific power  $5 \cdot 10^8 \text{ W/cm}^3$  allowed treating almost all available materials. The unit ELURO is employed to produce special articles for electronic engineering. The microscope and a displacement mechanism incorporated in the unit provide alignment of the electron beam and a joint zone with  $\pm 5 \mu\text{m}$  accuracy under brazing of gold wire  $80 \mu\text{m}$  in diameter to the nichrome-manganese silver on the glass (thickness of layers is 30 and 800 nm; a silver layer 600–800 nm thick as a filler alloy) [15]. EBH was applied to produce through leads in the dielectric and semiconducting materials with high density and location accuracy. In this case one and the same unit is employed to drill holes (several dozens of micrometers in diameter) to where the wires are inserted (kovar and others) and to braze with a «softer» electron beam. It is proved possible to achieve high accuracy in positioning of leads — five wires positioned on  $1 \text{ mm}^2$  gave only  $10 \mu\text{m}$  of deviation from the preset geometry [15]. The industry and research organizations launched the production of other types of units.

Scanning of the flow of electrons is used for EBH of large area of joints. To achieve a uniform heating of the brazing zone in the units of ELU-4 type the electron beam oscillates when pulse beams of different

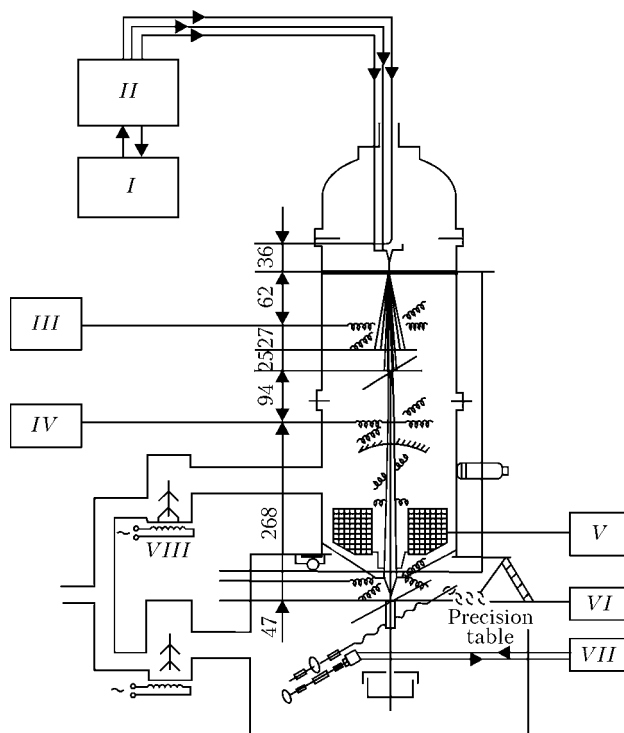


**Figure 1.** Schematic diagram of ELURO unit: I — high-voltage rectifier; II — voltage stabilizer, modulator, sections of glow and bias voltage; III–V — power sources of aligning coils of stigmator and lens; VI — power unit of raster electron microscope; VII — power supply to the table engine; VIII — pumping system

shape are fed to the deviating system. The unit is employed for brazing of complicated units of stainless steel medical instruments (Figure 2) [16].

A technology of brazing of massive parts of complex configuration using EBH and low-temperature solders was developed in the end of 1980s at the E.O. Paton Electric Welding Institute [17]. Brazing of components of space structures of aluminium alloys with nickel-copper and nickel-tin coating was conducted in the laboratory conditions. Heating with its duration reduced to the time of filling the clearance with the solder was performed by a defocused electron beam under pressure  $1 \cdot 10^{-2}$  MPa in the chamber. High fusion ability of the electron beam was used under development of the technology for producing the wheels of centrifugal compressors consisting of two disks and blades located between them. Electron beam fuses through the covering disc and melts down the solder between the disc and the blade [18].

Exploration of space requires production of special structures consisting of separate components on the orbit. Brazing in the space conditions is the leading technology of joining as well as in the Earth. However, the absence of gravity, vacuum, the necessity to work in the space-suites, limitation of the weight of the instruments and other equipment considerably complicate implementation of brazing as well as other technological operations. Besides, such new materials as composites with polymer, ceramic, metallic matrices and carbon fiber-reinforced plastics are used in these conditions with increasing frequency.

V.N. Kubasov was the first in the world to conduct experimental welding in space in 1969 in the spaceship «Soyuz-6». Processes of arc and electron beam heating were tested on the unit «Vulkan» created at the E.O. Paton Electric Welding Institute. Then the EB brazing was established as appropriate to use outside the spaceship [19]. EB units normally functioning in the orbital vacuum and consuming minimum energy as against other apparatus provide a high thermal efficiency of the welding, brazing and coating in the open space [20].

As a result of long-standing researches carried out under the leadership of Prof. B.E. Paton at the E.O. Paton Electric Welding Institute (V.F. Lapchinsky, E.A. Asnis, A.A. Zagrebely, V.F. Khorunov and others), in S.P. Korolyov Rocket Space Corporation «Energija» (Russia) (V.P. Nikitsky, A.V. Markov and others) and in the number of other organizations as well as the experiments in different spaceships the reliable and optimal design of the EB units, technologies for joining and repair of space structures, types of joints etc. were developed. Strong-focused electron beams are not needed for repair works, so a straight-channel diode gun was used as a source of EBH for brazing [21]. Research teams from the same organizations developed constructions of the orbit complexes, large-scale stations, whose erection in the space conditions requires brazing [22].

Optic sources of heating are underlain by a number of inventions of the middle of the 19th century, which

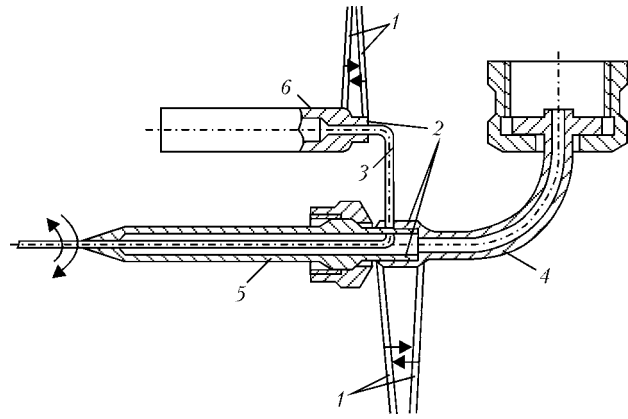


**Figure 2.** Scheme of brazing of the medical instrument unit: 1 — oscillating electron beam; 2 — cylinder; 3 — needle; 4 — branch pipe; 5 — working cylinder; 6 — brazing filler alloy

led to creation of electric sources of lighting, infrared and ultraviolet beams. Scientists and inventors from many countries (P.N. Yablochkov, V.N. Chikolev, A.N. Lodygin, T.A. Edison, V. Swan, I. Lengmur, N.P. Bulygin and others) were the pioneers of the lighting engineering. Electric lighting introduced into every day life in the first half of the 20th century is the most important and effective indication of the lighting engineering contribution into the development of civilization. Heating action of the radiant energy in lighting appliances (both arc and filament) observed in solving the problems with illumination, was often viewed as «harmful phenomenon». Nevertheless, already in the beginning of the 20th century the radiant heating started to be employed for technological purposes: for drying, melting of certain substances and others. Relevant appliances (reflectors, furnaces) were improved [23]. Solution of certain theoretical problems of thermal radiation (black light) in 1900 by M. Planck underlay modern quantum physics. Particularly, A.G. Stoletov's photoeffect was explained. The heating was attributed to absorption of energy and photon pulses by the illuminated body. Reflecting from mirror the photon changes its energy and pulse in compliance with the laws of collision of two material bodies but does not lose its heating ability [24].

Creation of the source of electromagnetic radiation of visible, infrared and ultraviolet range — the optic quantum generator opened a new epoch in the development of engineering. First quantum generators in the centimeter range of waves appeared in 1954. In 1960 the Soviet physicists N.G. Basov, A.M. Prokhorov and American physicist Ch. Townson created first ruby lasers. Soon the same year the first gas-discharge laser on the mixture of helium and neon was created and in 1962 — semiconducting lasers [25].

Laser has wide technological potentialities including high concentration of energy in the beam (up to  $1 \cdot 10^8$  W/cm<sup>2</sup>), practically inertialess control of the energy flow, high focusing accuracy of the beam, which provides minimization of the HAZ and deformation, penetration into hardly accessible places. The most important advantages of laser beam as against

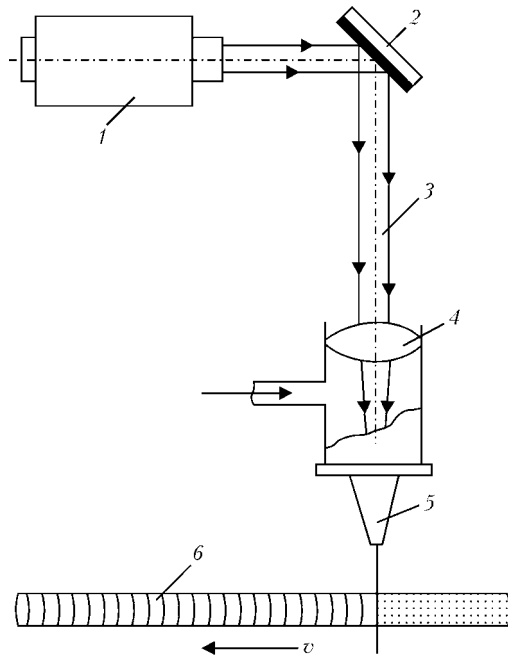


**Figure 3.** Diagram of CO<sub>2</sub>-laser system for metal treatment: 1 — laser source; 2 — mirror; 3 — laser beam; 4 — lens; 5 — nozzle; 6 — item

electron one is its ability to transmit radiation without losses to considerable distances by means of transmitting (on the basis of lenses) or reflecting (on the basis of parabolic mirrors) optical systems and distribution of heating energy by the working zones; non-contact treatment; ecological purity. Energy of the laser beam may concentrate into the spot about 0.2 mm in diameter.

Several laser systems were developed in the 1970s for technological purposes, however lasers on carbon dioxide (CO<sub>2</sub>) and on yttrium-aluminum garnet alloyed by neodymium (YAG) gained the wide use (Figure 3).

First technological laser units had maximal radiation energy not more than 2 J with pulse duration up to 8 ms and frequency rate up to 60 p/min. However, lasers were constantly improving. Pulse quantum generators were developed at the end of 1960s. In 1974 these lasers were used in the units of «Kvant» type for welding and other thermal operations [26]. In 1972 research workers from the E.O. Paton Electric Welding Institute and P.M. Lebedev Physical Institute for the first time in the Soviet Union conducted

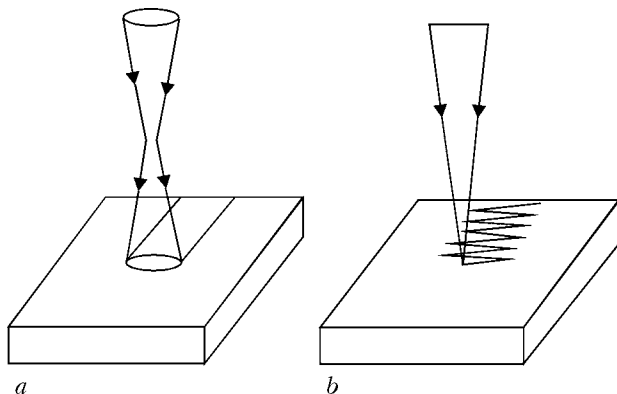


**Figure 4.** Diagram of defocusing (a) and scanning (vibrating) beam (b)

experiments on continuous laser welding. Industrial unit on the basis of CO<sub>2</sub>-laser was created at the I.V. Kurchatov Institute of Nuclear Energy in 1975 [27].

Application of CO<sub>2</sub>-lasers with a wide range of power and radiation for welding and related technologies is most effective. Their efficiency in this case may be increased by the pulse operating regime. Brazing requires, as a rule, smaller output power density than welding and cutting. It is achieved by regulation of the power and spot area by using lenses with a very short focusing distance.

Flexible light guides allow transporting a laser beam to any place of brazing with minimal energy losses. The unit of «Kvant» type was applied for production and repair of articles of titanium alloys. In many cases it is possible to make a repair only by local heating of the defected areas, which can be achieved by supplying concentrated energy. In those cases when a fast heating of a considerable area is needed, one uses beam defocusing or beam scanning (Figure 4). In the former case a narrow zone of the material is heated, in the latter — the spot area achieves several hundreds of square millimeters.

High-effective technologies for production of the elements of electronic engineering by laser beam brazing were developed in the 1970s at the E.O. Paton Electric Welding Institute (V.P. Garashchuk, O.A. Velichko, P.V. Avramchenko), A.A. Bajkov Institute of Metallurgy and a number of other organizations. It became possible to solve the problem of joining thin wires with thin films and formation of ohmic contacts in crystals of integral circuits [28, 29]. O.V. Yakubovich, V.E. Matyushkov and others proved in the course of the experiments a possibility to join the «spider» to the ball leads of the integral circuits by one-pulse laser radiation on the unit «Kvant-16» [30].

In the 1980s laser brazing came into wide use in the commercial production of steel structures, for example, for joining plates of the automobile bodies when the filler alloy is fed in the form of the wire (Figure 5) [31].

In recent years more attention is drawn to the problems of laser brazing of ceramics with metal. Particularly, mathematical models for brazing of plane and conic encasing metal-ceramic joints were created at the N.E. Bauman Moscow Higher Engineering College (B.A. Vinogradov, D.L. Kharichev and others) [32, 33].

Problems of joining heat resistant alloys and aluminium alloys with heat resistant brazing filler alloy of noble metals and aluminium were solved in Japan by laser brazing. In this case the diode laser was used that provided a suppression of erosion of the base metal and very accurate local control [34]. Laser brazing in the USA and Canada is successfully applied for repair of blades of hydraulic turbine engines [35]. There are reports on effective use of laser brazing in electronics (Germany) [36].

Currently the works on the seam laser brazing of galvanized steel continue at the E.O. Paton Electric Welding Institute (V.F. Khorunov, V.D. Shelyagin,

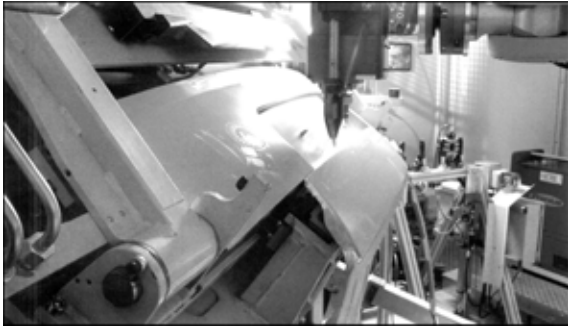


Figure 5. Laser brazing of the automobile body

V.Yu. Khaskin, I.V. Zvolinsky, S.V. Maksymova, A.V. Bernatsky, A.V. Siora). For this purpose a special stand on the basis of two-coordinate manipulator was created (Figure 6). Laser LT-104 developed and produced at the E.O. Paton Electric Welding Institute was used in the experiment [37]. Copper-base filler alloy was made in the form of a wire 1.2 mm in diameter. Butts of plate galvanized steel were brazed into clearance (0.6 mm). Satisfactory formation of the upper and lower reinforcing beads and a smooth transfer of the filler metal to the galvanized coating without disturbing the latter were obtained. Brazing rate was up to 2 m/min.

Quartz lamps may be classified as beam heating sources for brazing. Depending on technological conditions one uses the units with reflectors, light guide lenses, lamps of different types. Lamps of infrared heating are most often used for operations in the horizontal position (quartz iodine lamps of NIK-220-1000, KIO-220-2500 types and others) [38–40], whose power achieves several kilowatts with heating temperature above 2000 °C. In the 1970s brazing with quartz lamps in the inert gas was successfully used for production of honeycomb panels of titanium alloys, different structures of other metals and plastic [39].

Light beam plays a significant part for welding and brazing [40–44]. Since 1950s heating of light beams came into use for solving a number of problems of scientific and technical progress (manufacturing of electron devices, growing of single crystals and others). The first pilot unit for welding and brazing with radiant energy USPLE-1-MATI (M.I. Oparin) was designed in 1968 at the K.E. Tsiolkovsky Moscow Aviation Institute in compliance with the concept on development of light-beam manufacturing equipment formulated by G.D. Nikiforov. The first light-beam units with mobile torches in the form of arc xenon lamps with power up to 10 kW were created in the first half of the 1970s. Units with different focusing systems were also experimentally studied (Figure 7) [43, 44].

Pilot units include a unit with seven optic focusing systems and lamps, small-scale unit «Foton» and others [45]. Large-scale studies determined technological advantages: contact-free heating of the article with energy supply through optically transparent chambers in any gas medium and under any pressure, heating of the article irrespective of physical and chemical

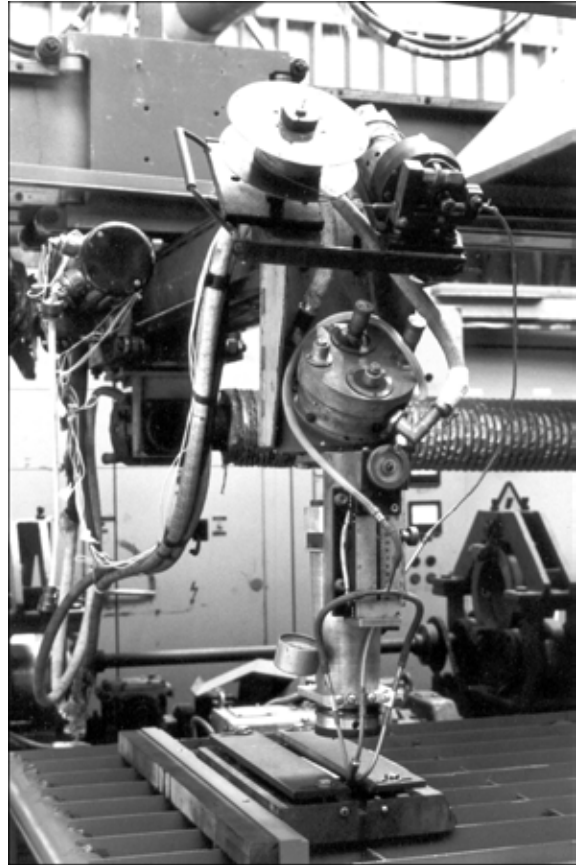


Figure 6. Stand for laser seam brazing

properties of the materials, high accuracy of the regime parameter control [37]. Similar results were obtained in the USA, Japan and other countries [46].

In the number of cases it is brazing with focused radiant energy that allows producing high-quality joints for electronic engineering. Industrial unit UPSL-1 was used to braze planar leads of microcircuits on printed-circuit boards and beam hermetic sealing of body components in vacuum [47].

In the 1980s a more powerful light-beam equipment was developed. Special metallic reflectors and pulse power mode permitted increasing the flow density up to 12 kW/cm<sup>2</sup>. Sphere ellipsoidal focusing systems allow obtaining a circular flow and a flow split into several beams [48].

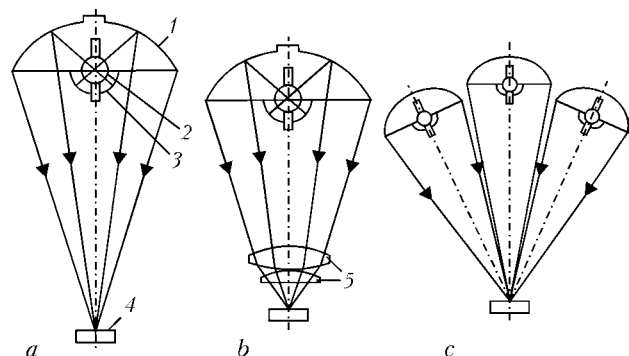
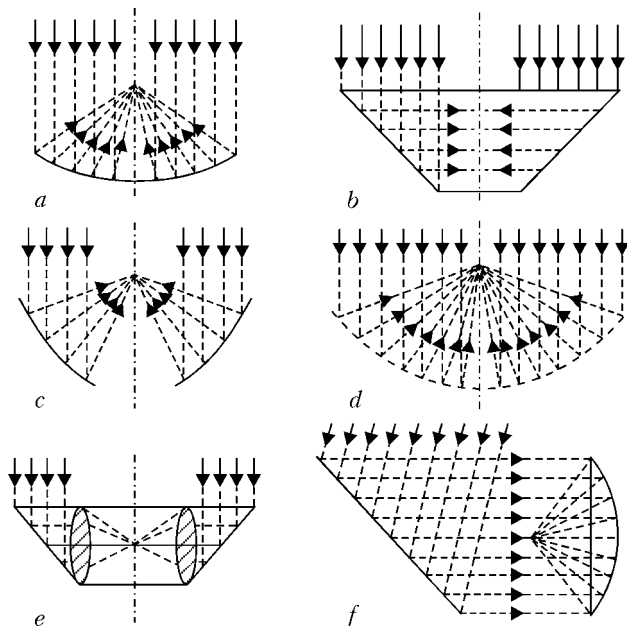


Figure 7. Optical schemes of pilot units monoellipsoidal (a), monoellipsoidal with lens objective (b) and polyellipsoidal (c) for welding, brazing and heat treatment with radiant energy: 1 — ellipsoidal reflector; 2 — arc xenon lamp; 3 — counter reflector; 4 — heated object; 5 — lens objective



**Figure 8.** Scheme of helio concentrators: *a* — paraboloidal (parabolic-cylindrical, cylindrical); *b* — conic; *c* — toroidal; *d* — composed of separate plane mirrors; *e* — mirror-lens; *f* — with movable mirror and immovable concentrator

The Sun as a natural source of light maintaining life on the Earth occupies a special place among beam sources. A method of concentrating the solar energy by optical lenses was used since ancient times. By this method a sacred fire was lighted in the temples of Ancient China, Ancient Rome and Ancient Greece. In the beginning of the last century a tradition to light the Olympic Fire from the sunrays was restored. In the ruins of town Ninevia (Mesopotamia) lenses were found, which dated back to the 8th century BC. The ancient Greek scientist Archimedes was the first, who performed studies on heating of objects with sunrays and described them in his tractates «On Lighting Glasses» [49]. He also invented and, as believed, for the first time applied the second method of concentration of the solar energy by reflection from mirrors. According to the Byzantine poet Ceces, Archimedes managed to set on fire the Rome fleet of Consul Marcellus laying siege to Syracuse proposing the women to direct sunbeams reflected from their mirrors to a single point on the vessels [50].

It is natural that energy of the Sun and seeming simplicity of its concentration time and again at-

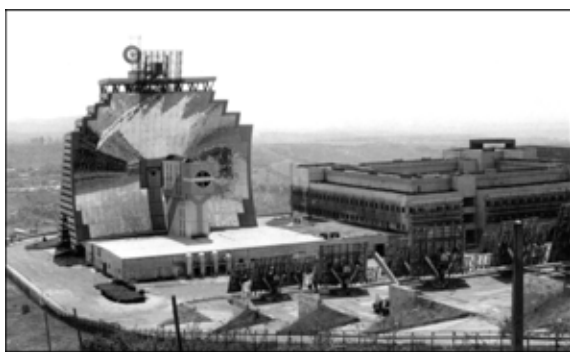


**Figure 9.** Two-mirror optic-power unit — sun furnace with power of 1 MW of the Research Production Institute of Materials Science, Association «Fizika-Solntse» (Parkent, Tashkent oblast)

tracted attention of the inventors. In the end of the 19th century a successful use of the sun heat in the steam engines was reported in Russia, Great Britain and France. The heating device even received a name «insolartor». However these devices were of very low efficiency and did not gain practical application.

In the second half of the 20th century the solar power engineering dealing with the problems of utilizing the energy of the Sun developed. Activities are centered around different methods of transformation of the solar energy into other types of energies suitable for practical application (first of all heat and power). Helio concentrators are the basic components of helio units for heating (Figure 8). Devices for concentration of radiant energy, which on the small area enhance the density of sun radiation  $10-10^{10}$  times are designed in the form of plane and concave reflectors of different shapes.

Sun furnace in addition to concentrators incorporate heating chambers, regulators of density of radiant energy flow and a system for the position control relative to the direction of lighting. In the end of the 20th century furnaces suitable for melting, welding, brazing and heat treatment where a heating temperature achieved  $3500-3800\text{ }^{\circ}\text{C}$  were created in different countries. Large sun furnaces with the power of more than 1 MW were constructed in Fon-Rome, Odejo (France), in settlement Parkent (Tashkent oblast, Uzbekistan) (Figure 9), in Turkmenistan (Research Production Association «Solntse»), in USA (California), in Las Salinas (Chile) and others. It is possible to judge about potentialities of solar energy by the results of the tests of helio unit in the USA (town Albuquerque, state New Mexico). Sunbeams from 1775 mirrors (1.5 m each) focused on the steel plate ( $400 \times 300 \times 20\text{ mm}$ ) incandesced it for 2 min to the temperature  $1000\text{ }^{\circ}\text{C}$ . It is noteworthy that such furnaces are developed mainly for heating of water for desalination, steam production and other purposes. However, there are technologies aimed at using the sun energy for chemical technologies and melting — remelting, welding, brazing [51, 52]. Most probable that welding and brazing by means of the sun will be used for construction and repair of engineering structures in the space. Solutions sought for under development of large-scale solar reflectors of polymer metal-sprayed film located on the near-earth orbit for lighting different objects on the Earth, large-diameter mirror concentrators and sun gas-turbine units [19] may serve as technical background for creation of special concentrators. Already available engineering solutions may be used for creation of the helio units. Several advanced designs of space optic systems with the enlarged diameter of metallic mirrors are known [53]. E.A. Korshenko, I.M. Zhdanov, S.I. Moravetsky, S.K. Fomichev and others (National Technical University of Ukraine «Kiev Polytechnic Institute») and V.F. Lapchinsky (E.O. Paton Electric Welding Institute) developed a light multilayer structure of corrugated thin-plate elements [54]. Even though the authors consider that such systems should be formed



by welding (one-sided spot-welded joints) a long-standing experience for production of similar grid structures (aviation and rocket) permits stating that brazing will be the most effective method of joining for construction of optic systems in the space [55].

## CONCLUSIONS

1. Owing to inventions in the sphere of physics of high energies, optics and due to development of devices radiating flows of electrons and light quanta the commercial units for transformation of kinetic energy of electron flows and electromagnetic radiation into heat energy suitable for practical brazing were developed in the second half of the 20th century.

2. Technological possibilities of electron-beam and optic units: inertialessness, high concentration of energy, accuracy in positioning allow effective solutions in production of complex assemblies and structures ranging from microelectronic elements to large-scale engineering structures in space using all structural metallic alloys, ceramic and other materials.

1. Petunin, I.E., Ekatoeva, A.S., Markova, I.Yu. (1976) *Metals science of brazing*. Moscow: Metallurgiya.
2. Lashko, N.F., Lashko, S.V. (1974) *Problems of theory and technology of brazing*. Saratov: SGU.
3. Rossoshinsky, A.A., Tabelev, V.D., Kislitsyn, V.M. (1971) *Pressure microwelding*. Kiev: Tekhnika.
4. (1975) *Reference book on brazing*. Ed. by S.N. Lotsmanov et al. Moscow: Mashinostroenie.
5. Frolov, V.P., Markova, I.Yu., Eroshev, V.K. et al. (2001) Development of brazing in the 20th century. In: *Brazing. Current technologies, materials, structures*. Moscow: TsRDZ.
6. Lashko, N.F., Lashko, S.V. (1981) Brazing of metals. In: *Welding in the USSR*. Vol. 1. Moscow: Nauka.
7. Shiller, V., Gajzik, U., Pantser, Z. (1980) *Electron beam technology*. Moscow: Energiya.
8. Wyman, W.L. (1958) High-vacuum electron-beam fusion welding. *Welding J.*, **2**, 49–53.
9. Stohr, J.A., Briola, J. (1958) Vacuum welding of metals. *Welding and Metal Fabrication*, **10**, 366–370.
10. Olshansky, N.A. (1959) Method of vacuum electron beam welding. *Avtomatich. Svarka*, **8**, 3–11.
11. Movchan, B.A., Rabkin, D.M., Gurevich, S.M. et al. (1959) Some technological features of vacuum electron beam welding. *Ibid.*, **8**, 32–33.
12. Khorunov, F.V., Malevsky, Yu.B., Nesmikh, V.S. et al. (1968) Effect of some technological parameters of welding-brazing process. *Ibid.*, **11**, 22–25.
13. Kabanov, A.N., Kafarov, A.A., Mikhajlovsky, G.A. (1967) Service characteristics of installation ELURO. *Ibid.*, **3**, 72–73.
14. Iliin, V.V., Klyujkov, A.G. (1967) Stabilized source of accelerating voltage for installation ELURO. *Ibid.*, 75–76.
15. Kabanov, A.N., Zolotov, L.A. (1967) Application of installation ELURO for microwelding and brazing. *Ibid.*, 74–75.
16. Pletnev, V.M., Ryzhkov, F.N., Drozdov, M.L. et al. (1971) Electron beam brazing of needle-less injector assembly unit. *Svarochn. Proizvodstvo*, **4**, 49–50.
17. Khorunov, V.F., Lapchinsky, V.F., Shvets, V.I. et al. (1993) Technology of vacuum brazing of aluminium alloy truss structure components. *Avtomatich. Svarka*, **2**, 52–53.
18. Tkachenko, G.G., Radzievsky, V.I., Gartsunov, Yu.F. (2000) Autovacuum brazing of impellers of centrifugal compressors of 07Kh16N6 steel. In: *Brazing*. Toliatti: TPI.
19. Paton, B.E., Lapchinsky, V.F. (1998) *Welding and related technologies in space*. Kiev: Naukova Dumka.
20. Khorunov, V.F., Shvets, V.I., Bulatsev, A.R. et al. (1999) Peculiarities of formation of brazed joints of thin-wall structures in space. *Avtomatich. Svarka*, **10**, 31–38.
21. Asnis, E.A., Zabolotin, S.P., Lapchinsky, V.F. et al. (1997) Technology of repair of pipelines using the electron-beam welding and brazing as applied to space conditions. *Ibid.*, **8**, 50–53.
22. Paton, B.E., Bulatsev, A.R., Mikhajlovskaya, E.S. et al. (1998) Truss structures in orbital complexes. *Ibid.*, **11**, 5–10.
23. Laslo, T.S. (1968) *Optical high-temperature furnaces*. Moscow: Mir.
24. Born, M., Volf, E. (1973) *Principles of optics*. Ed. by G.P. Motulevich. Moscow: Nauka.
25. Clouder, J.R., Sudarshan, E. (1970) *Principles of quantum optics*. Ed. by S.A. Akhmanov. Moscow: Mir.
26. Baranov, M.S., Kondratiev, V.A., Uglov, A.A. (1972) Kinetics of formation of wire splice in pulse laser beam welding. *Fizika i Khimiya Obrab. Materialov*, **5**, 11–14.
27. Rykalin, N.N., Uglov, A.A., Kokora, A.N. (1975) *Laser treatment of materials*. Moscow: Mashinostroenie.
28. Avramchenko, P.F., Velichko, O.A., Moravsky, V.E. (1978) Pulse laser brazing of conductors with films in microinstrument-making industry. *Avtomatich. Svarka*, **5**, 24–26.
29. (1975) Joining of integrated circuit elements by laser. In: *News in science and technique: Inform. commun. VINITI*. Issue 14.
30. Yakubovich, O.V., Matyushkov, V.E. et al. (1981) Laser brazing of electronic engineering items. *Ibid.*, **4**, 57–59.
31. Husner, J., Olaineck, C. (2003) Laser brazing in automobile production. *Thyssen Krupp Techforum*, **12**, 60–63.
32. Vinogradov, B.A., Kharicheva, D.L., Shvajka, D.S. (2001) Modelling of thermal processes in laser brazing of ceramics with metal. *Problemy Mashinost. i Nadyozhn. Mashin*, **4**, 71–75.
33. Vinogradov, B.A., Kharicheva, D.L., Styopochkin, V.A. et al. (2004) Determination of typical heat zones in laser brazing of metal with ceramics. *Svarochn. Proizvodstvo*, **8**, 23–26.
34. Saida, K., Nishimoto, K. (2003) Method of diode laser brazing. *Welding Technology*, **51**(6), 92–98.
35. Dodd, E., Bilakh, Ya. (2004) Repair of blades by laser is the technology of the future. *Svarshchik*, **3**, 34–35.
36. Azdasht, G., Zakel, E., Reiche, H. (1996) Implementation of low power diode laser for soldering by fibre push connection method. *Soldering and Surface Mount Technology*, **22**, 51–54.
37. Garashchuk, V.P., Shelyagin, V.D., Nazarenko, O.K. et al. (1997) Technological CO<sub>2</sub>-laser LT-104 of 10 kW power. *Avtomatich. Svarka*, **1**, 36–39.
38. (1965) Electric furnaces OKB-1152 and OKB-1153 with infrared heating. *Elektrotermiya*, Issue 43, 3–4.
39. Khorunov, V.F., Kuzhel, A.V., Malevsky, Yu.B. (1974) Production of brazed lamellar structures. *Avtomatich. Svarka*, **11**, 53–56.
40. Nikiforov, G.D., Oparin, M.I., Fyodorov, S.A. (1979) *Light beam welding and brazing*. Manual. Moscow: Mashinostroenie.
41. Frolov, V.A., Mamaev, V.S., Pronin, N.S. et al. (1993) Use of light beam energy for technological purposes. *Svarochn. Proizvodstvo*, **4**, 12–14.
42. Khorunov, V.F., Shal Dzigo. (1995) Welding and brazing of different materials using the light beam of arc xenon lamps (Review). *Avtomatich. Svarka*, **5**, 48–52.
43. Nikiforov, G.D., Diachenko, V.V., Oparin, M.I. et al. (1969) Use of focused light energy of high-capacity xenon lamps for welding and brazing of metals. *Svarochn. Proizvodstvo*, **9**, 1–3.
44. Nikiforov, G.D., Oparin, M.I., Fyodorov, S.A. (1974) Use of light heating for welding, brazing and heat treatment. *Ibid.*, **12**, 18–21.
45. Mironov, L.G., Ravaev, G.P., Petukhov, V.F. (1981) Experience of application of focused light energy of arc xenon lamps for brazing of items. In: *New developments in brazing*. Kiev: PWI.
46. Takagi, M., Yamaji, T. (1995) New soldering process using light beam technology. *Soldering and Surface Mount Technology*, **20**, 13–20.
47. Frolov, V.A. (1998) Engineering and design features of development of welded structures using the light beam welding. *Svarochn. Proizvodstvo*, **3**, 16–20.
48. Frolov, V.A., Proshin, N.S., Fyodorov, S.A. et al. (2003) Development and improvement of light-beam welding, brazing and heat treatment technologies. *Tekhnologiya Mashinostroeniya*, **5**, 28–29.
49. (1962) *Archimedes*. Treatises. Moscow: Fizmatgiz.
50. Veselovsky, I.N. (1957) *Archimedes*. Moscow: Uchpedgiz.
51. (1983) *Optic infrared telescopes in the 1990s*. Moscow: Mir.
52. Kornienko, A.N. *Reflector*. USSR author's cert. 350614. Int. Cl. B 23 K 27/00. Publ. 13.09.72.
53. Semyonov, Yu.P. (2003) Space technologies on the threshold of the centuries: results and prospects. *The Paton Welding J.*, **10/11**, 21–30.
54. Zhdanov, I.M., Kononchuk, V.V., Fomichev, S.K. et al. *Package for producing the multilayer structure*. USSR author's cert. 1684091. Int. Cl. 5 B 32 B 3/12. Publ. 15.10.91.
55. Belotserkovsky, S.M., Odnovol, L.A., Safin, Yu.Z. et al. (1985) *Lattice wings*. Moscow: Mashinostroenie.



# METHOD OF SOFTWARE DEVELOPMENT USING CONTROL GRAPHS AND LANGUAGES MEANS ISaGRAF FOR INTELLIGENT WELDING CONTROLLERS

F.N. KISELEVSKY, V.V. DOLINENKO and D.D. TOPCHEV  
E.O. Paton Electric Welding Institute, NASU, Kiev, Ukraine

A new method is proposed to develop software of intelligent welding controllers, using control graphs of the states and SFC language of ISaGRAF package. An example is considered of synthesis of a child program «Arc ignition» for the arc power source controller of TIG welding CAM system.

**Keywords:** arc welding, automatic control, control graphs, software

This study is devoted to the problem of development of object-oriented systems of automatic control of arc welding [1]. Development of the software for intelligent controllers of welding equipment can run into difficulties in some cases. On the one hand, low-cost requirements are made of them, and, on the other hand, they should implement data communication protocols accepted in the automated system and support in real time the realization of control graphs of the states of the lowest level of the control program. Application of a programmed logical controller (PLC) Smart-I/O (PEP Company, Germany) for development of intelligent welding controllers can be an interesting solution. Unlike the traditional PLC, Smart-I/O can run programs written both using the known programming languages ANSI-C and C++, and specialized ISaGRAF package [2]. The latter has the following advantages: use of standard programming languages IEC1131-3; graphic development interface; easy mastering and convenient use; built-in means for programming industrial networks; convenient and effective debugging aids.

According to IEC1131-3 standard, developers have five language means at their disposal: language of sequential functional circuits (SFC); functional

block-diagrams (FBD); relay diagrams (LD); structured text (ST) and instructions (IL).

PWI is working on development of a procedure of automated design of object-oriented CAM systems for welding, in particular, welding equipment controllers. Conducted investigations on development of a formal approach for synthesis of control programs in ISaGRAF language allowed formulating a method for development of programs for intelligent controllers of welding equipment. As an example, let us consider programming of a control graph for «Arc ignition» function in TIG welding of items of aluminium alloys (Figure).

The following conventions are taken, when assigning the graph ribs:

$$U_{ab}?:\{V_{ab}\}, \quad (1)$$

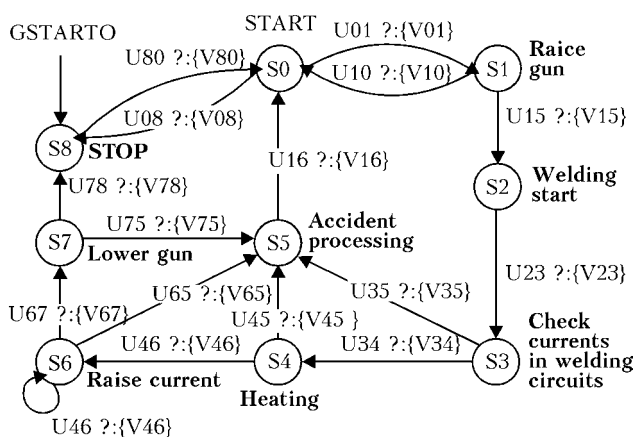
where  $U_{ab}$  is the condition, written as Boolean expression;  $V_{ab}$  is the operator, which is fulfilled at the true value of condition  $U_{ab}$ ; a, b are the numbers of graph points, between which the rib is located.

chPodjig module (child process) has the following purpose: after receiving a command from upper level controller «Welding start», perform the following functions: raise the welding head to a certain distance above the item surface; switch on the arc power source; raise the welding currents to required values; lower the welding torch to item surface level; transfer control to the next program module.

The structure of control program of the controller is developed in FBD language, and child programs are in SFC and ST languages.

Developed by us formal method of conversion of an object-oriented control graph of states into a block-diagram of SFC-program is a system of formal rules, which allow generating a SFC-program, the behaviour of which corresponds to the initial control graph in terms of the control problem.

**Rule 1.** Each rib of the oriented graph is replaced by a pair of «transition-step» objects of SFC-program. «Transition» object implements  $U_{ab}$  condition, and «step» is  $V_{ab}$  action for this rib.



Control graph of child program «Arc ignition»

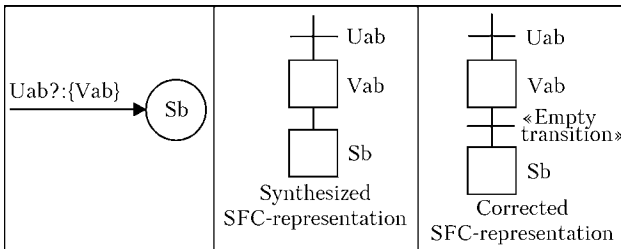


**Rule 2.** Each graph tip is replaced by «step» block of SFC-program.

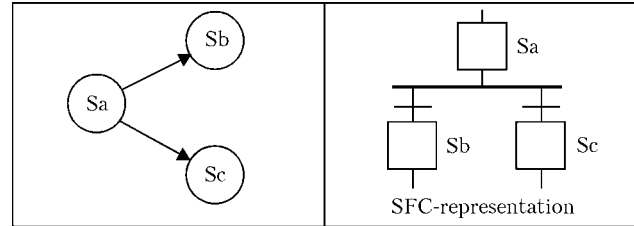


A step should not have any inner operators. However, in the case, if this tip has a rib-loop, «step» behaviour is described by «non-stored» action. In keeping with the terminology of SFC-program language a «non-stored» action is an operator block, which is repeatedly performed in each step of SFC-program operation, unlike «pulse» action, which is only performed once, having reached the information «marker» of this «step» (information «marker» indicates an active «step»).

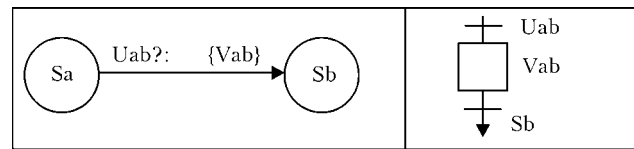
**Rule 3.** Follows from the rule of developing a SFC-program: a «transition» object should be present between two «steps» of SFC-program. If two successive «steps» do not have a «transition» object, it should be added, and the content of such a «transition» should be empty.



**Rule 4.** If several ribs oriented towards other tips are adjacent to the graph tip, SFC-object «divergence» is used.



**Rule 5.** As SFC-program is organized in the form of vertical chains of objects, it is allowed to disrupt the graph ribs. A pair of «transition» objects is applied in this case, using «unconditional transition».



SFC-program behaviour in real time is organized as follows. A variable earlier declared with «Timer» type is zeroed, in «step» object code, for instance:

$$T1 := t\#0 \text{ ms.}$$

An inequality is added to the «transition» following this step, for instance:

$$T1 > t\#1 \text{ s.}$$

In this case a time delay of 1 s will be executed.

1. Kisilevsky, F.N., Dolinenko, V.V. (2001) Object-oriented programming of systems of welding technological process control. *The Paton Welding J.*, **6**, 43–45.
2. (2000) ISaGRAF IEC1131-3 Version 3.00. In: *User guide*. C.J. International.



## THESES FOR SCIENTIFIC DEGREES

### **I.M. Gubkin Russian State University of Oil and Gas (Moscow)**

**Sidorenko A.V.** (I.M. Gubkin Russian State University of Oil and Gas) defended on the 12th of October 2004 his thesis for a Candidate degree on the subject «Peculiarities of Repair of Elements of Units for Cleaning of Gas from Acid Components».

Analysis of service conditions of units for cleaning of natural gas from acid components showed that the main causes of failure of the units were general non-uniform and pitting corrosion of metal.

It is shown that the use of high-alloy austenitic materials for cladding on carbon steels leads to substantial macroheterogeneity of the surface and, as a result, to its local damage. Formation of an active galvanic element between the repaired and non-repaired surfaces leads to fracture of the region of fusion with base metal.

It is indicated that in environments containing both passivating and activating agents even a small electrochemical heterogeneity causes an intensive pitting damage of the surface. As this heterogeneity is formed as a result of mixing of dissimilar base and filler metals, taking place during cladding, it is rational to use cladding consumables close in chemical composition to the base metal for joints operating in the above environments.

It is established that in the case of a comparable state of non-metallic inclusions, the bainitic component of structure, despite its high thermodynamic instability, provides increase in resistance to general and local corrosion due to higher homogeneity. The rational structural composition of deposited metal, consisting mostly of bainite (not less than 80 %), is determined.

The possibility of applying a generalised method by N.N. Rykalin to determine main geometric parameters of the cladding zone, temperature-time conditions of formation of deposited metal and parameters of argon-arc and plasma-arc cladding is proved. Calculation results are confirmed experimentally.

The field of a reasonable application of the argon-arc and plasma-arc cladding methods is identified. Unless thickness of the metal layer being restored is in excess of 2.0–2.5 mm, and the required cooling rate in a range of diffusion transformation of austenite is more than 40 °C/s, it is possible to use plasma-arc cladding. With increase in thickness of the deposited layer and keeping to the required cooling rates of less than 40 °C/s, it is indicated to use electric arc cladding by the GMA method.

The technology for restoration of the surface of equipment by the method of mechanised electric arc cladding using metal electrode in a mixture of gases (Ar + 20 % CO<sub>2</sub>) was developed. The technology provides structure of the deposited layer that contains not less than 80 % of the bainitic component, which is resistant to the corrosion effect by a working environment of the units for cleaning of natural gas from acid components.

Experimental-industrial tests proved validity of the application of the developed technology for cladding

carbon materials to repair elements of the units for cleaning of gas from acid components. In all cases the deposited metal has mechanical characteristics that are not inferior to those of the base metal, and a high resistance to general non-uniform and pitting corrosion.

The possibility of providing rational structural composition and required resistance of the deposited metal to the effect of a corrosive environment for a number of carbon cladding consumables is shown using the computer analysis.

The process instruction developed on the basis of the results of the work on restoration of internal surface of the U172 type unit for cleaning of gas from acid components was agreed upon with the All-Russian Research Institute of Gas and is recommended for application at the Astrakhan Gas Processing Plant.

### **Belarussian-Russian University (Mogilyov, Republic of Belarus)**

**Yakubovich D.I.** (Belarussian-Russian University) defended on the 16th of December 2004 the thesis for a Candidate degree on the subject «Improving Quality of Welded Joints in Thin-Sheet Steels Sensitive to Thermal Cycle through Redistribution of Heat Flow from a Heat Source».

The thesis analysed the effect of redistribution of heat input into a workpiece on the process of filling of gaps and edge displacement. Additional possibilities of regulating the rate of cooling of HAZ, preventing formation of martensite and accompanying cold cracks through redistribution of the heat flow in electrode weaving are revealed for steels sensitive to welding thermal cycle.

The effect of displacement of edges of the parts joined on the welding process was studied, and the maximum permissible edge displacements and edge gaps for butt welded joints in thin metal (0.1–2.0 mm) were established. The efficiency of electrode weaving for improving the quality of weld formation and prevention of burns-through is shown.

The expediency of using a more concentrated energy source for limiting size of the weakening zone in cold-worked steel in a temperature range of 1500 to 400 °C and reducing the time of growth of grain near the weld to 2–5 s is shown.

The mechanism of cold cracking of steels sensitive to welding thermal cycle is revealed. It consists in the beginning of fracture under the effect of interaction of hydrogen atmospheres with moving dislocations. Methods were developed for increasing technological strength through optimisation of oxidation potential of a shielding atmosphere.

The technology for robotic welding of steel 1 mm thick was developed, and optimal conditions were identified, providing sound welded joints at a welding current of 60–80 A, voltage of 17–20 V, amplitude of 4 mm and frequency of 3 Hz. The results of studies of butt welded joints 1.2 mm thick made in shielding gases with electrode weaving have found commercial application.